Chemical Consequences of Air Quality Standards and of Control Implementation Programs

Final Report

Contract No. A7-175-30

California Air Resources Board

June 1980

Principal Investigator

Dr. James N. Pitts, Jr.

Program Managers

Dr. Arthur M. Winer

Dr. William P. L. Carter

Program Research Staff

Dr. George J. Doyle

Dr. Richard A. Graham

Dr. Ernesto C. Tuazon

Technical Support Staff

Ms. Sara M. Aschmann

Mr. Frank R. Burleson

Mr. Dennis R. Fitz

Mr. L. Michael Kienitz

Ms. Minn P. Poe

Mr. Glen C. Vogelaar

Ms. Laurie A. Willis

Technical Editor

Dr. Marian C. Carpelan

STATEWIDE AIR POLLUTION RESEARCH CENTER

UNIVERSITY OF CALIFORNIA

RIVERSIDE, CALIFORNIA 92521

ABSTRACT

The environmental chamber facility established at the Statewide Air Pollution Research Center, University of California, Riverside, under a joint California Air Resources Board--University of California program has been employed in investigations:

To obtain data concerning the photooxidation of toluene, benzaldehyde, and cresols in NO_x-air systems; these data were then used to develop and validate a detailed chemical mechanism for the photooxidation of aromatic hydrocarbons;

To extend the previous oxidant-hydrocarbon-NO_x data base obtained at SAPRC by generating new data concerning the temperature dependence of photochemical smog formaton and of smog chamber effects;

To determine the dark and photooxidative reactivity of dimethylethanolamine (DMAE), a solubilizer in water-based paints.

Additional procedures or facilities were used in the following associated investigations:

Application of a combined chamber data-modeling technique to the determination of the effect of altering kinetic mechanisms and hydrocarbon composition on EKMA predictions of oxidant-precursor relationships;

Determination of the rate constants for the reactions of hydroxyl radicals with ethanol and propanol amines;

Elucidation of the gas- and aerosol-phase products of DMAE photooxidations;

Extension of previous measurements of the ambient concentrations of NH_3 and HNO_3 by kilometer pathlength FT-IR spectroscopy to experimental and theoretical investigations of the interrelationships between particulate nitrate and the concentrations of its gaseous precursors, NH_3 and HNO_3, under atmospheric conditions.

TABLE OF CONTENTS

ACKNOWLEDGMENTS

Stimulating discussion and valuable exchanges of technical information, for which we express our appreciation, took place at various times during this program with the following members of the California Air Resources Board and research staff: Dr. Alvin O. Gordon; Dr. John R. Holmes; Dr. Jack K. Suder; and Mr. Frank Bonamassa.

We gratefully acknowledge the assistance of Ms. Donna M. Shaw in typing this report.

This report was submitted in fullfillment of Contract No. A7-175-30 by the Statewide Air Pollution Research Center, University of California, Riverside, under the partial sponsorship of the California Air Resources Board. Work was completed as of October 31, 1979.

LIST OF FIGURES

LIST OF TABLES

I. EXECUTIVE SUMMARY

In order to provide an experimental data base relating to major unresolved issues concerning photochemical smog formation, the SAPRC environmental chamber facility was designed and constructed (1970-73) with support from the California Air Resources Board (ARB). The facility was initially (1973-75) utilized in a study of oxidant formation from hydrocarbon-oxides of nitrogen (HC-NO_x) mixtures irradiated under conditions simulating those found in the California South Coast Air Basin. The cumulative data base generated in these studies has been reported in previous SAPRC/ARB final reports and in 1979 was archived for the ARB in computer-readable formats to facilitate dissemination to other researchers.

An important result of these environmental chamber facility studies (1975-77) was the determination of OH radical rate constants for a large number of organic compounds under simulated atmospheric conditions, including some which were not amenable to study by more fundamental kinetic techniques. From the resulting extensive data base, a new reactivity scale based on the reaction of organics with the OH radical was formulated. The SAPRC/ARB surrogate hydrocarbon-NO_x-air data base has also been used in on-going studies reported in this volume on (a) the development of oxidant-precursor relationships for ambient air using combined chamber data-modeling techniques, (b) the development and validation of mechanisms of photooxidation of aromatic hydrocarbons, and (c) investigations of the effect of temperature on photochemical smog formation.

Additionally, in response to recent developments in atmospheric chemistry and air pollution control, studies during the contract period covered here included an investigation of the atmospheric reactivity of representative alcohol amines, and studies of the relationships between ammonia, nitric acid, and particulate nitrate in polluted atmospheres.

The results of the work undertaken for ARB Contract No. A7-175-30 (1978-79) are reported in this document. A summary of the results for each sub-program is given in the following pages of the Executive Summary, while Section II through VI provide a detailed report of the work carried out.

A. Photooxidation, Reactivity and Biological Studies of Ethanol and Propanol Amines Used in Water-Based Paints (Section II)

Because of a recent ARB rule aimed at further controlling solvent emissions in paint operations, interest has focused on the air pollution impact of increased use of water-based finishes. Such coatings contain significant quantities of alcohol amines, specifically, the tertiary amine dimethylaminoethanol (DMAE) and the primary amine 2-amino-2-methyl propanol (AMP). The chemical formulas of these two compounds are shown below.

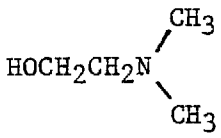

DMAE

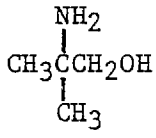

AMP

The atmospheric reactions of these compounds are of considerable current interest. In addition to their possible role as oxidant precursors a question arises as to their potential contribution to the formation of nitrosamines, nitramines, or other toxic species from the reactions of such amines with oxides of nitrogen in air.

Since AMP is a primary amine, it would not be expected to form nitrosamines. However, DMAE is a tertiary amine and by analogy with the reaction of triethylamine (Pitts et al., 1979a) it might be expected to form small amounts of nitrosamines in the dark and somewhat more in sunlight. Furthermore, during irradiation Pitts et al. (1978a) observed rapid photoconversion of nitrosamines to nitramines, and the same reaction might be expected with DMAE.

For these reasons, we have investigated the atmospheric reactivity of DMAE and AMP. Our study included: (1) development of a quantitative chromatographic analysis technique for DMAE and AMP; (2) indoor and outdoor smog chamber irradiations of DMAE-NO_x-air mixtures, and of DMAE-surrogate hydrocarbon-NO_x-air mixtures; (3) gas chromatographic-mass spectrometry characterization of the major DMAE photooxidation products; (4) examination of the mutagenic activity of DMAE, AMP, and products of DMAE-NO_x-air irradiations; and (5) determination of the rate constants for the reaction of hydroxyl radical with DMAE and AMP.

Results of these studies indicate that DMAE is less reactive than, for example, toluene in contributing to ozone formation or to photoconversion of NO to NO_2. However, DMAE photooxidation does result in the formation of large quantities of aerosol. There was no evidence for formation of nitrosamines from DMAE-NO_x-air reactions in the experiments performed, however traces of dimethylnitramine were observed from DMAE-surrogate hydrocarbon-NO_x-air runs. The latter observation could have resulted from the formation of nitrosamines which were rapidly photo-converted to nitramines but no direct evidence was obtained for this.

As noted a technique for chromatographic analysis of DMAE and AMP was developed. In attempting to calibrate this analysis by injection of known amounts of DMAE or AMP into the all glass chamber, we found that the measured gas phase concentrations of DMAE and AMP were variable and always smaller than expected based on the amount introduced. When a Teflon bag lining was employed with the glass chamber variability was greater and lower levels of DMAE were observed. These discrepancies were probably not due to the analytical techniques, which were varied without any change in results, but rather to absorption on the chamber walls; such "stickiness" is a characteristic of amines. Lower gas phase concentrations of DMAE were observed when the atmosphere contained NO_x than when the chamber contained only pure air. This observation might possibly be due to DMAE-NO_x-air dark reactions.

Exploratory experiments in the indoor chamber in which DMAE-NO_x-air mixtures with and without hydrocarbons were irradiated showed the conversion of NO to NO_2 and the growth of chromatographic peaks attributable to products of DMAE photooxidation. During such irradiations, concentrations of products apparently formed from interaction of DMAE with NO_2 in the dark increased. As expected a number of other products were formed during irradiation which were not formed in the dark. One of the three major photooxidation products was identified as dimethylformamide.

The SAPRC outdoor Teflon smog chamber facility was used in irradiations of DMAE-NO_x-air mixtures with and without a surrogate hydrocarbon mixture which has previously been described (Pitts et al., 1976a). In the absence of the surrogate hydrocarbon mixture, irradiation of DMAE-NO_x-air mixtures yielded significant aerosol formation and relatively little

NO_x reaction or ozone formation. The DMAE concentration-time profiles suggest that absorption and offgassing of DMAE on the surfaces occurred in these outdoor bag runs in a manner similar to that observed in most of the indoor chamber runs. There was also evidence for dark interactions between DMAE and NO_x in the outdoor bag runs, primarily an increase in condensation nuclei and aerosol particle number which occurred in the dark immediately upon NO_x injection. During irradiation, aerosol volume and b_{scat} increased markedly indicating formation of aerosol material due to photochemical reactions.

Experiments were performed to determine the effect of added DMAE on a surrogate hydrocarbon-NO_x-air irradiation in the outdoor dual chamber. Representative results are shown in Figures 1 and 2. A more extensive description of results is given in Section II. DMAE addition to the surrogate hydrocarbon-NO_x mixture enhanced ozone formation and the rate of NO_2 consumption. Aerosol formation occurred when as little as 20 ppb DMAE was added, while little or no aerosol formation occurred without DMAE present.

Gas chromatographic-mass spectroscopy (GC-MS) analyses were performed on gas phase samples and filter extracts of aerosol material collected during the DMAE-NO_x-air and the DMAE-surrogate hydrocarbon-NO_x-air outdoor chamber irradiations. Tenax samples of gas phase material taken from the DMAE-NO_x-air experiments contained only three products in detectable quantity: dimethylaminoacetaldehyde, dimethylformamide, and dimethylnitramine. Dimethylformamide and dimethylnitramine, but not dimethylaminoacetaldehyde were also observed on Tenax samples taken from DMAE-surrogate-NO_x-air runs. It is probable, however, that the detection of dimethylaminoacetaldehyde in the DMAE-NO_x-air sample is an artifact. In the DMAE surrogate hydrocarbon aerosol extracts, there were three major unidentified products. The observed products are consistent with those expected based on the most probable reactions for the atmospheric reaction of DMAE with OH in the presence of NO_x.

The Ames Salmonella typhimurium mammalian-microsome mutagenicity test was employed to screen for mutagenic activity of the parent compounds DMAE and AMP. In addition, reaction products from a DMAE-NO_x-air exposure in the outdoor chamber were tested using three different collection tech-

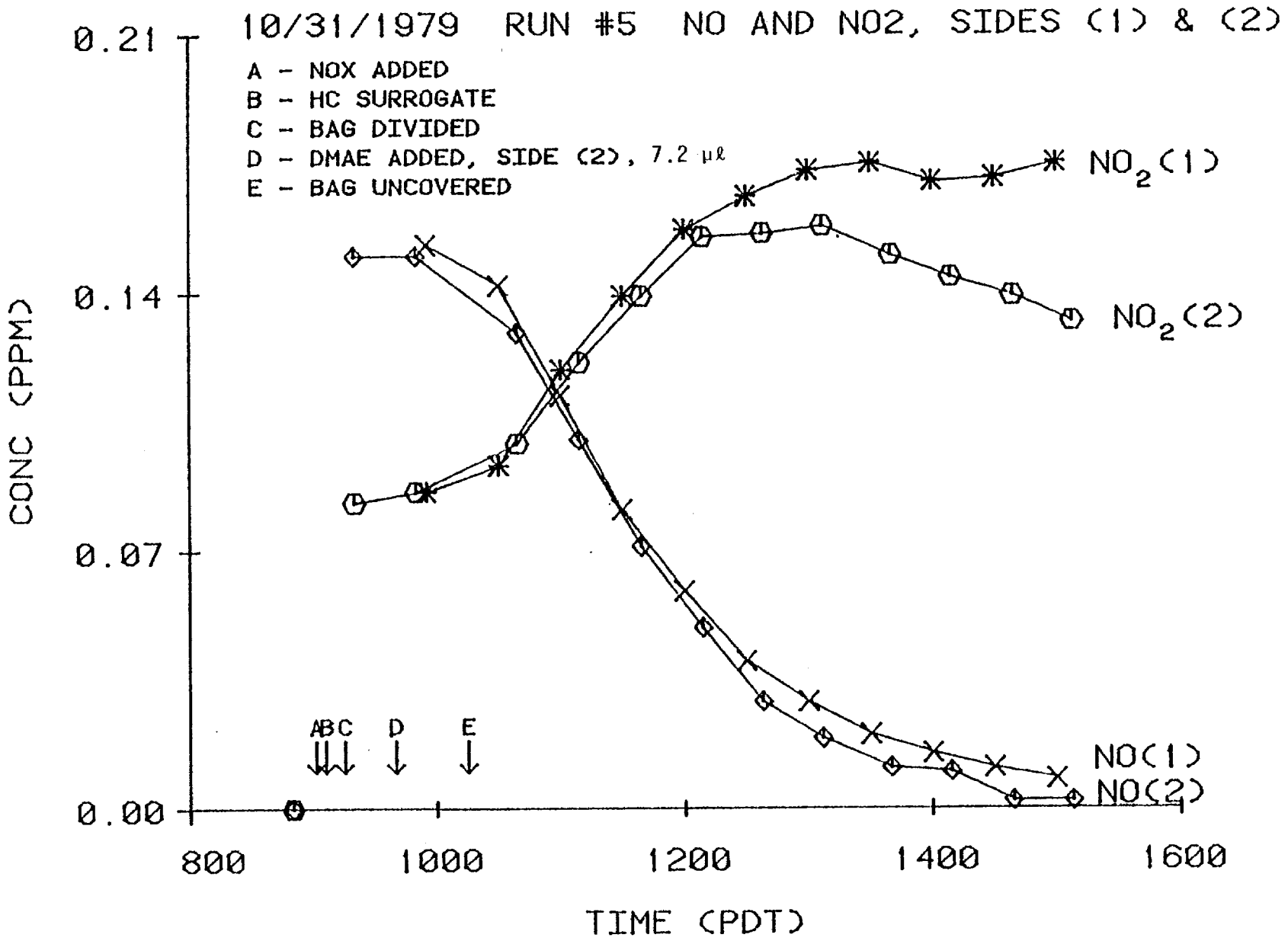

Figure 1. NO and NO_2 Concentration-Time Profiles for Dual-Outdoor Bag DMAE-Surrogate-NO_x-Air Run #5.

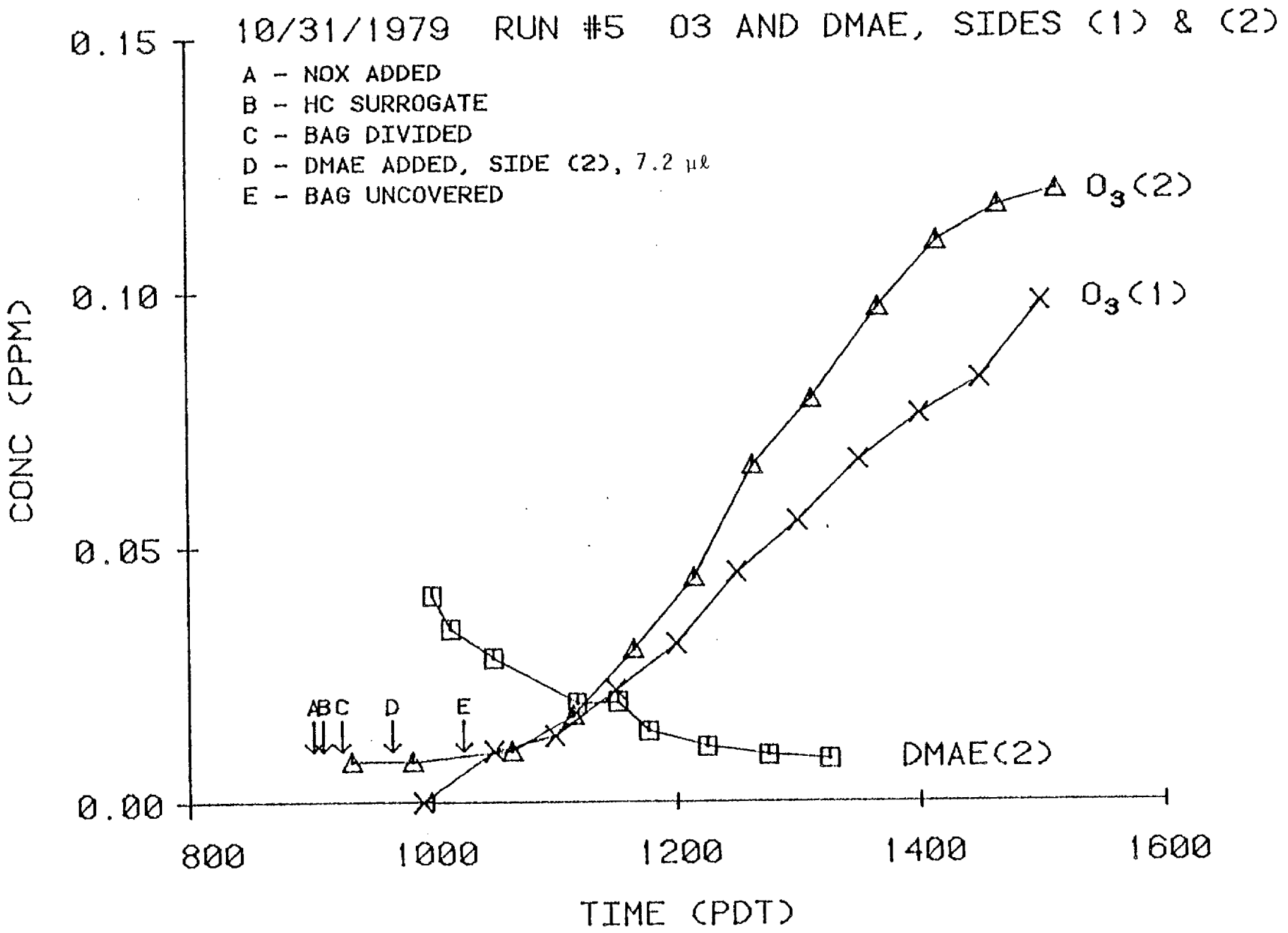

Figure 2. O_3 and DMAE Concentration-Time Profiles for Dual-Outdoor Bag DMAE-Surrogate-NO_x-Air Run #5.

niques: freeze-out samples, Tenax cartridge samples and direct exposure of the agar overlay containing the tester bacterial strains. Appropriate tester strains were used in each case both in the presence and absence of metabolic activation.

Although no mutagenic activity was found from any of the samples tested the following cautions must be emphasized. First, it was felt that the concentration of the reaction products in the gas exposure (sub ppm) and the freeze-out samples were probably below the threshold sensitivity for the tester strains employed. Secondly, it is well documented that many nitrosamines are only detected in milligram concentrations (Ames et al., 1975; McCann et al., 1975) in the Ames test. Finally, although the Tenax cartridge method can provide adequate concentration of sample, this technique is thought to produce artifact errors during the collection and elution procedure which might change, and possibly deactivate, any mutagens present. Thus, failure to obtain response in the Salmonella typhimurium mutagenicity assay cannot be taken as conclusive evidence for absence of mutagenic activity of the products of the thermal or photooxidation reactions of DMAE or AMP.

Rate constants for the reaction of hydroxyl radicals (OH) with both DMAE and AMP were determined by the flash photolysis resonance fluorescence (FPRF) technique. Reactions of OH radicals with DMAE and AMP were measured at temperatures of 300 $\pm$ 2K for 50 $\pm$ 1 torr total pressure of argon. The observed exponential OH decay rates yielded the following rate constants for the reaction of hydroxyl radicals with DMAE and AMP at 300 $\pm$ 2K:

$$k_1 \text{ (DMAE)} = 4.7 \pm 1.2 \times 10^{-11} \text{ cm}^3 \text{ molecule}^{-1} \text{ sec}^{-1}$$

$$k_1 \text{ (AMP)} = 2.8 \pm 0.5 \times 10^{-11} \text{ cm}^3 \text{ molecule}^{-1} \text{ sec}^{-1}$$

Estimates of the OH + DMAE rate constant were also obtained from an analysis of the results of the indoor and outdoor smog chamber experiments in which organic compounds with known OH rate constants were present. Using this technique, we obtained $k(\text{OH + DMAE}) \simeq 5 \times 10^{-11}$ cm^3 molecule^{-1} sec^{-1}. This value is in excellent agreement with that obtained by the FPRF technique.

The agreement of OH + DMAE rate constants using the FPRF technique and the smog chamber techniques indicates that the primary fate of gas phase DMAE emitted into the atmosphere must be reaction with the hydroxyl radical. This is probably also the case for AMP. Estimated lifetimes of gas phase DMAE and AMP are calculated to be approximately 3 hours and 6 hours, respectively, for urban atmospheres, assuming [OH] = 2 x 10^6 molecule cm^{-3}.

Although based on its rate of reaction with OH, DMAE is a quite reactive compound, results from our chamber experiments suggest that the tendency of DMAE to form large quantities of aerosols may be a more significant factor, in terms of environmental impact, than its ozone-forming potential. In particular the replacement of large quantities of organic solvents by substantially smaller amounts of the ethanolamines should lead to lower ozone production. Also working in this direction is the lower volatility and greater "stickiness" of DMAE and AMP compared with many of the organic solvents for which they are being substituted. On the other hand the propensity of DMAE and AMP to form aerosols must be considered in weighing the benefits of a water-based paint strategy since this is not a property of many of the solvents utilized in organics-based paints.

Finally, no positive results were obtained in any of the mutagenicity testing (Ames test) which was carried out for either DMAE and AMP or their reaction products. However, it must be emphasized that previous workers have shown that the Ames test is not sensitive to amines, or nitrosamines such as dimethylnitrosamine, a known carcinogen. The results of the mutagenicity tests are examined more fully in Section II.

B. Development of Ozone-Precursor Relationships for Ambient Air Using Combined Chamber Data-Modeling Techniques (Section III)

Quantitative relationships relating ambient ozone formation to its precursors, hydrocarbons and nitrogen oxides, are required if reliable predictions are to be made of the impact of changes in HC and NO_x emissions on ambient air quality. One technique currently advocated by the U. S. Environmental Protection Agency in making such quantitative predictions is the "empirical kinetic modeling approach" (EKMA). This approach involves the following steps: developing a hydrocarbon-NO_x-air kinetic model whose predictions of ozone formation can be made consistent with data obtained in smog chamber irradiations; modifying the model by removing "chamber effects"

and including appropriate diurnally-varying photolysis rate constants and realistic dilution rates and emission patterns; using the modified model to calculate isopleth plots of maximum ozone yields as a function of initial hydrocarbon and NO_x levels; and finally, using these isopleths to predict changes in ozone formation resulting from fractional changes in hydrocarbon and NO_x emissions.

A number of deficiencies and limitations of the EKMA technique (U. S. Environmental Protection Agency, 1977; Dimitriades, 1977; Bilger, 1978) are already well recognized by researchers and control officials. Other potentially important uncertainties of the EKMA technique which have not been adequately studied concern the validity of the chemical kinetic reaction mechanism (kinetic model) employed, and the most appropriate way to represent the nonmethane hydrocarbons in the mechanism. The kinetic model which has been used in applications of the EKMA technique is that developed for the EPA for this purpose by Dodge (1977a,b) (hereafter designated the EPA model), which employs the 75-step propene and n-butane mechanism developed by Durbin et al. (1975).

Studies concerning the effects of varying the mechanistic parameters or the representation of the nonmethane hydrocarbons used in the EPA model are limited. Dodge (1977a) used the EPA model to calculate the effect of varying hydrocarbon reactivity, solar energy, dilution rates, and post-9 a.m. emissions on calculated O_3 isopleths and on control strategies derived from them. It was found that changing these parameters changed the O_3 isopleths somewhat, but that changes in the isopleths had relatively little effect on control strategies derived from them, provided the control strategies were derived in terms of <u>relative</u> changes in hydrocarbon or NO_x emissions. It has been inferred from this that EKMA control strategy predictions are insensitive to details of how the hydrocarbons are represented and to uncertainties in the kinetic mechanism (U. S. Environmental Protection Agency, 1977). However, we are aware of no published calculations in which different kinetic mechanisms were compared, or in which other aspects of hydrocarbon representation, such as oxygenate content, were varied. Therefore, the assumption of general insensitivity of EKMA control strategy predictions to changes in details of the kinetic mechanism or the hydrocarbon representation remains to be tested thoroughly.

In this section we describe the results of calculations characterizing the dependence of EKMA isopleths and control strategy predictions on the kinetic model and the representation of the hydrocarbon mixture. In our EKMA calculations, we used an updated, independently-developed kinetic model which was validated against the SAPRC smog chamber data base (mechanism C); and the mechanism of Durbin et al. (1975) which was incorporated in the standard EPA EKMA model developed by Dodge (1977b) (mechanism D). In addition to varying the kinetic mechanism, calculations were made using different representations of the reactive hydrocarbons.

Table 1 outlines the matrix of mechanisms and hydrocarbon mixtures used in this study with the corresponding model designations. With respect to the designations for the hydrocarbon mixtures, mixtures SD and S represent the SAPRC detailed surrogate and propene-n-butane-aldehyde surrogate, respectively. Mixture E consists of propene, n-butane, formaldehyde and acetaldehyde in the relative amounts used in the standard EPA EKMA model. Mixture E- is the same as the E mixture but without the aldehydes.

Table 1. Designations of Models (Kinetic Mechanism + Hydrocarbon Mixture) Used in Ambient Air Simulation Calculations

Hydrocarbon Mixture	Kinetic Mechanism (C)[a]	Kinetic Mechanism (D)[b]
SAPRC detailed surrogate (SD)	C_{SD}	Not used
SAPRC propene-butane-aldehyde (S)	C_S	Not used
Standard EPA propene-butane-aldehyde (E)	C_E	D_E
EPA propene-butane (E-)	C_{E-}	D_{E-}

[a]Carter et al. (1979); Atkinson et al. (1980)

[b]Durbin et al (1975); Dodge (1977b)

Use of the EKMA isopleth analysis technique requires that the kinetic mechanism employed be validated against results of smog chamber irradiations of a reactive mixture representing polluted ambient air. Mechanism C is the simplified propene-n-butane-NO_x-air kinetic mechanism of Carter et al. (1979) with updated rate constants. For the purpose of validating mechanism C, four sets of chamber-simulation calculations were performed and the results of these calculations were compared to experimental chamber results. Good fits between predicted and observed ozone dependence on initial hydrocarbon and NO_x could be obtained, provided appropriate account was taken in the model for chamber effects. In order to give the best fit to the chamber data, a constant radical input rate of 0.4 ppb min^{-1} was assumed, and the $N_2O_5 + H_2O$ reaction was assumed to be negligible. Thus, mechanism C can be considered to be validated for the purpose of using it in EKMA calculations.

Ozone isopleths were calculated using mechanisms C and D and the four different hydrocarbon representations designated in Table 1. The effect on the isopleths of varying both the mechanism and the mixture is shown in Figure 3. Figure 4 shows the effects of added aldehyde in the EPA hydrocarbon mixture on the calculated O_3 isopleth for mechanism C. It can be seen from Figure 3 that although calculations using the SAPRC propene-butane-aldehyde mixture (S) give different isopleths than those using the EPA propene-butane-aldehyde mixture (E), this effect is not as great as that resulting from varying the kinetic mechanism. Thus, mechanism C predicts that increasing NO_x concentration inhibits O_3 formation more efficiently than does mechanism D. Mechanism C also predicts a larger effect of added aldehydes on the calculated O_3 isopleths than does mechanism D.

In order to evaluate the extent to which differences in ozone isopleths calculated by the various models and using different hydrocarbon representations will affect predictions of control strategy impacts, the isopleths were calculated for ozone levels of 0.45, 0.30 and 0.12 ppm. As a specific illustration, the isopleths were analyzed to determine their predictions of the degree of hydrocarbon control required to reduce O_3 levels from 0.3 ppm to the current federal air quality standard of 0.12 ppm. For this analysis the relative EKMA isopleth analysis technique was

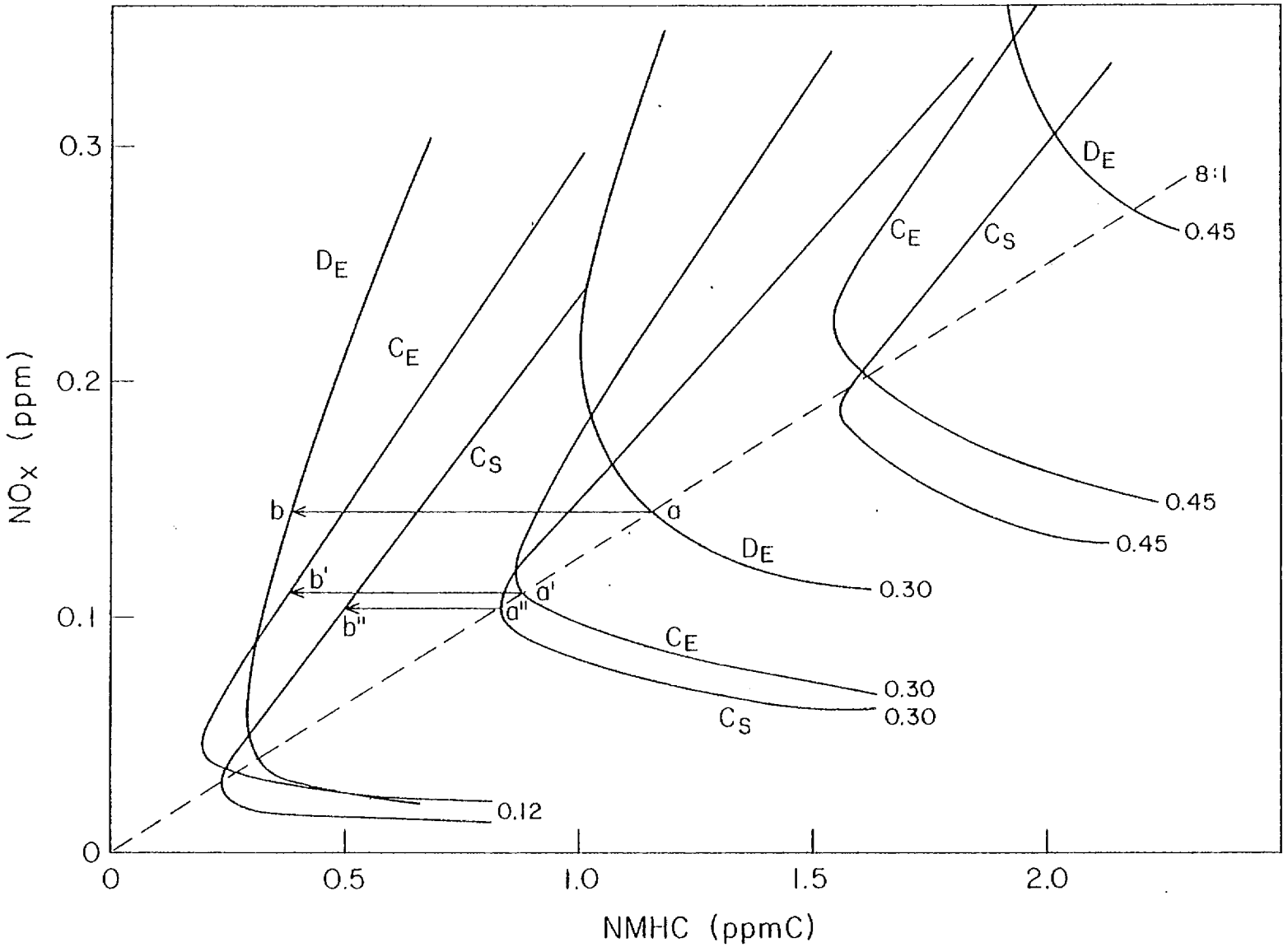

Figure 3. Isopleth Plots for O_3 = 0.12, 0.30 and 0.45 ppm Calculated for Mechanism D and the EPA Hydrocarbon Mixture (D_E); Mechanism C and the EPA Hydrocarbon Mixture (C_E); Mechanism C and the Propene-Butane-Aldehyde Representation of the SAPRC Surrogate Hydrocarbon Mixture (C_S). --- = $NMHC/NO_x$ = 8:1.

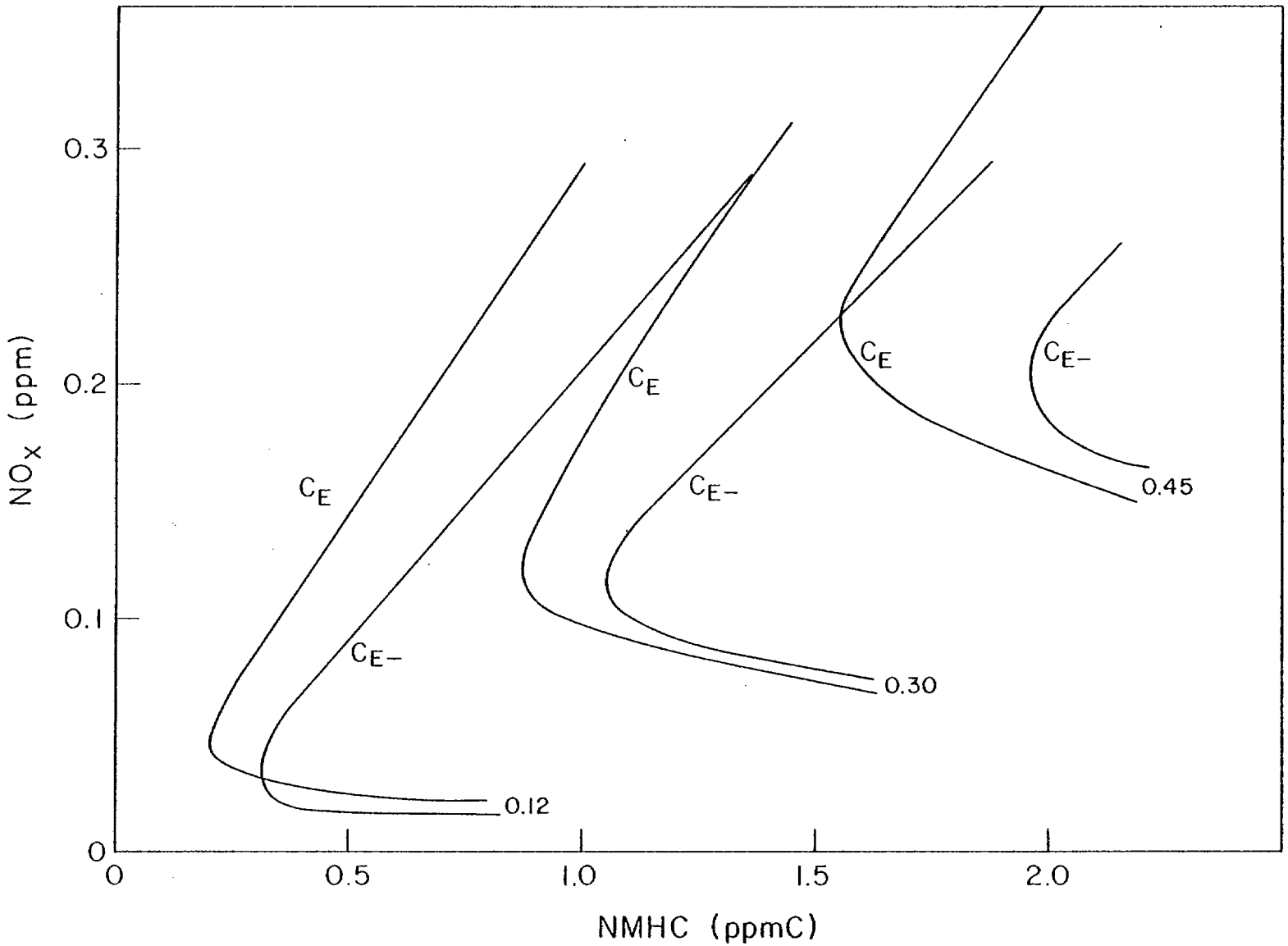

Figure 4. Isopleth Plots for O_3 = 0.12, 0.30 and 0.45 ppm Calculated for Mechanism C and the EPA Hydrocarbon Mixture With Aldehydes (C_E) and Without Aldehydes (C_{E-}).

used and is illustrated in Figure 3. Referring to Figure 3, if we assume the nonmethane hydrocarbon (NMHC) to NO_x ratio is 8 and construct isopleths calculated using the standard EPA model (D_E), the situation for O_3 = 0.3 ppm is indicated by a. In order to achieve a reduction of O_3 from 0.3 ppm to 0.12 ppm the D_E isopleths indicate a reduction of NMHC is required corresponding to moving from point a to point b. This amounts to a 67% reduction in hydrocarbon emissions. Analogously, the C_E and C_S isopleths in the same figure indicate reductions corresponding to moving from points a′ to b′ and from a" to b", respectively, amounting to required NMHC reductions of 58% and 41%, respectively.

The results of our analyses are summarized in Figure 5 in which percent hydrocarbon control predicted from the isopleths are plotted against initial NMHC/NO_x ratios. Thus, for an 8:1 NMHC/NO_x ratio and the EPA hydrocarbon representation, mechanism D predicts that a 66% NMHC reduction is required, while mechanism C predicts that a 57% reduction is needed. The difference between the predictions of the respective kinetic mechanisms is greater if aldehydes are excluded from the hydrocarbon representation; in that case mechanism D predicts a 62% reduction is required, while mechanism C predicts only 34%. Thus, our updated SAPRC mechanism predicts ~10-30% less hydrocarbon emissions reduction is required to achieve the O_3 federal air quality standard than previously predicted. In addition, predictions using mechanism C were more sensitive to the hydrocarbon representation than was mechanism D.

In a validation study of the EKMA isopleth analysis technique, Trijonis and Hunsaker (1978) compared historical air quality trends for the Los Angeles region and predictions of the EKMA isopleth method. They found a much better fit was obtained of EKMA "predicted" oxidant to the 1965-1974 historical oxidant data if an NMHC/NO_x ratio of 7:1 were used rather than their estimated summertime ambient ratio of ~12:1.

We examined the question of what the results of the Trijonis and Hunsaker (1978) study would have been if different kinetic mechanisms or hydrocarbon mixtures were employed. Their analyses were repeated for a sample case using the same techniques and input data, but employing the isopleths calculated for this study. Oxidant trends observed in the 95th percentile of the daily maxima at Azusa were chosen as being representative. Results of predicted trends, derived using models D_E, D_{E-}, C_E,

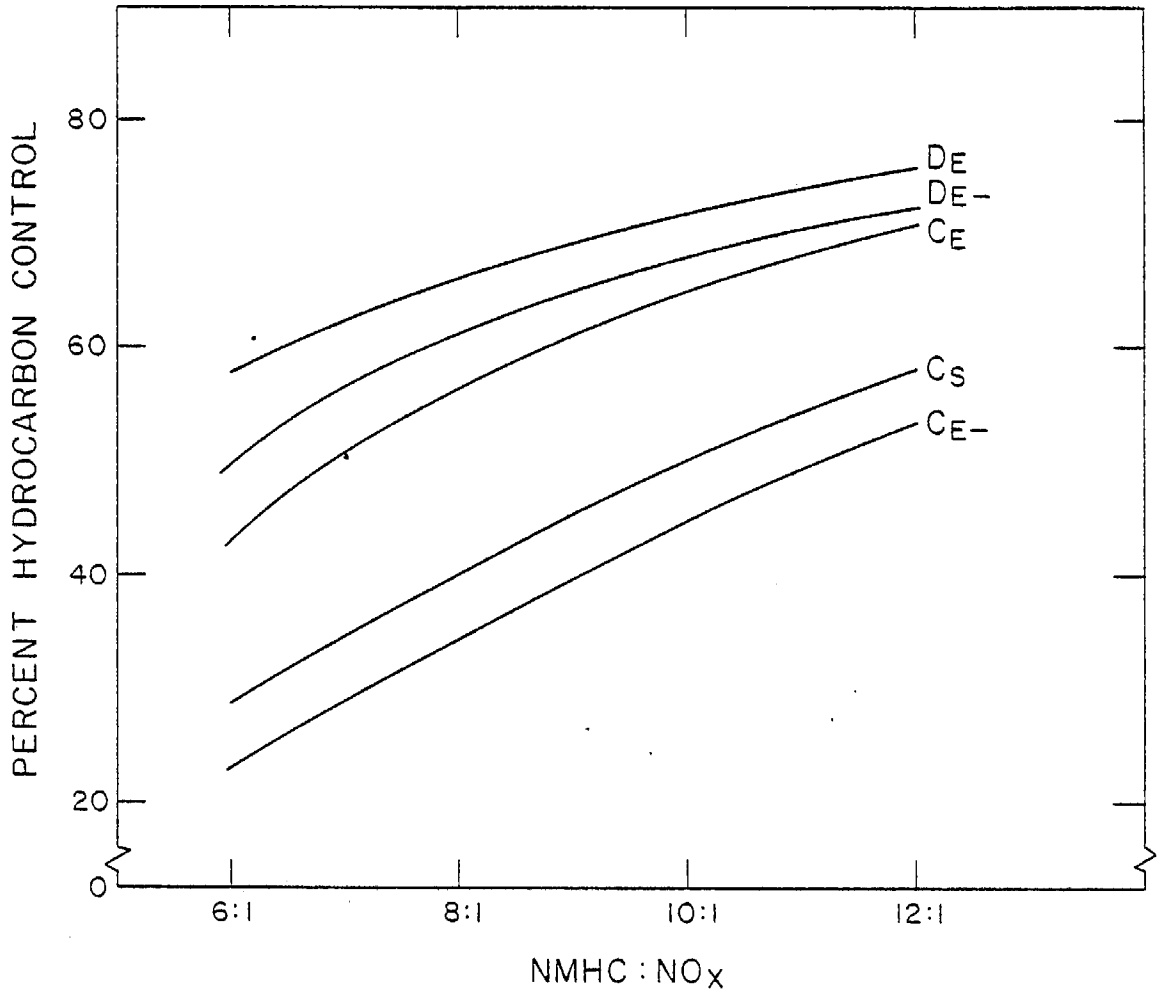

Figure 5. Percent Hydrocarbon Control Required to Reduce Ambient O_3 from 0.3 ppm to the Federal Air Quality Standard of 0.12 ppm as a Function of Initial NMHC/NO_x Ratios Derived from EKMA Isopleth Analysis. Calculations for Mechanisms C and D and the EPA Hydrocarbon Mixture With and Without Aldehydes (C_E, C_{E-}, D_E, D_{E-}, respectively) and for Mechanism C and the Propene-Butane-Aldehyde Representation of the SAPRC Surrogate Hydrocarbon Mixture (C_S).

C_{E-} and C_S, assuming the estimated initial NMHC/NO_x ratio of 12:1, are shown in Figure 6 and compared with the historic oxidant trend data.

It can be seen that the predicted oxidant trends, like the predicted hydrocarbon requirements, are affected by the kinetic mechanism and the hydrocarbon mixture used to calculate the isopleths. Predictions of mechanisms C and D are similar if the standard EPA hydrocarbon mixture (E) is used but are dramatically different if aldehydes are removed from the mixture (E-). Again the predictions using mechanism C are more sensitive to the hydrocarbon mixture than mechanism D and the aldehyde content of the mixture appears to be more important in affecting the results than total OH reactivity.

The sources of discrepancies between predictions derived from mechanism D and mechanism C were examined with respect to six different factors involving rate constants and mechanistic aspects which are given in detail in Section III. The discrepancies were examined by changing each of the six specific aspects of mechanism C to resemble mechanism D. It was determined that the major source of discrepancy concerns radical initiation or termination, which results from making different assumptions during model validation about unknown chamber radical sources.

In summary, the EKMA analyses based on isopleths calculated using our validated kinetic mechanism and hydrocarbon representation differ from analyses based on isopleths calculated using the EPA kinetic model currently used in EKMA analyses. These differences occur even though the isopleth analyses employed the "relative" technique recommended by the EPA and contrasts with the results of the sensitivity study by Dodge (1979a). Dodge also found that the NMHC/NO_x ratios assumed in the analyses are among the most important of the input data to effect EKMA predictions.

Our study confirmed that the NMHC/NO_x ratio is important; but in addition we found that the magnitude of differences in predictions derived by assuming different kinetic mechanisms or aldehyde content can approach the magnitude of the differences which occur by using the same model but changing the NMHC/NO_x ratio by a factor of 2. Therefore in terms of their impact on EKMA model predictions, uncertainties in the kinetic mechanism and the aldehyde content of the hydrocarbon can be of equal or perhaps even greater importance than uncertainties in the NMHC/NO_x ratio.

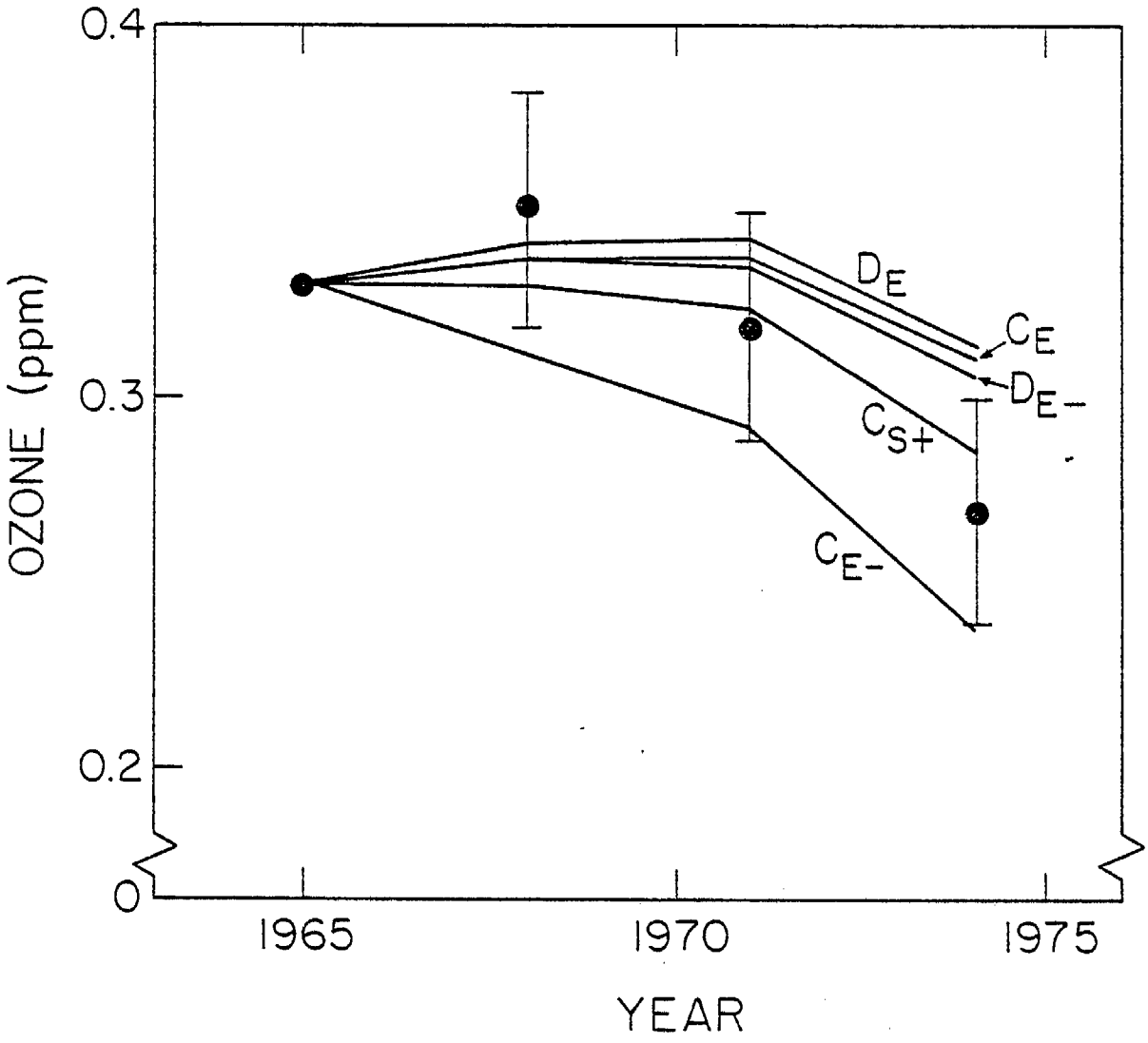

Figure 6. Oxidant Trends for the 95th Percentile of the Daily Maximum at Azusa: • = Observed, (error bars indicate measurement uncertainty); —— = Predicted from EKMA Isopleth Analysis. Calculations for Mechanisms C and D and the EPA Hydrocarbon Mixture With and Without Aldehydes (C_E, C_{E-}, D_E, D_{E-}, respectively) and for Mechanism C and the Propene-Butane-Aldehyde Representation of the SAPRC Surrogate Hydrocarbon Mixture (C_S).

C. The Role of Aromatic Hydrocarbons in Polluted Urban Atmospheres: Development and Validation of Mechanisms of Photooxidation (Section IV)

Aromatic hydrocarbons are recognized to be an important constituent of anthropogenic emissions in polluted urban atmospheres (Lonneman et al., 1974). In order to develop chemical kinetic computer models of photochemical air pollution as an integral part of urban airshed models used in the formulation of emission control strategies, the chemistry involved in the photooxidation of these aromatic hydrocarbons under atmospheric conditions must be reasonably well understood (Finlayson-Pitts and Pitts, 1977). As a first step, such computer kinetic models must, as far as possible, be validated against accurate smog chamber data.

We report here the development of a detailed chemical mechanism for the photooxidation of toluene, and of its major oxidation products benzaldehyde and o-cresol, in NO_x-air systems. The mechanism, which can be generalized to apply to other aromatics, was derived from an experimental and modeling study of irradiated toluene-NO_x-air, toluene-benzaldehyde-NO_x-air and cresol-NO_x-air mixtures at ppm concentrations. These mixtures were irradiated at 303 $\pm$ 1 K in the SAPRC 5800-liter Teflon-lined evacuable environmental chamber and temperature, humidity, light intensity, spectral distribution, and the concentrations of O_3, NO, NO_2, toluene, PAN, formaldehyde, benzaldehyde, o-cresol, m-nitrotoluene and methyl nitrate were monitored as a function of time.

Ten toluene-NO_x-air smog chamber irradiations were performed using a variety of initial reactant concentrations and the results were compared with those of two toluene-benzaldehyde-NO_x-air irradiations and one each o-, m-, and p-cresol-NO_x-air irradiations. The organic product yields in the cresol runs were very low, cresol being much less reactive in terms of O_3 formation and NO to NO_2 conversion rates than toluene, with the relative reactivity of the cresol isomers being the order meta >> ortho > para. The addition of benzaldehyde to toluene-NO_x-air mixtures also decreased the reactivity, in agreement with previous studies.

Calculations were carried out to examine the effect of alternative mechanistic pathways on model predictions for toluene- and o-cresol-NO_x-air systems. The various mechanistic options concerned (a) the reactions of the species formed by the addition of hydroxyl radicals and then O_2 to

the aromatic ring, (b) the reactions of the predicted conjugated γ-dicarbonyl products, (c) the relative importance of the chain-terminating formation of organic nitrates from the RO_2 + NO reaction, (d) the photolysis of benzaldehyde, and (e) the reaction of o-cresol with NO_3 radicals. The alternative mechanistic pathways are discussed in detail in Section IV.

As illustrated in Figure 7, fits of the calculations to most of the experimental concentration-time profiles could be obtained to within the experimental uncertainty for two of the mechanistic options considered. In both cases it is assumed that (a) O_2 adds to the OH-toluene adduct ~75% of the time, forming, after a further addition of O_2, a C_7 bicyclic peroxy radical, and (b) that this C_7 bicyclic peroxy radical reacts with NO ~75% of the time to ultimately form α-dicarbonyls and conjugated γ-dicarbonyls (e.g., methylglyoxal + 2-butene-1,4-dial) and ~25% of the time to form organic nitrates.

These chemical kinetic models predict the formation of products and reactive intermediates in aromatic-NO_x-air photooxidations which have not yet been detected in such systems, and whose atmospheric chemistry is at best poorly characterized, such as glyoxal, methylglyoxal, etc. The major uncertainties in the mechanisms concern (a) the structure of the bicyclic peroxy intermediate and (b) the γ-dicarbonyl photooxidation mechanism. Good fits to the o-cresol concentration-time profiles in the toluene-NO_x runs are obtained if it is assumed that o-cresol reacts rapidly with NO_3 radicals. However, the model underpredicts nitrotoluene yields by a factor of ~10. Further experimental work will be required to adequately validate the assumptions incorporated in the aromatic photooxidation mechanisms presented in this study.

D. Investigation of the Effect of Temperature on Photochemical Smog Formation (Section V)

Temperature is an important factor in affecting the formation of photochemical smog, but quantitative information concerning its effect has been limited. In order to satisfy the need for well-characterized smog chamber data suitable for the validation of models of the effect of temperature on photochemical smog formation, a series of variable-temperature chamber experiments have been performed employing the SAPRC evacuable chamber-

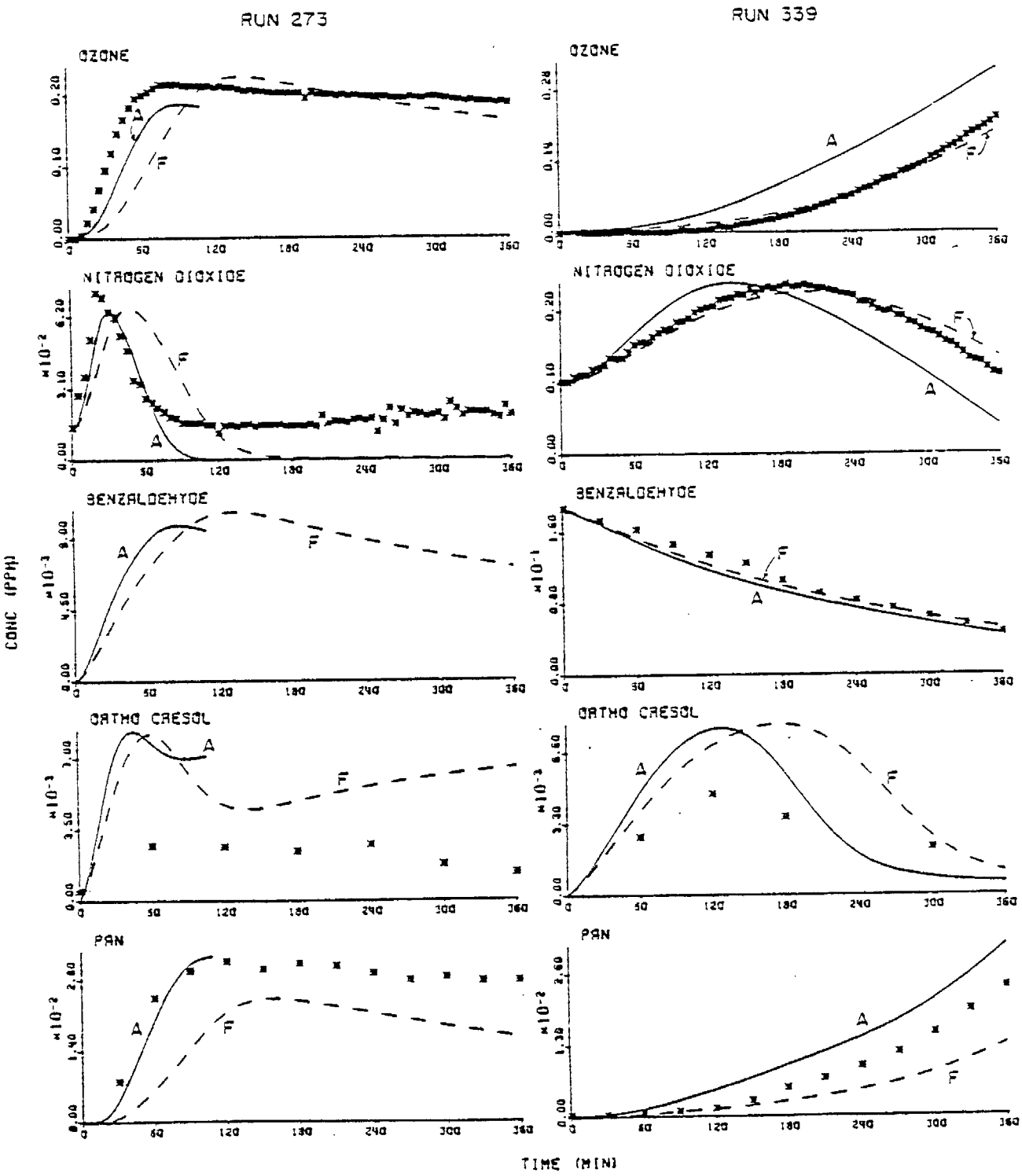

Figure 7. Experimental and Calculated Concentration-Time Profiles for Selected Reactants and Products in Toluene-NO_x Run EC-273 and in Toluene-Benzaldehyde-NO_x Run EC-339.
* = Experimental Data; ——, --- = Calculated.

solar simulator facility. Efforts have been made to insure that these experiments are well characterized, with experimental variables unrelated to temperature effects, such as light intensity, spectral distribution, reactant injections, moisture content, etc., held constant. The results of these experiments are reported here.

The experiments consisted of examination of both surrogate hydrocarbon-NO_x-air mixtures and, for control purposes, alkane-NO_x-air mixtures at a variety of initial hydrocarbon and NO_x levels and at average temperatures of 8°C, 30°C, and 51°C. The surrogate hydrocarbon mixture consisted of a number of representative alkanes, olefins, aromatics, alkenes, and oxygenates designed to represent the ambient air pollutant burden in the South Coast Air Basin (Pitts et al., 1976a). The alkane system consisted of equal amounts of n-butane and neopentane, and was chosen for control purposes because its chemistry was reasonably well understood; it has also been shown to be sensitive to chamber effects.

Detailed tabulations of the results of these experiments, suitable for model validation, are given in Appendix D of this report. Since the primary purpose of this study is to provide data suitable for model validation, a full discussion of the implications of the results of this study must await the results of model calculations simulating these runs. However, several observations can be made without the benefit of such calculations. For example, Tables 2 and 3 show the six-hour ozone yields and the estimated average hydroxyl radical (OH) levels for the surrogate hydrocarbon-NO_x-air and the alkane-NO_x-air runs, respectively. It can be seen that as the temperature increases, both the ozone yields and the OH levels increase significantly, with the OH levels increasing by factors of 3 to 4 as the temperature is increased from 8°C to 50°C for both types of runs.

From a mechanistic standpoint, the increase of radical levels with temperature is probably the most fundamental result, since the increased ozone yields and most of the other major temperature effects can ultimately be attributed to dependence of radical levels on temperature.

The increase in OH radical levels with temperature could be due to increasing rates of radical initiation reactions, or to decreasing rates of radical termination processes, or to a combination of both. Prior to the

Table 2. Six-Hour Ozone and Estimated Hydroxyl Levels Observed in Surrogate-NO_x-Air Evacuable Chamber Experiments

Nominal Initial Concentrations[a]		T = 8°C			T = 30°C			T = 51°C		
NMHC (ppmC)	NO_x (ppm)	Run No.	6-hr O_3 (ppm)	Est. [OH][b] (molec cm^{-3})	Run No.	6-hr O_3 (ppm)	Est. [OH][b] (molec cm^{-3})	Run No.	6-hr O_3 (ppm)	Est. [OH][b] (molec cm^{-3})
0.45	0.05	382	0.068	4.4×10^6				381	0.237	1.3×10^7
0.45	0.1	368	0.039	2.3×10^6				367	0.237	9.5×10^6
0.7	0.1	365	0.056	3.1×10^6	362	0.176	5.8×10^6	366	0.327	1.2×10^7
					387	0.167	5.6×10^6			
2.2	0.05	371	0.085[c]	3.1×10^6				372	0.359	6.0×10^6
2.2	0.1	379	0.176[c]	1.4×10^6				380	0.477	7.8×10^6
2.2	0.3	375	0.044	2.1×10^6				376	0.576	7.6×10^6

[a]Concentrations given are desired initial concentrations. Actual initial concentrations may be slightly different.

[b]Calculated from the relative decay rates of n-butane and 2,3-dimethylbutane using k(OH + n-butane) = 2.8×10^{-12} cm^3 $molecule^{-1}$ sec^{-1} and k(OH + 2,3-DMB) = 5.7×10^{-12} cm^3 $molecule^{-1}$ sec^{-1}.

[c]Maximum O_3 observed prior to 6 hours.

Table 3. Six-Hour Ozone and Estimated Hydroxyl Levels Observed in Alkane-NO_x-Air Evacuable Chamber Experiments

Nominal Initial Concentrations[a]		T = 8°C			T = 30°C			T = 51°C		
Alkane (ppm)[b]	NO_x (ppm)	Run No.	6-hr O_3 (ppm)	Est. [OH][c] (molec cm^{-3})	Run No.	6-hr O_3 (ppm)	Est. [OH][c] (molec cm^{-3})	Run No.	6-hr O_3 (ppm)	Est. [OH][c] (molec cm^{-3})
3	0.05	383	0.098	7×10^5				384	0.391	1.8×10^6
3	0.2	369	0.042	6×10^5	363	>0.076[d]	1.1×10^6	370	0.696	3.0×10^6
					386	0.196	1.3×10^6			
3	0.5	373	0.010	5×10^5				374	0.332	2.0×10^6
6	0.5	360	0.027	6×10^5				361	0.989	2.3×10^6

[a]Concentrations given are initial concentrations desired. Actual initial concentrations may be slightly different.

[b]Given as concentration of neopentane + n-butane (ppm). Equal quantities of each used.

[c]Calculated from the relative decay rates of n-butane and neopentane using $k(OH + \text{n-butane}) = 2.8 \times 10^{-12}$ cm^3 $molecule^{-1}$ sec^{-1}, and $k(OH + \text{neopentane}) = 8.7 \times 10^{-13}$ cm^3 $molecule^{-1}$ sec^{-1}.

[d]4-hour value. Compare with 4-hour O_3 value of 0.098 ppm for EC-386.

consumption of NO_x, the major termination reactions are organic radical + NO_2 reactions forming nitrates or peroxynitrates. In the alkane system the major known radical initiation processes are ozone and aldehyde photolysis. In the surrogate system, reactions of ozone with olefins and photolysis of the α-dicarbonyls will also contribute to initiation and the higher radical levels observed in surrogate runs can be rationalized on the basis of these reactions. Although the OH radical levels in the surrogate runs are on the average over four times higher than those of alkane runs at the same temperature, the fact that the relative increase in OH concentration with an increase in temperature from $8^{o}C$ to $50^{o}C$ is the same in both systems suggests that the cause of this strong influence of temperature on radical levels may result from some aspect of the mechanism common to both systems.

In the alkane-NO_x system, where the major organic photooxidation products can be monitored, it is possible to estimate the total extent of initiation or termination from the known processes. The result of such analysis indicates that at all three temperatures the total amount of termination is significantly greater than the total amount of initiation from known processes, with the discrepancy increasing strongly with temperature. Since initiation and termination must balance, there is an unknown radical source which becomes greater with increasing temperature.

The existence of unknown radical sources in smog chamber systems is now generally recognized, and it represents a serious problem in modeling such systems. It is frequently attributed to photolysis of HONO formed during the injection of NO_x through the interaction of NO and NO_2 with water vapor. Evidence obtained in our laboratory indicates that formation and photolysis of HONO may be minimal and that radical initiation is probably due to offgassing of some highly photoreactive contaminant from the chamber walls. It is reasonable to expect such offgassing to increase with increasing temperature. Additional evidence for this comes from the fact that at the higher temperature, there are indications that the total concentration of NO_x + HNO_3 actually increases during the runs.

As a result of this study we can conclude that there is a major effect of temperature on photochemical smog simulations in smog chamber systems, but current evidence suggests that most of this could be an artifact introduced by chamber effects. Until chamber effects relating to

radical initiation are more completely understood, it will not be possible to use smog chamber data to validate unambiguously photochemical models concerning temperature effects. More chamber characterization experiments are required, particularly those with more quantitative data concerning offgassing at higher temperatures. We are currently conducting additional chamber characterization and offgassing experiments aimed at elucidating this problem and thus increasing the utility of the experiments reported here.

E. Studies of the Relationships Between Ambient Ammonia and Nitric Acid and Particulate Nitrate: Implications for Nitrate Artifact Formation (Section VI)

The need to reliably establish ambient levels of ammonium nitrate particulates in ambient air and the evidence for "artifact effects" in sampling methods for particulate nitrate have led to recent interest in the roles that the precursors ammonia and nitric acid play in the formation of ammonium nitrate in the atmosphere and on filters. This study extends the previous analysis of Stelson et al. (1979) concerning the applicability of the equilibrium relationship in Equation 1 to the atmosphere:

$$NH_4NO_3(s) \rightarrow NH_3(g) + HNO_3(g) \qquad (1)$$

Simultaneous concentrations of NH_3 and HNO_3 in ambient air were measured in Riverside, California in 1977 using a kilometer pathlength FT-IR spectrometer. Data chosen for analysis from these measurements met two conditions: (1) NH_3 and HNO_3 concentrations exceeded the detection limits of 4 and 6 ppb, respectively; and (2) measurements were made during oxidant episodes ($O_3 \geq 100$ ppb). During selected episodes, 24-hr high-volume particulate samples were also collected on washed Gelman AE glass fiber filters and were subsequently analyzed for ammonium, nitrate, and sulfate ions.

Multiple linear regressions using the particulate data values for mass concentrations of NH_4^+, NO_3^-, and $SO_4^=$ ions suggest that the mixture consists of ammonium nitrate and two sulfates of ammonia. Data from the FT-IR measurements showed a small negative correlation between NH_3 and HNO_3

concentrations which indicates qualitatively that these concentrations are being affected by chemical reaction or an equilibrium relationship such as equation (1). The logarithm of the NH_3-HNO_3 concentration product has a significant positive correlation with temperature, as expected for the NH_4NO_3 equilibrium. The effect of temperature on the logarithmic concentration products at the low to moderate humidities of the experiments is well represented by a regression coefficient of about 0.2 deg^{-1}.

The means of the concentration product and temperature data and their least squares regression coefficients are given in Table 4 as changes in the free energy and enthalpy for reaction (1); the same quantities, as estimated from compilations of thermochemical data, are also given in Table 4 for comparison. The experimental data and thermodynamic calculations presented in this study support the hypothesis that gaseous ammonia and nitric acid are in equilibrium with solid ammonium nitrate in the atmosphere.

Table 4. Thermodynamic Data for the NH_4NO_3 Equilibrium at 306.6 K[a]

	Derived from Experimental Data[b]	Calculated from Thermodynamic Data[c]
Free-energy Change, kcal/mol	22.08 ($\pm$0.12)	21.78
Enthalpy Change, kcal/mol	30 ($\pm$12)	43.79

[a]Average of all temperatures in these experiments.

[b]The temperature and free-energy change are the means of the 54 observations. Enthalpy is calculated from the slope of the unweighted regression line. The uncertainties in parentheses are 95% confidence intervals.

[c]Calculated at 306.6 K from heat of formation data given by JANAF Tables (Stull and Prophet, 1971) and by Wagman et al. (1968) using gas heat capacities from Benson (1968) and solid heat capacities from Wagman et al. (1968). The small heat of transition contribution for NH_4NO_3 at 305.4 K was included (ΔH = 0.410 kcal/mol).

The ammonium nitrate equilibrium constant derived from tabulated thermochemical data is consistent with our atmospheric measurements of NH_3 and HNO_3 and is of direct utility in atmospheric models for calculating particlate nitrate concentrations. However, its implications for nitrate-sampling artifacts are unclear. Transfer of ammonium nitrate to and from a filter sample via the precursors is a complex mass transfer process, and its rate seems sensitive to surface conditions. Further investigation into nitrate sampling artifacts is needed.

II. PHOTOOXIDATION, REACTIVITY AND BIOLOGICAL STUDIES OF ETHANOL AND PROPANOL AMINES USED IN WATER-BASED PAINTS

Because of a recent ARB rule (ARB, 1978) aimed at further controlling solvent emissions in paint operations, interest has focused on the air pollution impact of increased use of water-based finishes. Such coatings contain significant quantitites of alcohol amines, and if their use is widely adopted by industry increased emissions of alcohol amines could result. In view of the high reactivity of simple amines in the atmosphere (Pitts et al., 1978) and their tendency to form toxic species such as nitrosamines and nitramines (Tuazon et al., 1978; Pitts et al., 1978), the possibility of increased use of the alcohol amines causing more environmental problems than use of the solvents they replace must be considered. Therefore, we have investigated the atmospheric reactivity and photooxidation products of representative alcohol amines.

Our studies have primarily focused on the most widely used alcohol amine in water-based finishes, N,N-dimethylaminoethanol (DMAE). Its structural isomer 2-amino-2-methyl-propanol (AMP) is used to a lesser extent, and limited studies were made of its atmospheric reactivity. The chemical formulas of these compounds are shown.

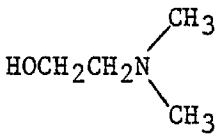

N,N-Dimethylaminoethanol

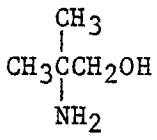

2-Amino-2-Methyl Propanol

In this report we describe (1) development of a quantitative chromatographic analysis technique for DMAE, AMP and other amines; (2) results of indoor and outdoor smog chamber irradiations of DMAE-NO_x-air mixtures and of the effects of added DMAE on surrogate hydrocarbon-NO_x-air irradiations in the dual outdoor chamber facility; (3) characterization of the major DMAE photooxidation products using gas chromatographic-mass spectrometry (GC-MS); (4) determination of the mutagenic activity of DMAE, AMP, and the gas and aerosol phase products of DMAE-NO_x-air irradiations using the Ames assay system; and (5) determination of the rate constants for the reaction of the hydroxyl radical (OH) with DMAE using both the flash photolysis resonance fluorescence (FPRF) and the smog chamber techniques, and of OH + AMP using FPRF.

A. Development of Chromatographic Analysis Techniques and Exploratory Indoor Chamber Experiments

Chromatographic Analysis. Determination of the best packing material for alcohol amines analysis was done using an HP5710A gas chromatograph (GC) equipped with a flame ionization detector and standard liquid injection features. Neat liquid injections enabled the determination of separation factors and retention times of the alcohol amines with a minimum of additional variables. Of the various columns tried, the FEP Teflon column packed with 4% Carbowax 20-M/0.8% KOH on Carbopack-B (C 20-M) used in our previous amine study (Pitts et al., 1978) gave the best separation and retention times at ~200°C for DMAE and AMP, and the C 20-M packing material was subsequently used in this study.

Determination was next made of the best method for gas sampling of the alcohol amines and their products, and for injecting them on the column. The analysis routine consisted of trapping the organics by pumping a known volume of the gas to be sampled through 5-in x 1/4-in o.d. Pyrex tubes silylated with dimethyldichlorosilane (DMCS) and packed with ~100 mg of Tenax GC (60/80 mesh). Initially, trapped materials were thermally desorbed onto the inlet side of a relatively cool (~100°C) column, which was then temperature programmed to ~200°C to elute the amines. At the time, this technique was thought to give better peak shape than desorption onto an isothermally operated column. It was found that 1/8-in o.d. FEP Teflon columns were unsuitable for temperature programming due to uncorrectable carrier gas flow rate variations caused by the flexibility of the Teflon at elevated temperatures. A 10-ft x 1/4-in x 2 mm i.d. glass column was decided upon as the logical second choice. This column was modified for Tenax cartridge injection by lengthening the inlet side 2 inches and inserting it through a drilled-out injection port of a Varian Aerograph Model 1400 gas chromatograph. The column was then silylated with DMCS and packed with the C 20-M column material.

Because of rapid baseline changes occurring during temperature programming, complicating quantification of the DMAE peak, it was desirable to operate the column isothermally. This required very rapid and uniform desorption of the sample off the Tenax cartridges to avoid unacceptable degeneration of peak shapes, separation factors and reproducibility. In

order to accomplish this desorption, a novel Tenax cartridge heater was designed and built. This heater consists of two 1-in x 1-in x 3.5-in brass blocks, each with an internal heating element, which can be instantaneously clamped around the Tenax cartridge after it is introduced into the carrier gas flow path. Using this technique, no carrier gas flows around the outside of the Tenax cartridge, dead volume is minimized, and isothermal operation at 175°C is achieved without noticeable degradation of peak shapes or resolution.

Initial gas samples taken were ~10 liters in volume, drawn at ~0.5 liter per minute by vacuum pump. However, there was significant amine breakthrough with 10 liter samples, so the sample size was reduced to <2 liters to hold breakthrough at less than 1.5%.

Chamber Injections. Trial introductions of DMAE into the SAPRC 6800-liter all glass chamber (AGC) were performed in order to determine whether DMAE can be quantitatively injected into the gas phase, and to calibrate the chromatographic analysis procedure described above. The AGC is shown in Figure 8, along with associated instrumentation. In addition, some injections were done using an ~5800-liter FEP Teflon bag located within the AGC (AGC-BAG), since the original intent was to use that as the reaction chamber for the indoor experimental runs. Prior to the injections, the AGC was flushed for several hours with air provided by the SAPRC air purification system (Doyle et al., 1977). The AGC-BAG was completely collapsed between experiments, and was filled with pure air immediately prior to the injections.

Introduction of the amine into the chamber was accomplished by depositing a known (weighed) amount of the compound on a 1/4-in x 3-in glass tube packed with Pyrex wool. This tube was then purged into the chamber with prepurified nitrogen and reweighed to determine the exact amount injected and to verify that the amine had indeed been introduced into the chamber. We have employed this technique successfully in performing gas-phase chamber calibrations for other difficult compounds, specifically aromatic photooxidation products. Despite the success we had in using this technique with other systems, we found that the chromatographic response (i.e., peak height or areas) for DMAE following chamber injections was variable and was always smaller than expected based on the

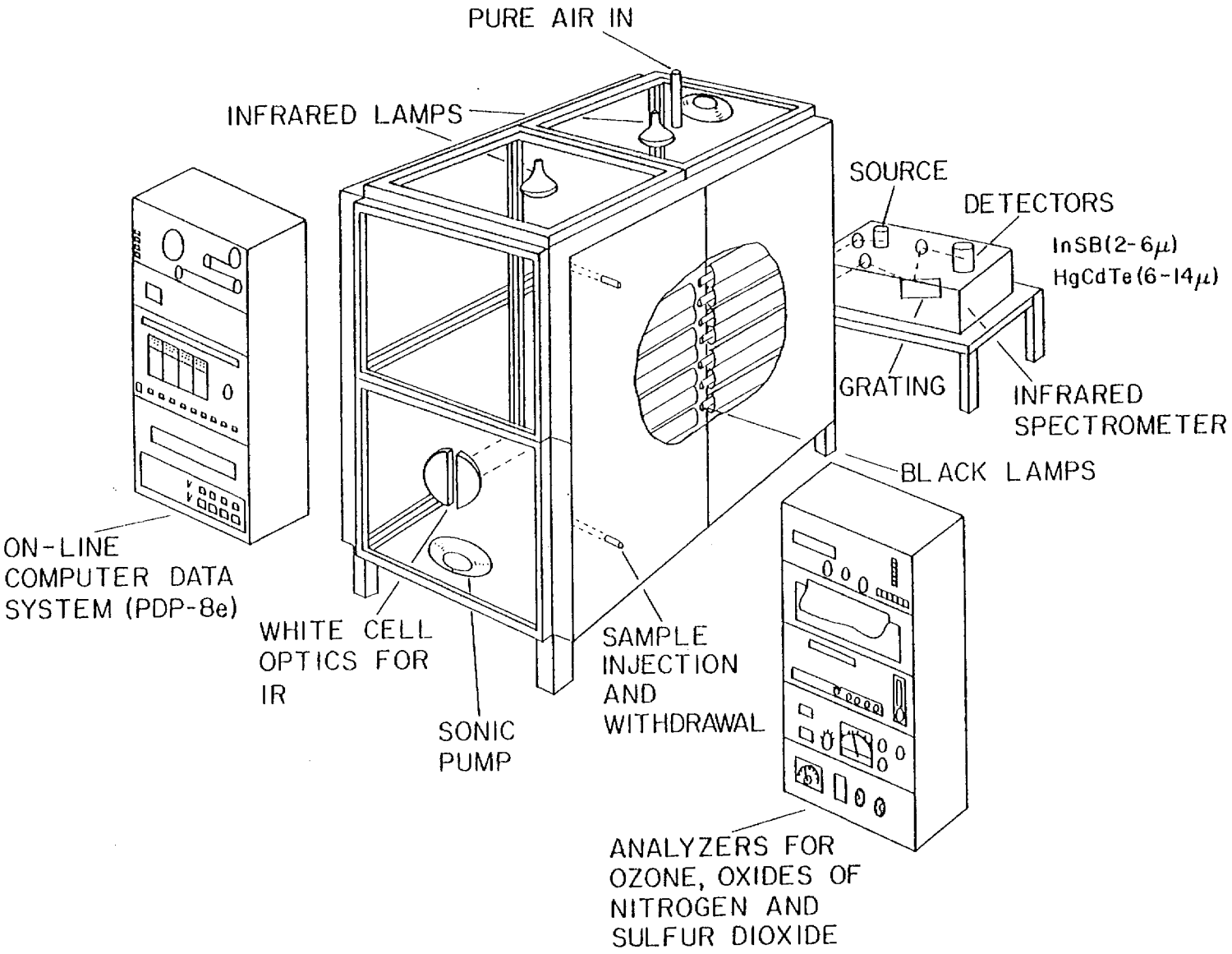

Figure 8. SAPRC All-Glass Chamber with Associated Analytical Data-Acquisition Systems.

amount injected and/or the results of "direct liquid" calibrations. The "direct liquid" calibrations consisted of placing known amounts of DMAE in methanol on the Tenax sampling cartridges, and then desorbing the sample onto the GC columns exactly as done when taking gas samples. The ratios of observed chromatographic responses relative to those expected for the DMAE injections into the AGC or the AGC-BAG are summarized in Table 5.

It can be seen from Table 5 that the results of the injections into the AGC were more consistent than those into the AGC-BAG. Even for the AGC injections the day-to-day variability of the injections (~±15%) was considerably greater than the sample-to-sample precision of our analysis (~±5%), or the uncertainties in the weighed amount of DMAE introduced (usually <1%). In addition, on one occasion (3/13) no response for DMAE was observed, though we have every reason to believe it was injected.

Despite the fact that the same DMAE introduction and sampling techniques were employed in both AGC and AGC-BAG runs, on only one occasion (3/20) did injection of DMAE into the AGC-BAG containing pure air give results comparable to those in the AGC. In the experiments of 3/22 and 3/23 considerably lower levels of DMAE were observed, though when the mixture in the chamber was allowed to sit for several hours without irradiation or addition of other reactants (3/23), the apparent gas phase DMAE levels increased, approaching levels characteristic of AGC injections, e.g. runs of 3/8, 3/12.

In attempts to determine whether these problems could be caused by irreversible absorption onto the Tenax traps, sampling cartridges with other packing materials were tried. Chromosorb 103 and the C 20-M column packing material gave the same results as Tenax, though in some cases extra peaks were observed on the chromatogram. The amount and ratios of gas sample passed through the traps, and the methods by which the sample volume was measured were also varied, but similar results were obtained. Therefore, we do not believe the analysis technique was the source of the problem, but that absorption onto the chamber walls was probably occurring.

Evidence for Dark Interactions Between DMAE and NO and NO_2. The results of some of the chamber injections shown in Table 5 suggest that the presence of NO_x tends to increase the discrepancy between the amounts of DMAE injected and the apparent gas phase concentrations. When DMAE was

Table 5. Ratio of Observed to Calculated[a] Chromatograhic Responses to N,N-Dimethylaminoethanol (DMAE) Injected into the All Glass Chamber (AGC) or into the FEP Teflon Bag Reactor (AGC-BAG)

Date (1979)	Reactor	Observed/Calculated[a] Response (%)	DMAE Injection (μℓ)	Conditions
2/27	AGC	61-82	24	Pure air
3/1	AGC	65	25	Pure air
3/6	AGC	64	21	Pure air
3/7	AGC	60	2	Pure air
		55	5	3 μℓ DMAE added
3/8	AGC	60	14	Pure air
3/9	AGC	62	26	Pure air
3/12	AGC	50	12	Pure air
3/13	AGC	~0	9	Pure air
		~0	19	~9 μℓ DMAE added
3/14*	AGC	47[b]	24[b]	24 μℓ DMAE added to previous day's mixture
3/19	AGC-BAG	2	5	NO = NO_2 = 0.5 ppm, HC's[c]
		1	10	Add 5 μℓ DMAE
3/20	AGC-BAG	71	25	Pure air
		47 → 62[d]	25	Add NO = NO_2 = 0.5 ppm, HC's
3/21*	AGC-BAG	5	5	NO = NO_2 = 0.1 ppm, HC's
		11	5	Pure air
3/22*	AGC-BAG	30-40	15	Add 10 μℓ DMAE, HC's
		14	15	Add NO = 0.9, NO_2 = 0.1 ppm
3/23	AGC-BAG	20 → 40[d] → 52[f]	15	Pure air
		40 → 50[d]	15	Add NO = ~1 ppm
		47 → 45[e]	15	Add NO_2 = ~1 ppm

[a]Calculated from the mass or the volume of DMAE injected, from the AGC or the estimated AGC-BAG volumes, and the "direct liquid" calibrations. The AGC-BAG volume was estimated at ~80% of the AGC volume.

[b]Does not count DMAE injection on previous day.

[c]HC's = Mixture of cis-2-butene, n-butane, neopentane, toluene and/or m-xylene.

[d]One hour after injection.

[e]15-30 minutes after injection.

[f]3 hours after injection.

*Irradiation experiment (all data given is prior to lights on).

injected into a NO_x-containing atmosphere, the DMAE measured ranged from 1-5% of the expected amount, while with injections into pure air it ranged from 11-71%. Furthermore, when NO and NO_2 were injected into the atmosphere containing DMAE, the DMAE concentrations were observed to decrease.

The data from the 3/23 dark run are perhaps the most useful in determining possible DMAE-NO_x dark reactions. After DMAE was introduced into the AGC-BAG filled with purified air, the initial gas phase DMAE concentration was 20% of the expected amount, but increased over 3 hours to almost the percentage obtained in AGC runs. Upon injection of ~1 ppm NO, the DMAE amount decreased temporarily, then returned to its pre-NOx-injection value within one-half hour. Such a temporary decrease could possibly be due to poor mixing following injection. Upon injection of ~1 ppm of NO_2 to this mixture, the DMAE again decreased, but this time it did not return to its initial value after one-half hour. In addition, in the C 20-M/KOH chromatographic samples taken following addition of NO_2, at least two peaks were observed which were either not present or much smaller in the DMAE-pure air or the DMAE-NO mixtures. The identities of the compounds causing these peaks have not been determined.

Exploratory DMAE-NO_x-Air Irradiations. Three indoor chamber irradiation experiments were done in which chromatographic samples were taken. These included one DMAE-NO_x-air run done in the AGC, and two DMAE-hydrocarbon-NO_x-air runs done in the AGC-BAG. In all runs, conversion of NO to NO_2 and growth of chromatographic peaks attributable to still unidentified products of DMAE photooxidation were observed. Upon irradiation, concentrations of products apparently formed from interaction of DMAE with NO_2 in the dark increased. No products formed in the dark were observed to decay upon irradiation. This would appear to be evidence against formation of nitrosoamines in the dark, since these are destroyed upon irradiation in other amine systems (Pitts et al., 1978).

As expected a number of products were formed in the light reactions which were not formed in the dark. At least three photooxidation products were observed on the C 20-M column, one of which was subsequently identified to be dimethylformamide on the basis of GC-MS analysis (see Section II-C) and injection of authentic samples. However, the identity of the

product formed in the largest yields based on its GC peak areas has not been determined.

The DMAE exhibited unexpected concentration-time profiles in the irradiation experiments and its behavior differed somewhat in the 3/21 run from that in the 3/14 or 3/22 runs. The results of the latter two were quite similar, despite the fact that one was done in the AGC and the other was done in the AGC-BAG. In both the 3/14 and 3/22 runs, the NO_x was injected after DMAE, and the DMAE concentration decreased prior to the irradiation. After the irradiation began, the DMAE concentration increased for the first 30 to 60 minutes and then declined exponentially with a half-life of less than 2 hours. This exponential decay is expected as a result of the photochemical reactions; if it is assumed that it is due primarily to the reaction of DMAE with OH, the decay rates can be used to determine the DMAE + OH rate constant, provided a reference compound is also present. The results of these and other OH rate constant determinations are given in Section II-E.

In the 3/21 run, in which the NO_x was added to the AGC-BAG before the DMAE, the observed DMAE concentration was never more than ~20% the expected value, even after the irradiation. Upon irradiation, the DMAE concentration increased slightly in the first hour, then decreased slowly, with a half life of $\gtrsim$ 10 hours. Thus it appears that the injected DMAE which did not appear initially in the gas phase was being offgased from the chamber walls during the course of the irradiation.

B. Outdoor Chamber Irradiations

Three types of outdoor chamber irradiation experiments were done: (1) DMAE-NO_x-air irradiations, to determine the atmospheric fate and reactivity of DMAE in the absence of other organic reactions; (2) surrogate hydrocarbon-NO_x-air mixture with and without DMAE in dual chamber irradiations, to determine the incremental effect of adding DMAE to existing atmospheric emissions; and (3) control surrogate hydrocarbon-NO_x-air dual chamber irradiations, to characterize the results of the DMAE-surrogate hydrocarbon runs. The experimental procedures employed and the results of the experiments are described below.

Experimental. All outdoor chamber experiments were performed using the SAPRC outdoor Teflon smog chamber facility which was designed for the

purpose of studying aerosol formation under a variety of conditions (Pitts and Grosjean, 1978). The outdoor chamber is constructed of 2 mil thick FEP Teflon sheets heat-sealed together using a double lap seam and externally reinforced with Mylar tape. A new Teflon bag reactor was constructed for the DMAE experiments using 9 panels each 25-ft x 58-in. The volume of the undivided bag when fully inflated was approximately 50 m^3. As shown in Figure 9, the reactor can be optionally operated in a dual mode configuration for the purpose of conducting parallel experiments under the same lighting and temperature conditions.

The reactor is supported by ropes running across a 25-ft x 20-ft cast iron pipe tubing frame held ~2-ft off the ground to allow air circulation under the chamber. No mechanical stirring device is used in our experiments since Wilson et al., (1971) showed that mechanical stirring dramatically inhibits aerosol formation in smog chambers. Wind action on the flexible chamber and the temperature gradient within the chamber are sufficient to ensure adequate mixing during an experiment. The chamber is held on the frame by a net connected to the frame by a system of ropes, and can be divided into two compartments by means of three 1.5-in diameter cast iron pipes running across the supports. Each compartment has an 8-in x 10-in port for introduction of pure air from the SAPRC air purification system (Doyle et al., 1977) and initial pollutants as well as for sampling during the experiment.

Gas and aerosol monitoring instruments are housed in an air conditioned monitoring facility immediately adjacent to the chamber, and are connected to the reactor through a Pyrex sampling manifold and a 5-m long, 15-mm i.d. Pyrex sampling line equipped with a switching valve. The pollutant transit time from the chamber compartments to the instruments is ~2 seconds.

During a typical run, the following parameters were monitored: NO, NO_2, NO_x, O_3, hydrocarbons, peroxyacetyl nitrate (PAN), condensation nuclei (CN), light scattering aerosol (b_{scat}), particle size distribution, relative humidity and temperature. Changes in solar radiation intensity and spectral distribution were measured using a EG&G integrating spectral radiometer. Table 6 lists the physical and chemical methods, instrumentation and range for each of the parameters measured. DMAE was monitored using the GC method described in Section II-A.

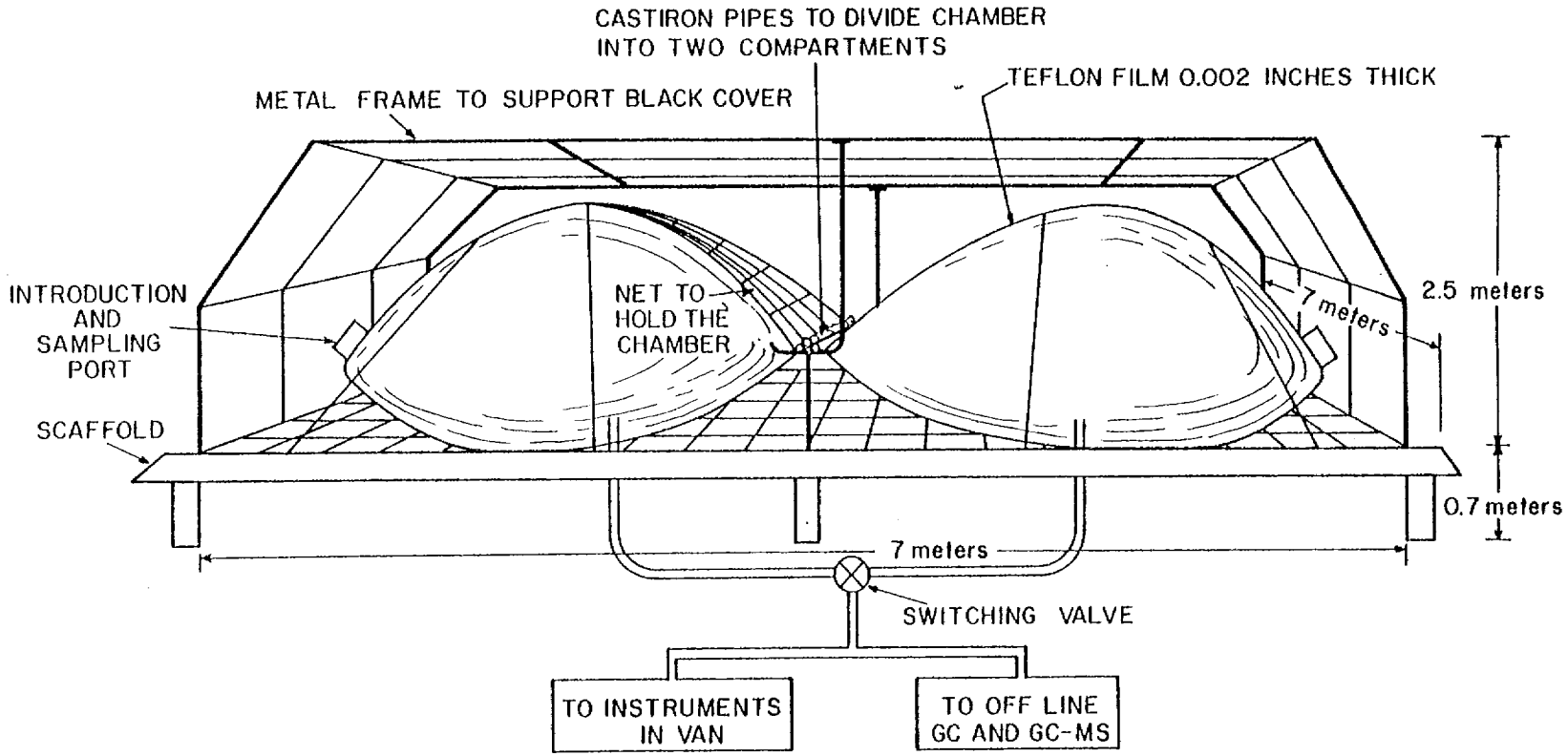

Figure 9. SAPRC Outdoor Teflon Chamber Shown in Dual Mode Configuration.

Table 6. Instrumentation for the Outdoor Teflon Chamber

Parameter Measured	Range	Instrument	Method
Aerosol light scattering coefficient (b_{scat})	0–10 x 10^{-4} m^{-1}	Nephelometer (MRI Model 1550)	Broad band photometry
O_3	0 - 1 ppm	Ozone Analyzer (Dasibi Model 1003 UV analyzer)	UV photometry
NO, NO_2	0 - 0.5 ppm	Nitrogen Oxides Analyzer (Bendix Model 5513802 chemiluminescent analyzer)	Chemiluminescence
Peroxyacetyl nitrate (PAN)	0 - 50 ppb	PAN-Analyzer (Varian gas chromatograph with electron capture detector)	Gas chromatography
Particle size distribution (0.0075 μm to 0.750 μm)		Electrical Mobility Analyzer (TSI Model 3030)	Electrical mobility
Particle size distribution (0.3 μm to 3.0 μm)		Optical Particle Counter (Climet)	Optical scattering
Condensation nuclei		Condensation Nuclei Counter (Environment One Model Rich 100)	Photometry
Light intensity		Eppley UV Radiometer	Photometry

During the reactant and injection procedure and prior to the beginning of the irradiation, the reactor was kept darkened by a black opaque cover supported by the top and sides of the metal frame over the reactor. With the exception of the DMAE, which was introduced as described in Section II-A, all reactants were injected via syringe injections into a flask followed by a nitrogen flush into the bag port. In all cases, the bag was mixed thoroughly after reagent introduction to minimize the reaction of the species of localized high concentrations. The irradiations were initiated by removal of the opaque cover.

Samples were taken in some experiments for GC-MS analysis and for mutagenic testing before and after irradiation. GC-MS samples were taken by passing ~5 liters through Tenax absorption tubes at ~0.5 liter min^{-1}. Gas phase samples for mutagenic testing were taken using two methods. One method involved pumping a large quantity of sample through a freeze-out trap covered by liquid nitrogen; the other involved passing a 50 liter sample through a large absorption tube packed with 10 gm of Tenax.

At the end of the irradiation, if significant quantities of aerosol were produced, the entire contents of the reactor was pumped through a high volume sampler containing a Pallflex quartz filter for aerosol entrapment. The organic contents of the filters were extracted with methanol, which was evaporated off after dividing the sample into two parts. One part was redissolved in dichloromethane for GC-MS analysis; the other part was redissolved in dimethylsulfoxide for mutagenic testing. The techniques employed and results obtained in the GC-MS analyses and mutagenic tests are described in Sections II-C and D, respectively.

DMAE-NO_x-Air Runs. Two irradiations were done using DMAE and NO_x in the undivided bag without other organic reactants. In both cases, DMAE was introduced ~2 hours prior to the injection of NO_x, which in turn was injected ~2 hours prior to uncovering the bag to begin irradiation. This protocol was chosen to observe the behavior of DMAE in the dark with and without NO_x, since exploratory indoor chamber experiments indicated that surface absorption effects and possible dark reactions might occur.

Figures 10 and 11 show the O_3, NO, NO_2 and DMAE concentration-time profiles for the two DMAE-NO_x-air irradiations. Figures 12 and 13

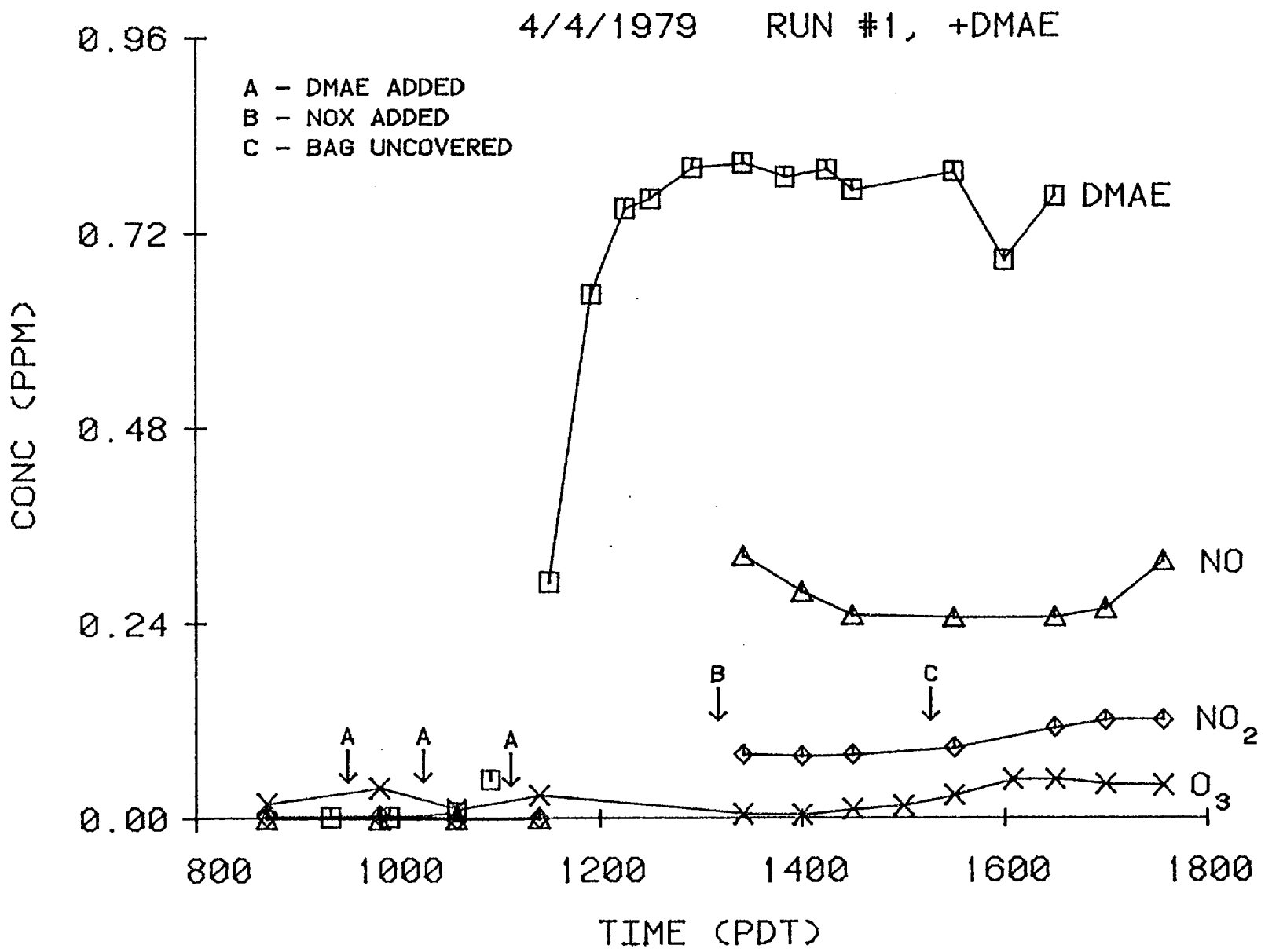

Figure 10. O_3, NO, NO_2 and DMAE Concentration-Time Profiles for Outdoor Bag DMAE-NO_x-Air Run #1.

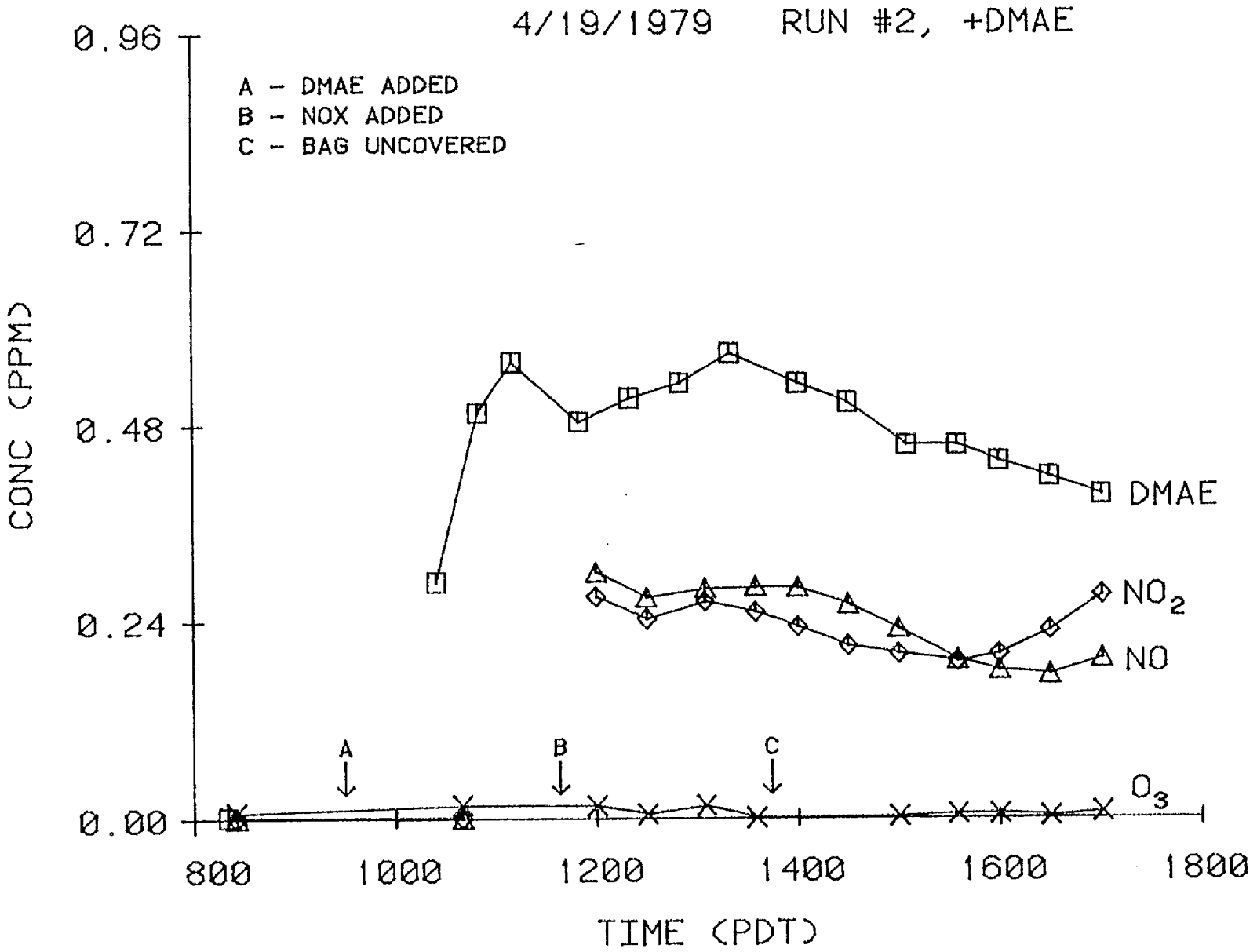

Figure 11. O_3, NO, NO_2 and DMAE Concentration-Time Profiles for Outdoor Bag DMAE-NO_x-Air Run #2.

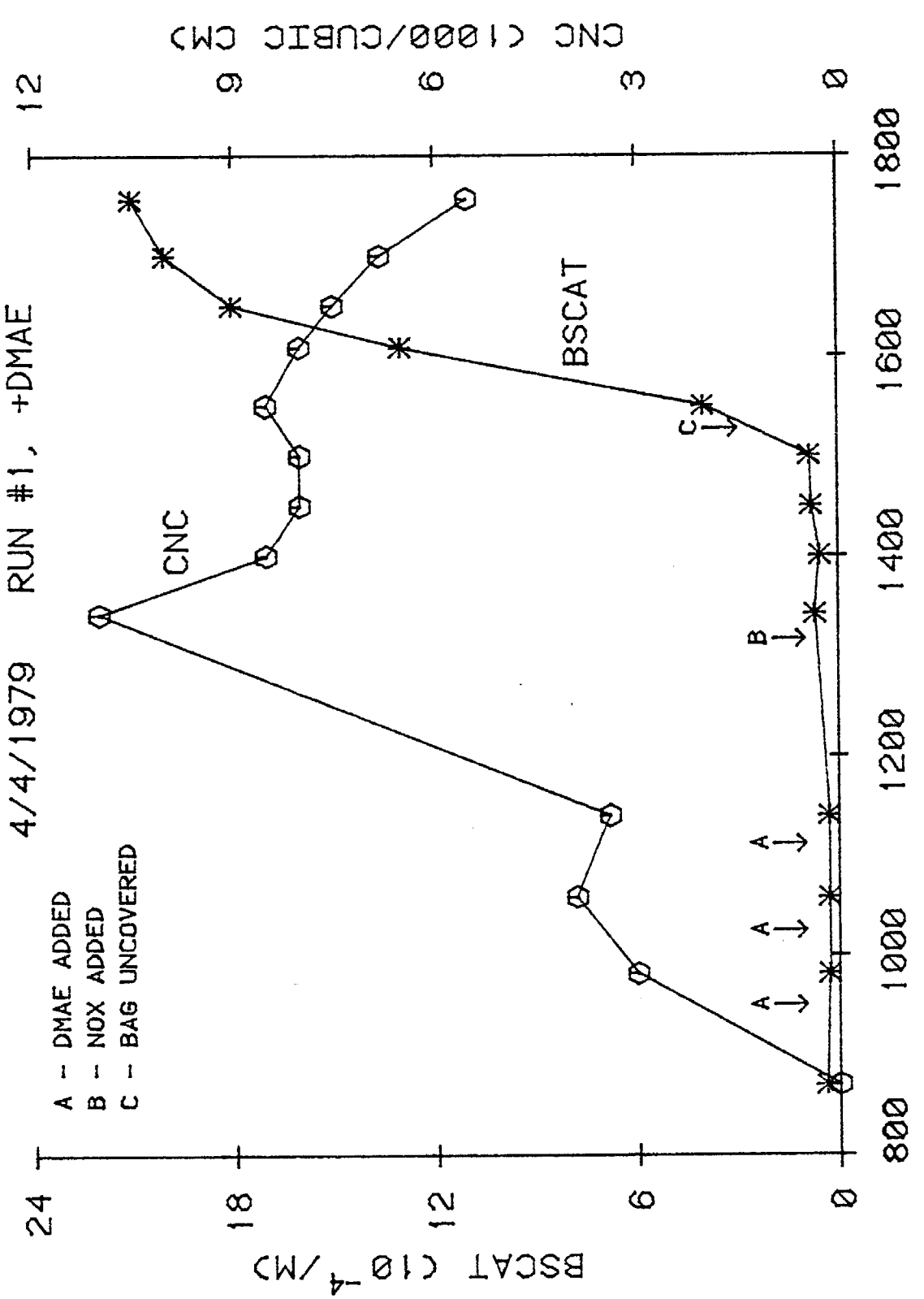

Figure 12. Concentration-Time Profiles for Condensation Nuclei and Light Scattering Aerosol (b_{scat}) for Outdoor Bag DMAE-NO_x-Air Run #1.

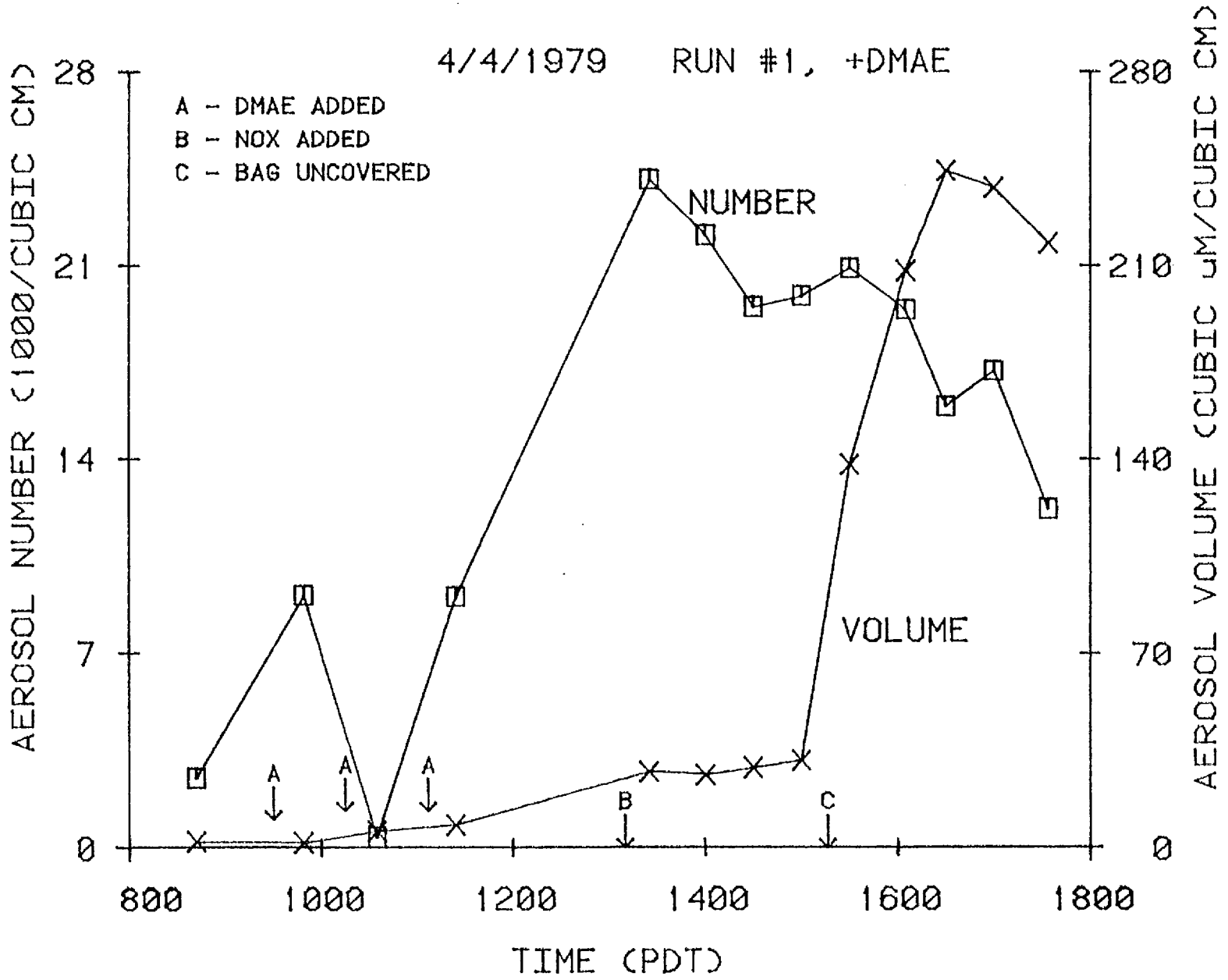

Figure 13. Concentration-Time Profiles for Aerosol Number and Volume for Outdoor Bag DMAE-NO_X-Air Run #1.

show the concentration-time profiles for condensation nuclei, light scattering aerosol (b_{scat}) and total aerosol number and volume for the first irradiation; the aerosol results in the second irradiation were similar. In both ~3-hr irradiations there was significant aerosol formation and relatively little NO_x reaction and O_3 formation. Detailed data tabulations for these runs are given in Appendix C1.

The DMAE concentration-time profiles suggest that absorption and offgasing of DMAE on the surfaces occurred in the outdoor bag runs, as was observed in most of the indoor AGC and AGC-BAG runs. In run #1, introduction of 200 μℓ DMAE (~ 1.0 ppm) was made three times. The extra introductions were made because unexpectedly low levels of gas phase DMAE were observed following the first introduction. Approximately 1 hr after the third introduction, the gas phase DMAE levels rose from ~10% the introduced amount to ~25%. A similarly delayed increase in DMAE concentrations was observed following DMAE introduction in run #2. The very slow rate of consumption of gas phase DMAE upon irradiation in run #1 indicates that offgasing of DMAE occurred, though this seems to be less important in run #2, where more rapid consumption of gas phase DMAE was observed. These varible results are consistent with the observations from the indoor chamber runs.

As in the indoor chamber runs, there is evidence for dark interactions between DMAE and NO_x. No significant increase in unknown products was observed in the dark chromatographic samples after NO_x injection (unlike the indoor runs), yet a dramatic increase in condensation nuclei and aerosol particle number occurred in the dark immediately upon NO_x injection. Smaller increases in total aerosol volume and b_{scat} also occurred.

Upon irradiation, aerosol volume and b_{scat} increased markedly (Figures 12, 13), indicating formation of aerosol material due to photochemical reactions. Those reactions did not result in significant formation of new particles, since the aerosol number and condensation nuclei were relatively unaffected by irradiation. Aerosol volume peaked and declined toward the end of irradiation, probably due to aerosol destruction on the walls, since the surface/volume ratio decreased throughout the run due to the collapse of the bag caused by sample withdrawal.

DMAE-Surrogate-NO_x-Air Dual Chamber Runs. Three dual chamber experiments were performed to determine the effect of added DMAE on a surrogate hydrocarbon-NO_x-air irradiation. One side of the dual chamber contained a surrogate hydrocarbon-NO_x-air mixture with 30 to 70 ppb added DMAE; the other contained the same surrogate and NO_x concentrations but no added DMAE. The composition of the surrogate hydrocarbon mixture, shown in Table 14, was designed to represent hydrocarbon emissions from all sources in the South Coast Air Basin and is based on the mixture previously used in SAPRC-ARB experiments (Pitts et al., 1975; 1976a; 1979a).

The experimental protocol employed in the dual chamber DMAE-surrogate runs was: surrogate hydrocarbon (~2 ppmC total) and NO_x (~0.3 ppm) were added to the undivided bag previously filled with pure air. The chamber was then divided, DMAE was introduced into one side, and the bag uncovered ~1 hour after DMAE addition.

DMAE introductions were made into side 1 for runs #3 and #4, and into side 2 for run #5, side 1 and side 2 referring to the chamber frame sides, hence to the spatial orientation of the chamber. The bag was rotated 180° in the chamber frame prior to run #5, therefore in all three runs the same half of the reactor bag was exposed to DMAE.

The results of the three DMAE-surrogate runs, which differed primarily in the amount of DMAE added, are given in Table 7. Figures 14 through 19 show the O_3, DMAE, NO and NO_2 concentration-time profiles for these runs. Figures 20 and 21 show measured aerosol parameters observed in the intermediate run, #5. Results of the aerosol measurements in the other two runs were similar, except for different maximum levels observed in the DMAE side (see Table 7). Detailed data tabulations for these runs are given in Appendix C2.

The results shown in Figures 14 through 19 indicate that DMAE addition to the surrogate hydrocarbon-NO_x mixture enhances O_3 formation and the rate of NO_2 consumption following its maximum, provided sufficient DMAE is added. Thus, the effect of DMAE on the inorganic concentration-time profiles is small at the low DMAE concentration, ~20 ppb (Figures 16, 17) but is significant for the higher DMAE concentration, ~80 ppb (Figures 14, 15). The enhancement in reactivity occurs primarily after NO is converted to NO_2, with NO_2 on the DMAE side being more rapidly consumed and larger

Table 7. Selected Results of DMAE-Surrogate Hydrocarbon-NO_x Dual Outdoor Bag Experiments

Run	DMAE #3		DMAE #4		DMAE #5	
Initial surrogate NMHC (ppmC)	2.4		2.1		2.1	
Initial NO_x (ppm)	0.19		0.26		0.23	
Photolysis duration (min.)	300		310		295	
Integrated UV (cal/cm^2)	0.90		0.91		1.10	
Side	1	2	1	2	2[a]	1
Injected DMAE (μl)	12.24	0	3.5	0	7.2	0
Injected DMAE (ppm)[b]	0.07	0	0.03	0	0.06	0
Observed maximum DMAE (ppm)	0.08	0	0.016	0	0.04	0
Maximum O_3 (ppm)	0.24	0.12	0.05	0.03	0.12	0.10
Maximum aerosol number ($particle/cm^3$)	9×10^4	2×10^3	5×10^5	3×10^3	1×10^5	2×10^3
Maximum aerosol volume (m^3/cm^3)	500	3	90	4	$\gtrsim 80$[c]	4

[a]Bag was rotated for this experiment. Side number refers to chamber frame sides, hence to spatial orientation. DMAE was added to side 1 for runs #3 and #4, and to side 2 for run #5.

[b]Calculated from volume of liquid DMAE injected and estimated volume of bag, assuming the density of DMAE = 0.89 g/cm^3.

[c]No data available after 54 minutes into the irradiation.

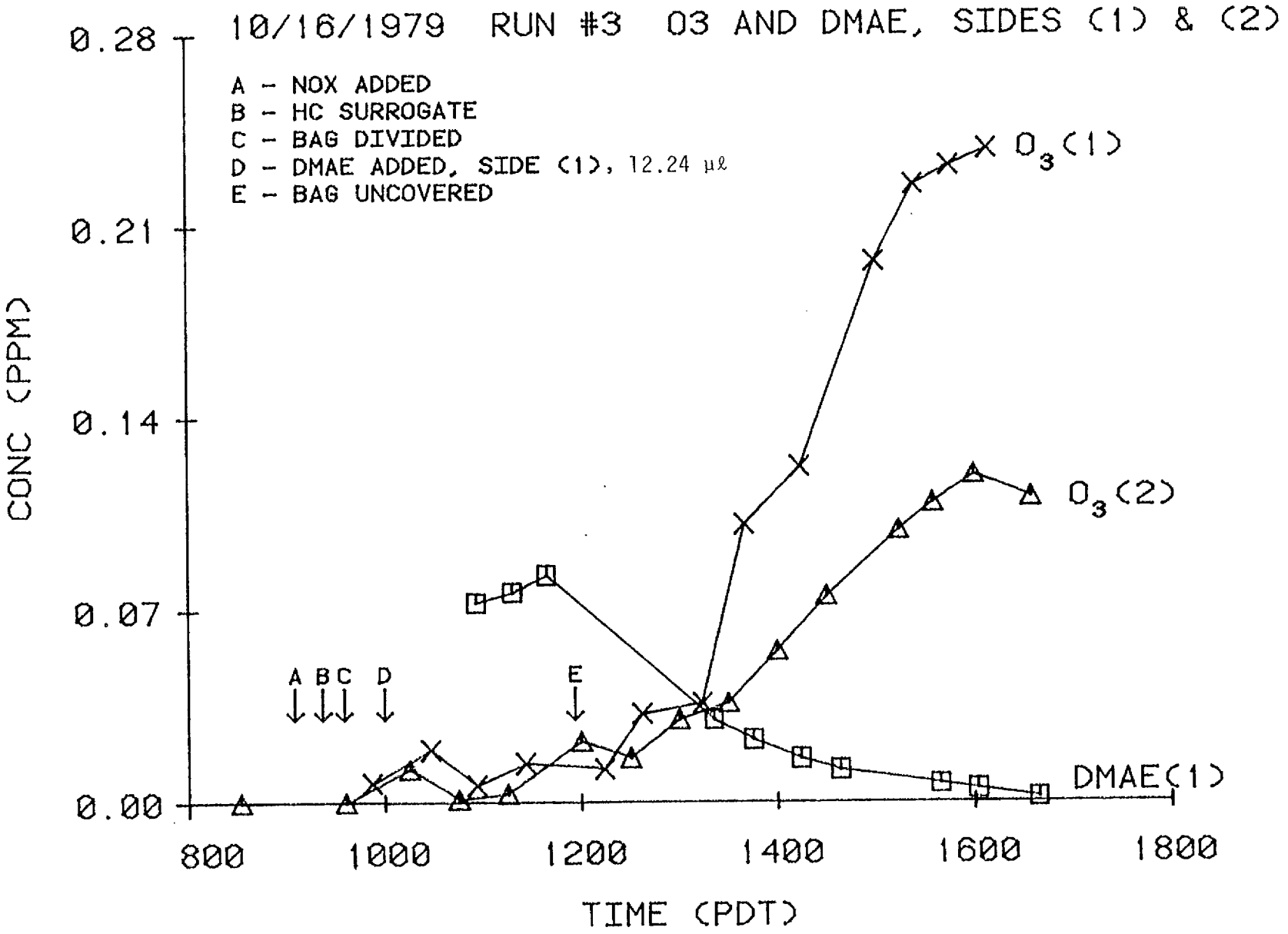

Figure 14. O_3 and DMAE Concentration-Time Profiles for Dual-Outdoor Bag DMAE-Surrogate-NO_x-Air Run #3.

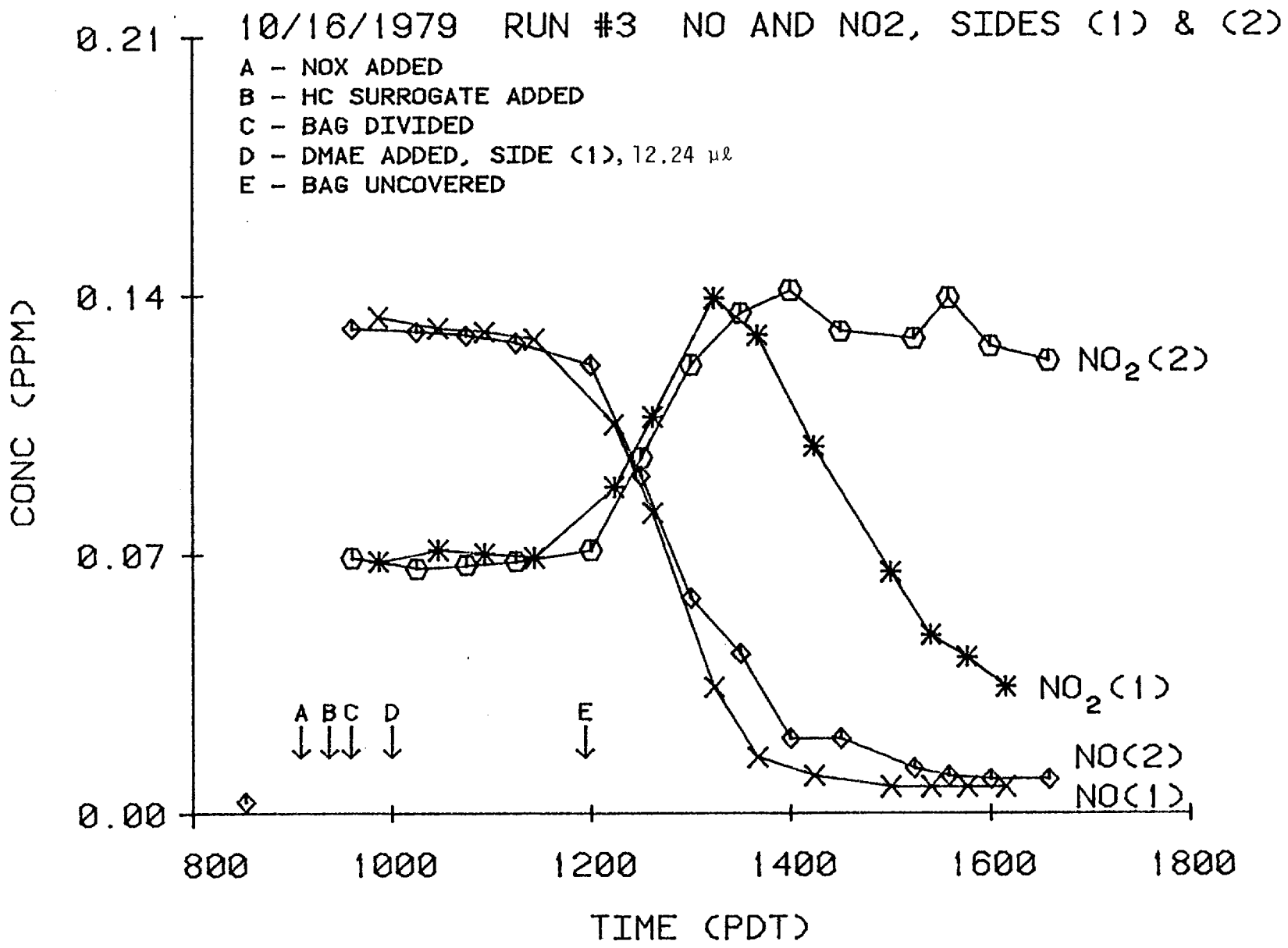

Figure 15. NO and NO_2 Concentration-Time Profiles for Dual-Outdoor Bag DMAE-Surrogate-NO_x-Air Run #3.

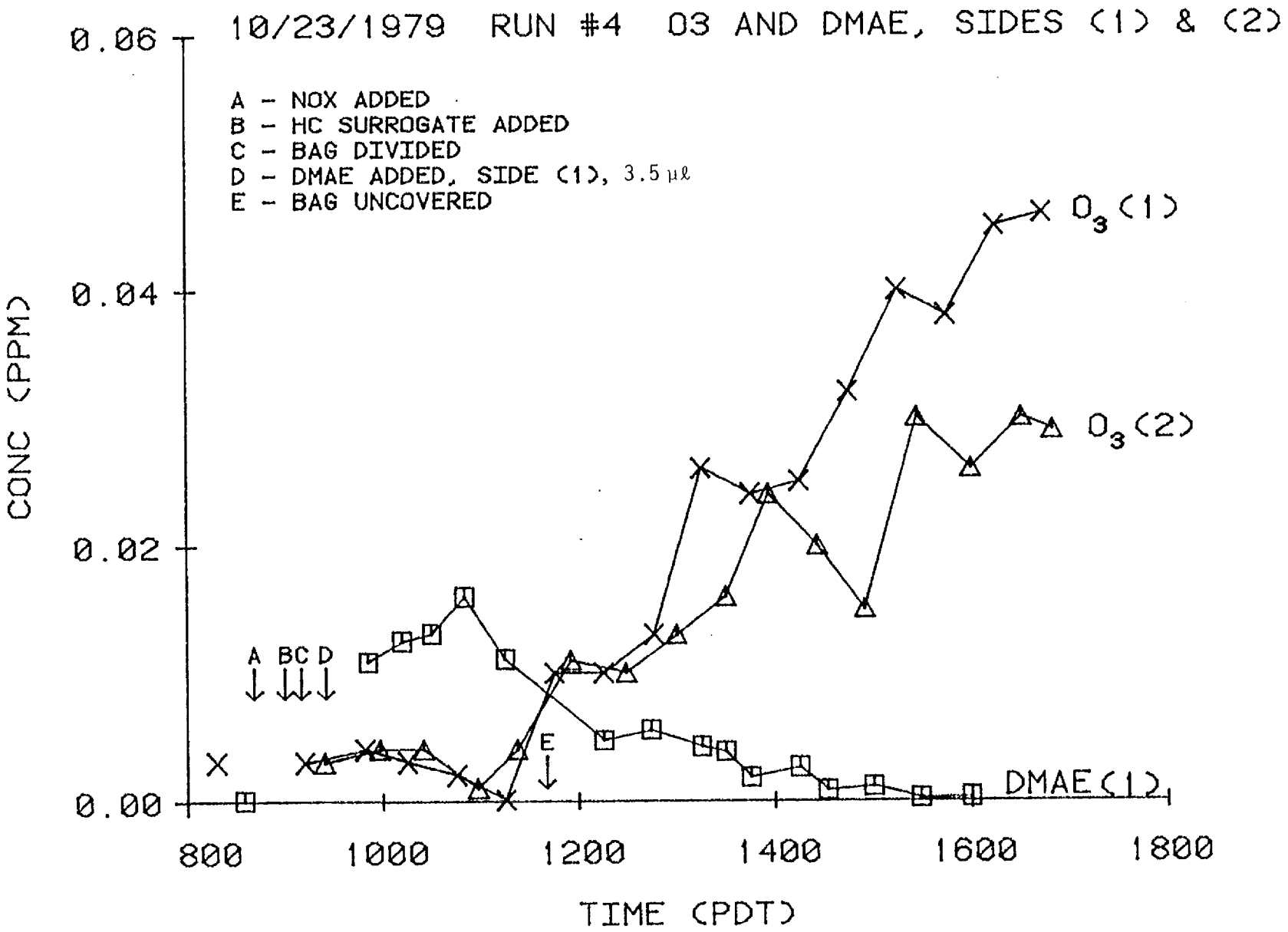

Figure 16. O_3 and DMAE Concentration-Time Profiles for Dual-Outdoor Bag DMAE-Surrogate-NO_x-Air Run #4.

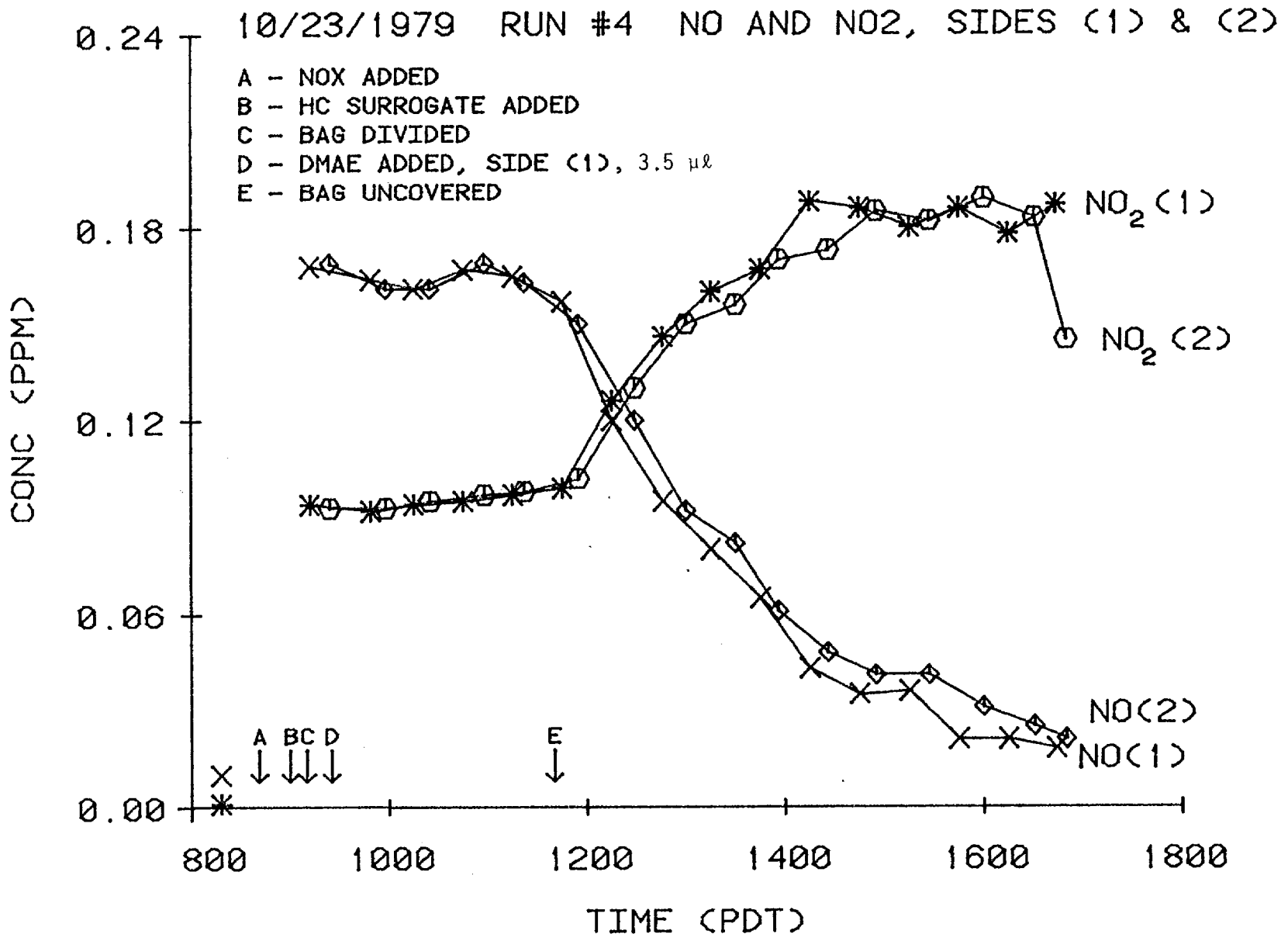

Figure 17. NO and NO_2 Concentration-Time Profiles for Dual-Outdoor Bag DMAE-Surrogate-NO_x-Air Run #4.

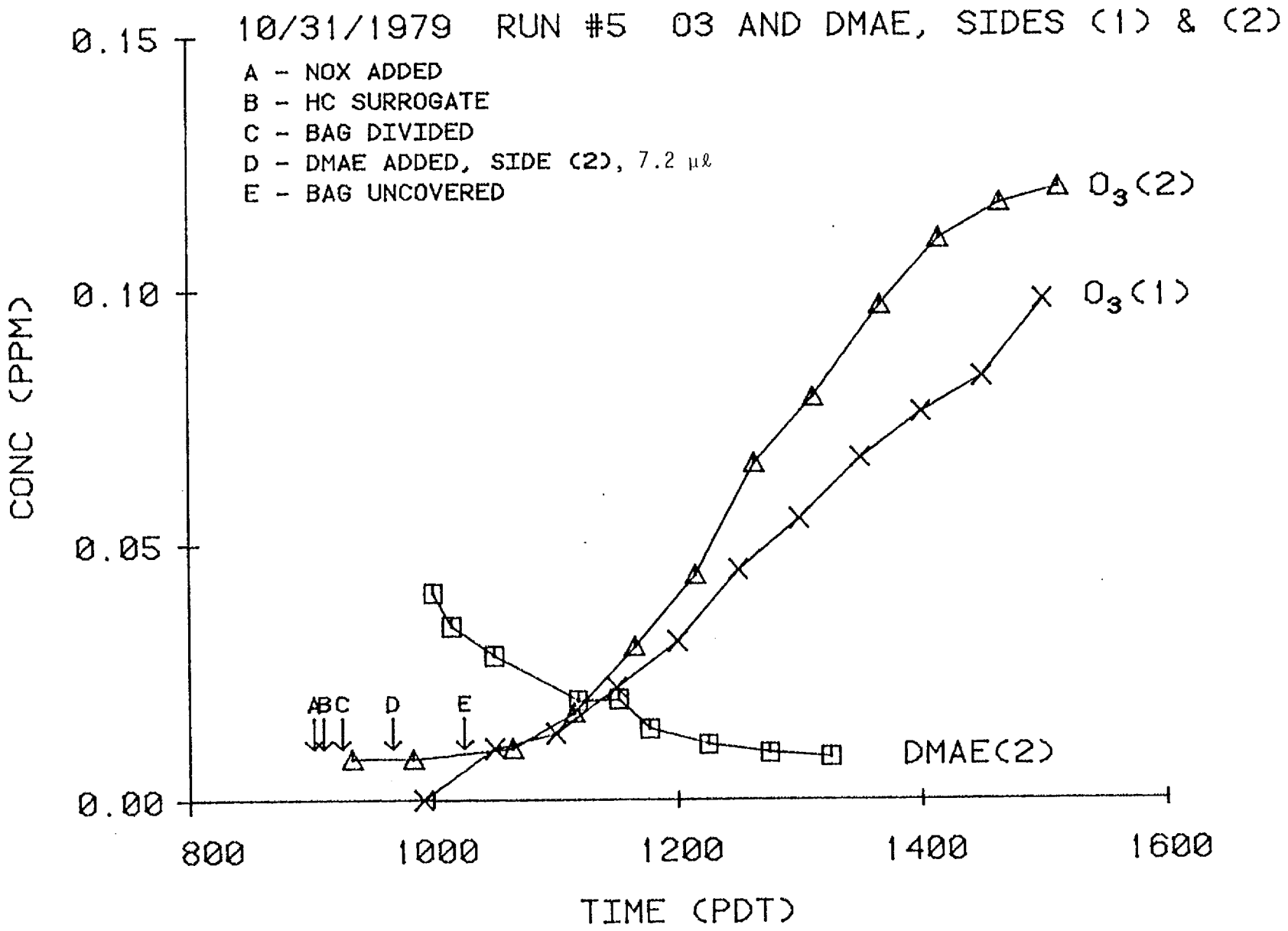

Figure 18. O_3 and DMAE Concentration-Time Profiles for Dual-Outdoor Bag DMAE-Surrogate-NO_x-Air Run #5.

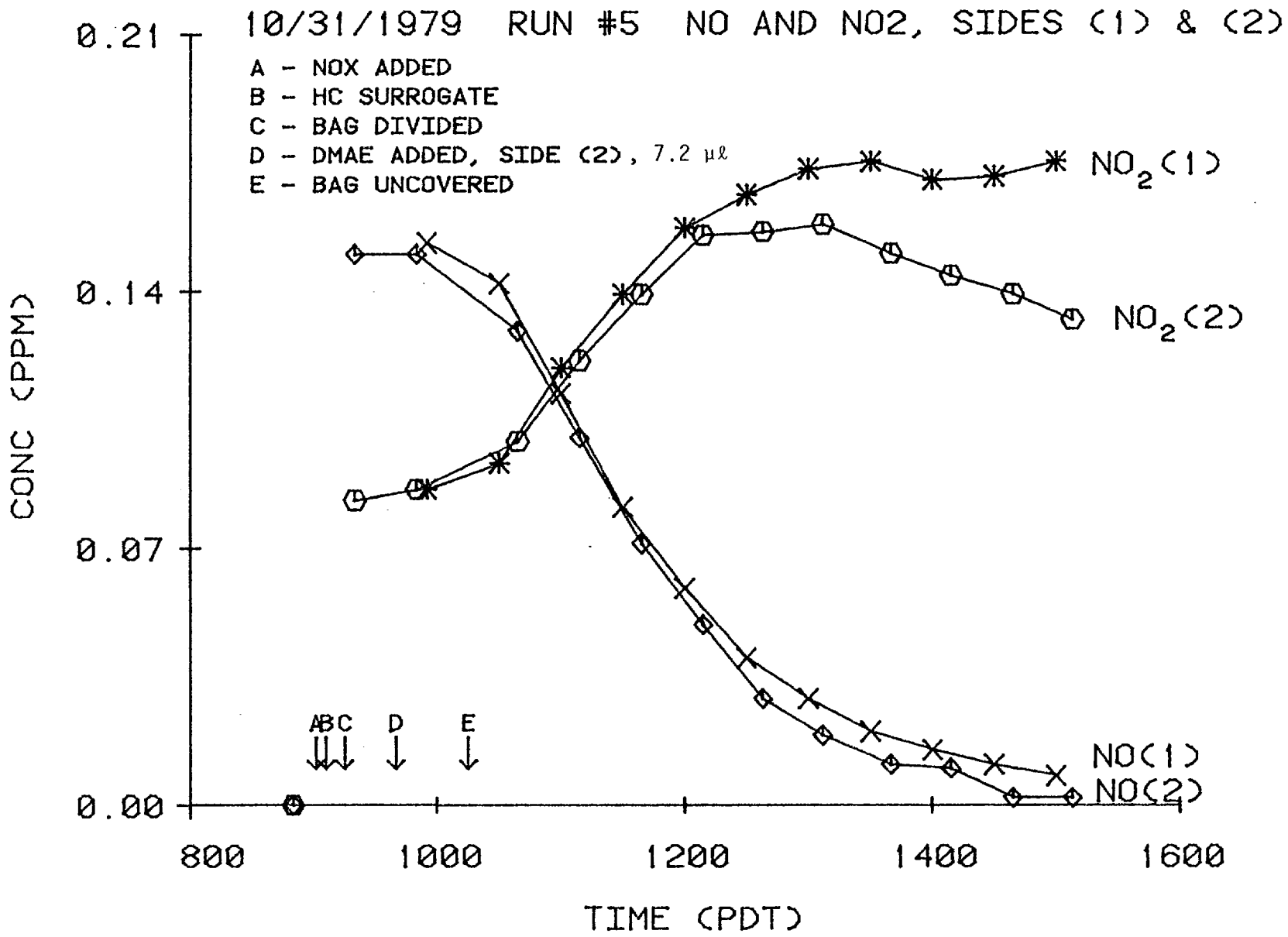

Figure 19. NO and NO_2 Concentration-Time Profiles for Dual-Outdoor Bag DMAE-Surrogate-NO_x-Air Run #5.

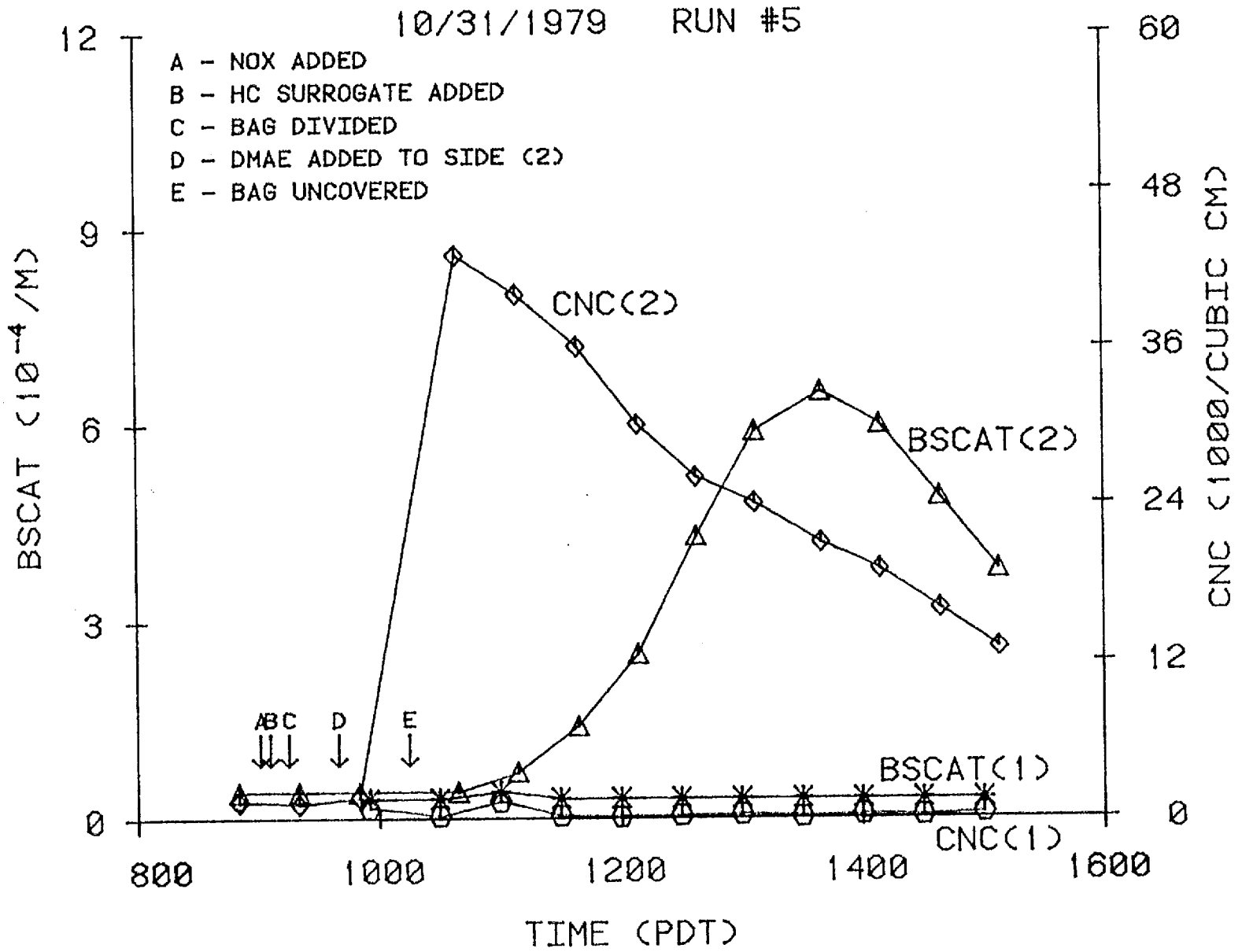

Figure 20. Concentration-Time Profiles for Condensation Nuclei and Light Scattering Aerosol (b_{scat}) for Dual-Outdoor Bag DMAE-Surrogate-NO_x-Air Run #5.

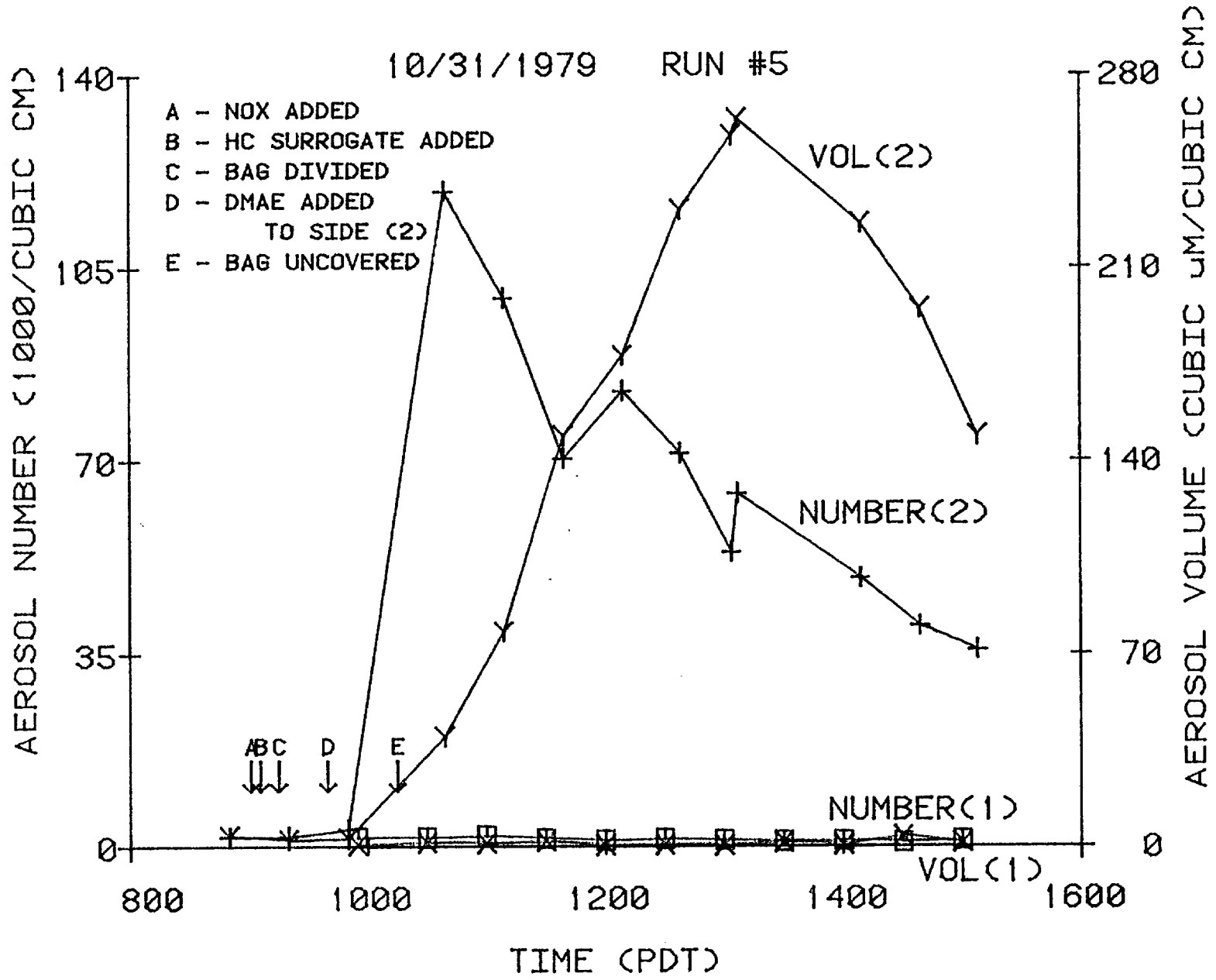

Figure 21. Concentration-Time Profiles for Aerosol Number and Volume for Dual-Outdoor Bag DMAE-Surrogate-NO_x-Air Run #5.

yields of O_3 and PAN being formed. There is no evidence of inhibition of reactivity by DMAE in the first hour of the experiment, as is the case for addition of 0.5 ppm diethylhydroxylamine [Heicklen (1976); Pitts et al. (1977)].

Control experiments (described below) indicated that there was a slight enhancement of reactivity on side 1, possibly due to its spatial orientation being such that it received slightly more sunlight. In order to test this possibility, the bag was rotated 180° so that the sides were reversed, side 2 being the previous side 1, and in run #5 DMAE was added on side 2. As can be seen in Table 7, and in Figures 18 and 19 the added-DMAE side was more reactive than the non-DMAE side, and the results of run #5 were similar to the the results of runs #3 and #4. Thus the effect of added DMAE is greater than any effect of nonequivalency of the chamber sides due to orientation.

In addition to enhancing ozone formation, the experiments indicate that DMAE has an even greater effect on aerosol formation. From Figures 20 and 21, and Table 7, it can be seen that aerosol formation occurred even when ~20 ppb of DMAE was added, while little or no aerosol formation occurred without DMAE. Unlike the DMAE-NO_x-air single bag irradiations in which ~2 to 3 ppm DMAE were added prior to injection of NO_x, there was no evidence for dark formation of particulates. In the dual bag experiment particle formation occurred immediately upon uncovering the bag, their number being less dependent on the amount of added DMAE than on the total aerosol volume formed later in the irradiation (see Table 7). The aerosol volume in these runs reached a maximum prior to the end of the irradiation presumably due to destruction of aerosol on the surface of the collapsing bag.

Control Experiments: Side Equivalency and the Effect of DMAE Contamination of the Bag. In order to test for any effects due to differing light intensity received by the two sides or possible effects of DMAE contamination, several control experiments without added DMAE were done in which equal reaction mixtures, injected and mixed prior to dividing the bag, were irradiated in the divided bag. For the first and third control runs, the reactants consisted of approximately the same surrogate hydrocarbon-NO_x-air mixture as used in the DMAE runs. In the second control

run, the surrogate hydrocarbons were replaced by a simpler propene + n-butane mixture which was expected to have similar reactivity. Detailed data tabulations on the results of these experiments are given in Appendix C3.

In the first control experiment the bag was oriented so the half previously exposed to DMAE was on side 1; the rate of NO oxidation and amount of O_3 produced was slightly higher on side 1 compared to side 2 (~30 vs. ~40 ppb O_3). For the second and third control runs, the bag was rotated so the half previously exposed to DMAE was on side 2. The second experiment yielded insignificant differences in the inorganic concentration-time profiles. In the third experiment slightly more NO_2 and O_3 were produced on side 1 than side 2 (~11 vs. ~9 ppb O_3), despite the fact that side 1 had not been exposed to DMAE. These results indicate that side 1 may be slightly more reactive than side 2 and that this effect, though small, is larger than any effect of DMAE contamination.

The results of the control experiments also suggest that some contamination of the bag by DMAE occurred. In all control runs an increase in condensation nuclei (to ~3 to 5 x 10^3 particles) was observed upon irradiation in the half of the bag which had been previously exposed to DMAE. Formation of condensation nuclei occurred regardless of the spatial orientation of the DMAE-exposed half of the bag. There was no significant difference, however, in b_{scat} or aerosol number or volume between the DMAE-exposed or -unexposed sides.

C. GC-MS Studies of DMAE Photooxidation Products

GC-MS analyses were performed on gas phase samples and filter extractants of aerosol material collected during the DMAE-NO_x-air and the DMAE-surrogate hydrocarbon-NO_x-air outdoor chamber irradiations described above. The methods for obtaining these samples are given in Section II-B, and the techniques employed and the results of the GC-MS analyses are described below.

Experimental. Analyses were performed on a Finnigan 3200 GC-MS instrument interacting with a Finnigan 6100 mass spectral data system. Ionization was by electron impact. The chromatographic column was a WCOT glass capillary (Ucon HB, 40 x 0.3 mm i.d.) prepared by barium carbonate deactivation followed by dynamic coating (Grob and Grob, 1976; Grob et al.,

1977). Cyclic scanning of the quadrapole mass filter produced a mass spectrum (35 a.m.u. - 500 a.m.u.) every two seconds.

Gas phase samples were desorbed from Tenax cartridges by heating from 30°C to 250°C under a 30 ml min^{-1} flow of high purity helium. They were heated for 20 min and frozen out into a loop of glass-lined stainless steel (30 cm x 0.5 mm i.d.) immersed in liquid nitrogen. After desorption the end of the loop was connected to the capillary column and the helium flow adjusted appropriately. Upon replacing the liquid nitrogen bath with a boiling water bath the samples were rapidly tranferred to the column. The column was held at 25°C for five minutes and then programmed from 30°C to 130°C at 4°C min^{-1}.

Aerosol samples were extracted for organic compounds and 1 μℓ aliquots in dichloromethane were injected onto the column using a Grob-type injector (Grob and Grob, 1972). The temperature was held at 25°C for 30 seconds and then programmed from 25°C to 150°C at 6°C min^{-1}.

A potentially significant modification was made to the system between the analyses of the samples from the DMAE-NO_x-air single outdoor bag runs and the analyses of the samples from the DMAE-surrogate hydrocarbon-NO_x-air dual outdoor runs. In the former case, the interface between the end of the column and the mass spectrometer consisted of a platinum-iridium transfer line which causes "sticking" problems with the amines and was a potential source of artifacts. Before analyzing the DMAE-surrogate hydrocarbon-NO_x-air samples this interface was replaced by a glass-lined stainless steel transfer line.

Results. The Tenax samples of gas phase material taken from the DMAE-NO_x-air experiments contained only three products in detectable quantities: dimethylaminoacetaldehyde, the major product, was tenatively identified on the basis of its mass spectrum (authentic samples are unavailable); dimethylformamide; and a trace of dimethylnitramine. Dimethylformamide and traces of dimethylnitramine were also observed on the Tenax samples taken from the DMAE-surrogate runs, but dimethylaminoacetaldehyde was not detected. Its detection in the former sample may be an artifact due to the platinum-iridium transfer line in the GC-MS. A number of other products were detected in the samples taken from the DMAE-surrogate runs which are attributed to products of the surrogate photooxidation, since

they appear on both sides of the bag. In addition, a very small amount of 3-butene-nitrile appeared only on the DMAE side of the bag.

The filter extracts of aerosol material from the DMAE-NO_x-air experiments were considerably more complex than the Tenax samples for gas phase products, but aerosol extracts from the DMAE-surrogate runs were surprisingly less complex than the corresponding gas phase Tenax samples. In the DMAE-surrogate aerosol extracts, there were three major unidentified products. In the DMAE-NO_x-air aerosol extracts, dimethylaminoacetaldehyde was observed, dimethylformamide, methylformamide, and a trace of dimethylnitrosamine were tentatively identified by their known mass spectra, N,N-dimethylglycine was tentatively identified on the basis of its known fragmentation pathways, and mass spectra for eight unidentified constituents were obtained. It is now believed that most of these products may be artifacts, since they were not detected in the subsequent DMAE-surrogate runs.

D. Microbiological Studies

The Ames Salmonella typhimurium mammalian/microsome assay was employed to test for mutagenic activity of DMAE, AMP and product samples collected during DMAE-NO_x-air outdoor chamber runs. The techniques for collecting the gas and aerosol phase samples during the DMAE-NO_x-air runs is described in Section II-B. The complete microbiological screening protocol and procedures used are documented for the SAPRC-ARB mutagen program (Pitts et al., 1980). Changes in procedure, strains, levels of activation, samples and tests are described below.

Fresh samples of DMAE and AMP were screened with tester strains TA1535, TA1537 and TA98 with and without two levels of microsomal activation. Strain TA1535 detects base-substitution mutagens, and strains TA1537 and TA98 are responsive to frame-shift type mutagens. The samples were diluted in dimethylsulfoxide and plated in duplicate at concentrations of 1, 10, 100, and 1000 μg/plate with and without 2% and 10% Aroclor 1254-induced rat liver S9 (liver vol/vol mix). Test plates were incubated at a uniform temperature of 37°C for 63 hours and counted using a calibrated electronic colony counter. Under the experimental conditions, no mutagenic activity was found for either compound.

Testing of samples from a DMAE-NO_x-air exposure was also carried out. Freeze-out samples of both the light and dark reaction products were screened with strain TA98, a strain responsive to frame-shift mutagens. Samples were tested at 1, 5, 10, 20, 40 and 100 µl/plate with and without 2% S9 (liver vol/vol mix). Tenax cartridge samples were tested with strain TA98 and TA100 at concentrations of 1, 2, 5, 10, 20, 50, 100, 200, 500, and 700 µg/plate with and without 2% S9 (liver vol/vol mix). Glass-fiber filter extracts were also screened with TA98 at sample concentrations of 10, 30, 90, 270, and 500 µg/plate with and without 2% and 10% S9 (liver vol/vol mix). No significant mutagenic activity was found under these test conditions.

Gas exposure mutagenicity screens were performed on a DMAE-NO_x-air sample using a modified overlay plating method. In this procedure petri plates containing base agar are overlayed with a top agar coat containing a tester strain in the presence and absence of metabolic activation (Rannug et al., 1974). The gas exposure took place in Billups-Rothenberg chambers which were used to expose the petri plates without plate covers. It was thought that this method should create enhanced gas-agar exchange for detection of mutagenicity. In the process 516 liters of the reaction mixture were pumped out of an outdoor bag through the B-R chambers over a 3-hr period. The chambers were housed in a dark container to prevent exposure of the light-sensitive bacterial strains. In this test five tester strains were employed: TA1535, TA1537, TA1538, TA98, and TA100. These strains were plated in the presence and absence of 2% and 10% S9 (liver vol/vol mix) to screen for potential activation. No mutagenic activity was detected with this technique.

Although no mutagenic activity was found in any of the samples tested, several caveats which are outlined in our conclusions to this section, page 81, preclude accepting tests reported here as conclusive evidence for absence of mutagenic activity of products of thermal or photooxidation reactions of alcohol amines.

E. Determination of Rate Constants for the Reactions of DMAE and AMP With Hydroxyl Radicals (OH)

The rate constant for the reaction of OH with both DMAE and AMP was determined by the flash photolysis resonance fluorescence (FPRF) technique.

A description of this experimental technique and the results of these determinations are given below. In addition, estimates of the OH + DMAE rate constant can be obtained from an analysis of the results of the indoor and outdoor smog chamber experiments described in Sections II-A and II-B. The results of those analyses, which agree within the estimated uncertainty with the FPRF results, are also given below.

FPRF Studies: Experimental. The apparatus and techniques used in this study have been described previously (Atkinson, et al., 1975a,b) hence only a brief summary will be given here. Hydroxyl radicals were produced by the pulsed vacuum ultraviolet photolysis of H_2O at wavelengths longer than the LiF cutoff ($\geq$1050 Å). OH radical concentrations were monitored as a function of time after the flash by resonance fluorescence using a cooled EMI 9659QA photomultiplier fitted with an interference filter transmitting the 3064 Å band of OH ($A^2\Sigma^+$, $v' = 0 \rightarrow X^2\Pi$, $v'' = 0$). The intersection of the detection system aperture and the resonance radiation beam defined a fluorescence viewing zone at the center of the reaction vessel whose cross-section was ~2 cm in diameter. This region was well separated from the reaction vessel walls, minimizing wall losses of the OH radicals. The reaction cell temperature was held constant during a run to better than $\pm$1 K with the gas temperature being measured by a Chromel/Alumel thermocouple mounted inside the reaction vessel.

The flash lamp was typically operated at discharge energies of 10-25 joules per flash at repetition rates of one flash every three seconds. Signals were obtained by photon counting in conjunction with multichannel scaling. Decay curves of OH radicals were accumulated from 200-2500 flashes, depending on the signal strengths. OH half-lives ranged from 1.48-46.2 msec and radical concentrations were monitored over at least three half-lives. In all cases the flash duration ($\leq$1 μsec) was negligible in comparison with the OH radical half-lives encountered.

In order to avoid the accumulation of photolysis or reaction products, all experiments were carried out under flow conditions so that the gas mixture in the reaction vessel was replenished every few flashes. The partial pressure of H_2O in the reaction cell ranged from 0.10 to 0.20 torr.

A known fraction of the total argon flow was saturated with the

amine vapor at 273 K (DMAE) or 298 K (AMP) and amine partial pressures in this fraction of the total flow were determined by their UV absorption at λ = 200-225 nm using a 9.0 cm pathlength cell and a Cary 15 spectrophotometer. The absorption cell was calibrated using known pressures of the amines as measured by an MKS Baratron capacitance manometer.

All flows were monitored by calibrated flowmeters and the gases were premixed before entering the reaction vessel. Prolonged flowing of the amine reactants was necessary in order to obtain steady state gas phase concentrations during the determination of rate data.

FPRF Studies: Results. The reaction of OH radicals with DMAE and AMP was studied at temperature of 300 $\pm$ 2 K and at 50 $\pm$ 1 torr total pressure of argon. Under the experimental conditions used, the pseudo-first order decays of the OH radical concentrations, [OH], are given by the integrated rate expression

$$[OH]_o/[OH]_t = S_o/S_t = \exp[(k + k_1[R])(t-t_o)]$$

where $[OH]_o$ and $[OH]_t$ represent the concentrations of OH at times t_o and t, respectively, S_o and S_t are the corresponding resonance fluorescence intensities, k is the first order rate constant for removal of OH in the absence of added reactant (primarily attributed to diffusion out of the viewing zone and to reaction with impurities), and k_1 is the bimolecular rate constant for the reaction of OH radicals with DMAE or AMP.

The observed decays of the hydroxyl radical concentration were always exponential and the first order decay rates are shown as a function of DMAE and AMP concentration in Figure 22 and 23, respectively. Variation of the flash energy by a factor of two had no effect on the decay rates within experimental error nor had an increase in the total pressure of argon to ~100 torr. The slopes of the least squares lines shown in Figures 22 and 23 can be used to derive the following rate constants for the reaction of hydroxyl radicals with DMAE and AMP at 300 $\pm$ 2 K:

$$k_1(\text{DMAE}) = 4.7 \pm 1.2 \times 10^{-11} \text{ cm}^3 \text{ molecule}^{-1} \text{ sec}^{-1}$$

$$k_1(\text{AMP}) = 2.8 \pm 0.5 \times 10^{-11} \text{ cm}^3 \text{ molecule}^{-1} \text{ sec}^{-1}.$$

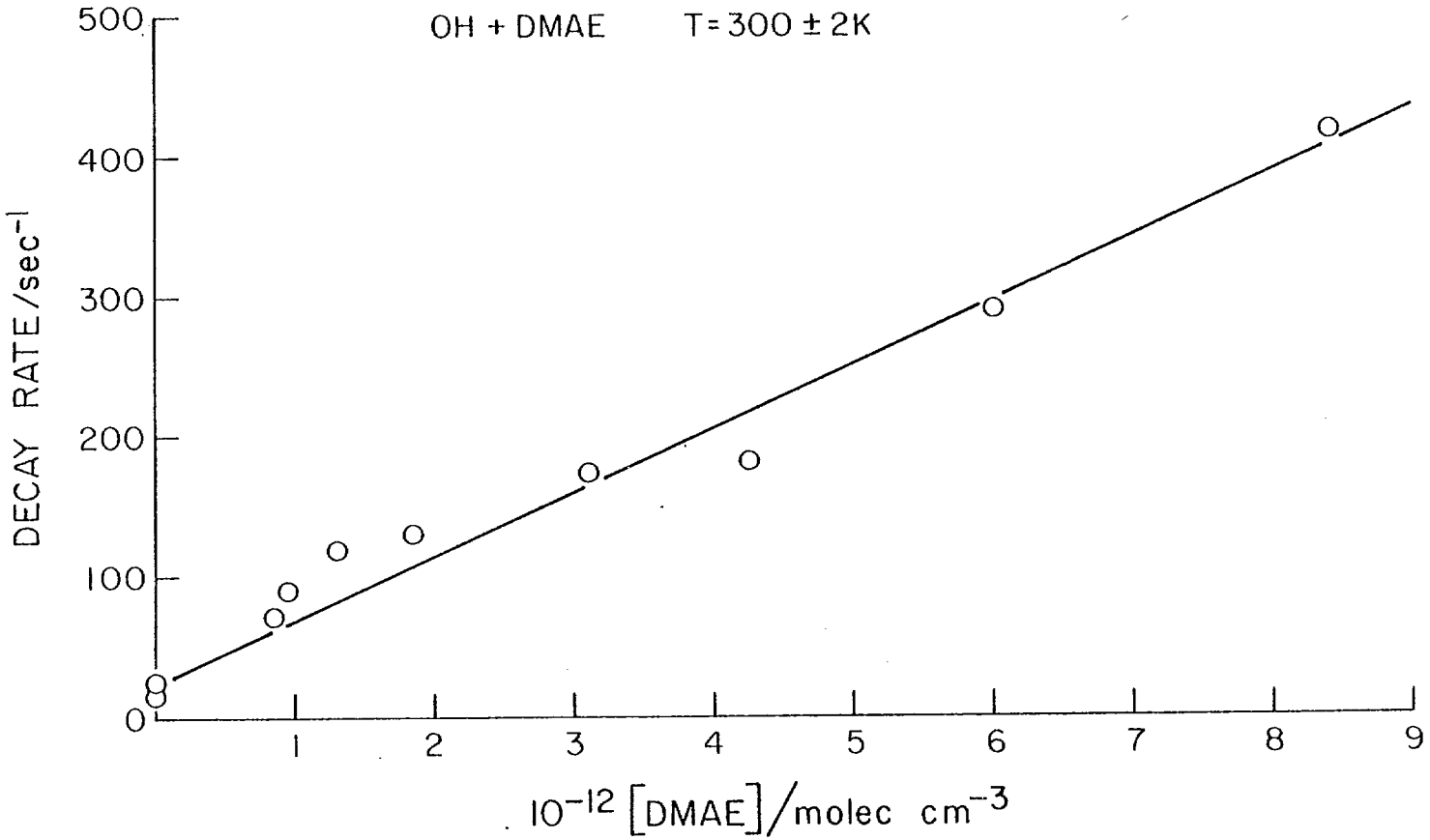

Figure 22. Pseudo-First Order Hydroxyl Radical Decay Rates due to Reaction with Dimethylaminoethanol.

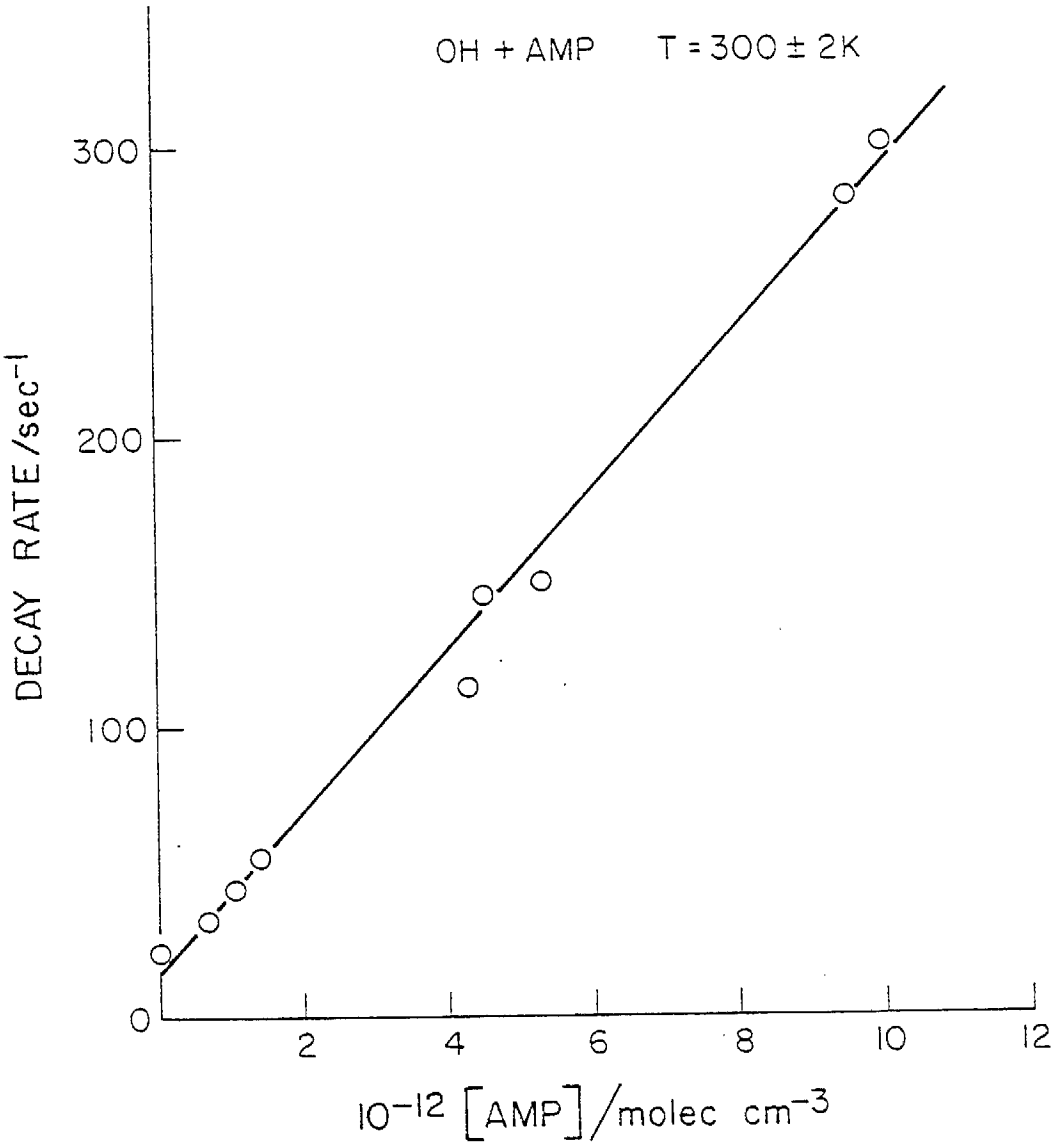

Figure 23. Pseudo-First Order Hydroxyl Radical Decay Rates due to Reaction with 2-Amino-2-Methyl-Proponal.

The error limits reflect three times the standard deviation of the slopes in Figures 22 and 23 plus the estimated uncertainties involved in measuring flow rates, pressures and optical density, the last of these being larger than would otherwise be the case because of the absence of suitably sharp peaks in the UV-visible absorption spectrum of either reactant compound.

Estimates of k(OH + DMAE) from Smog Chamber Data. If it is assumed that the only significant reaction depicting two organic reactants in smog chamber systems is reaction with hydroxyl radicals, the relative rates of decay of those reactants can be used to obtain the ratio of their OH rate constants (see for example, Doyle et al., 1975). Using this technique, estimates of the rate constant for OH + DMAE were derived from the results of the smog chamber experiments in which organic compounds with known OH rate constants were present, as was the case in two of the indoor chamber irradiations and the three outdoor DMAE-surrogate hydrocarbon-NO_x-air irradiations.

Of the two indoor chamber DMAE-added hydrocarbon-NO_x-air irradiations (the 3/21 and 3/22 runs, Table 5), only the data of the 3/22 run is usable because of evidence of significant DMAE offgasing during irradiation in the 3/21 run. Of the three outdoor DMAE-surrogate hydrocarbon-NO_x-air irradiations, we will restrict our analysis to run #3, since that run had sufficiently high DMAE for precise analysis, an adequate amount of hydrocarbon decay data, and sufficient reactivity to allow the decay rate of the less reactive hydrocarbons to be determined with reasonable accuracy. It should be noted that because of the evidence for the importance (albeit variable) of DMAE offgasing during chamber irradiations, the measured DMAE decay rates, and thus the DMAE + OH rate constants derived from them, must be considered to be lower limits.

The AGC-BAG run of 3/22 contained cis-2-butene, n-butane, neopentane, and toluene as well as DMAE and NO_x. Of these, toluene will be used as the reference compound since it is analyzed on the same column as DMAE and had the most rapid decay (except for cis-2-butene, which also reacts with O_3). Plots of the log DMAE/toluene concentration ratios (which are more precisely known than the DMAE concentration, since variabilities in sampling sizes factor out) vs. time and of the log toluene concentrations

vs. time (obtained on a different GC column on which toluene analyses were more precise) are shown in Figure 24. It can be seen that the plots are reasonably linear, indicating essentially constant [OH] during the period shown. Making the assumption of constant [OH] and that DMAE and toluene are consumed only by reaction with OH, the following can be derived:

$$[OH]_{avg} \cong \frac{\frac{d \ln [\text{toluene}]}{dt}}{k(OH + \text{toluene})} \cong \frac{\frac{d \ln ([DMAE]/[\text{toluene}])}{dt}}{k(OH + DMAE) - k(OH + \text{toluene})}$$

From this, and using least squares slopes of the ln [toluene] and ln([DMAE] /[toluene]) vs. time of respectively 7.4×10^{-4} ($\pm$7%) min^{-1} and 4.6×10^{-3} ($\pm$9%) min^{-1} (for the 120-215 minute time interval), and using k(OH + toluene) = 6×10^{-12} cm^3 $molecule^{-1}$ sec^{-1} (Atkinson et al., 1979), we obtain $[OH]_{avg} \cong 2.2 \times 10^6$ molecule cm^{-3}, and k(OH + DMAE) $\cong 4.5 \times 10^{-11}$ cm^3 $molecule^{-1}$ sec^{-1}. Considering the uncertainty introduced by possible DMAE offgasing in smog chamber irradiations, this value is in remarkable agreement with the $(5 \pm 1) \times 10^{-11}$ cm^3 $molecule^{-1}$ sec^{-1} value obtained by FPRF.

The DMAE-surrogate hydrocarbon-NO_x-air outdoor runs contained a number of hydrocarbons which could be used as the reference compound, but we will use toluene for consistency with our above analysis of AGC-BAG run 3/22. Plots of the log DMAE and toluene concentrations vs. time monitored in the outdoor chamber run #3 are shown in Figure 25. As can be seen in the figure, the decays are reasonably exponential for the time period between 75-min to 250-min. During that period log [DMAE] and log [toluene] vs. time plots had least square slopes of 1.12×10^{-2} ($\pm$3%) min^{-1} and 1.23×10^{-3} ($\pm$11%), respectively. Assuming relationships similar to that given above, and using an OH + toluene rate constant of 6×10^{-12} cm^3 $molecule^{-1}$ sec^{-1} (Atkinson et al., 1979), we obtain $[OH]_{avg} \cong 4 \times 10^6$ molecule cm^{-3}, and k(OH + DMAE) $\cong 5.5 \times 10^{-11}$ cm^3 $molecule^{-1}$ sec^{-1}. This is essentially the same as the OH + DMAE rate constant obtained by FPRF, and is in excellent agreement with that obtained from the AGC-BAG data.

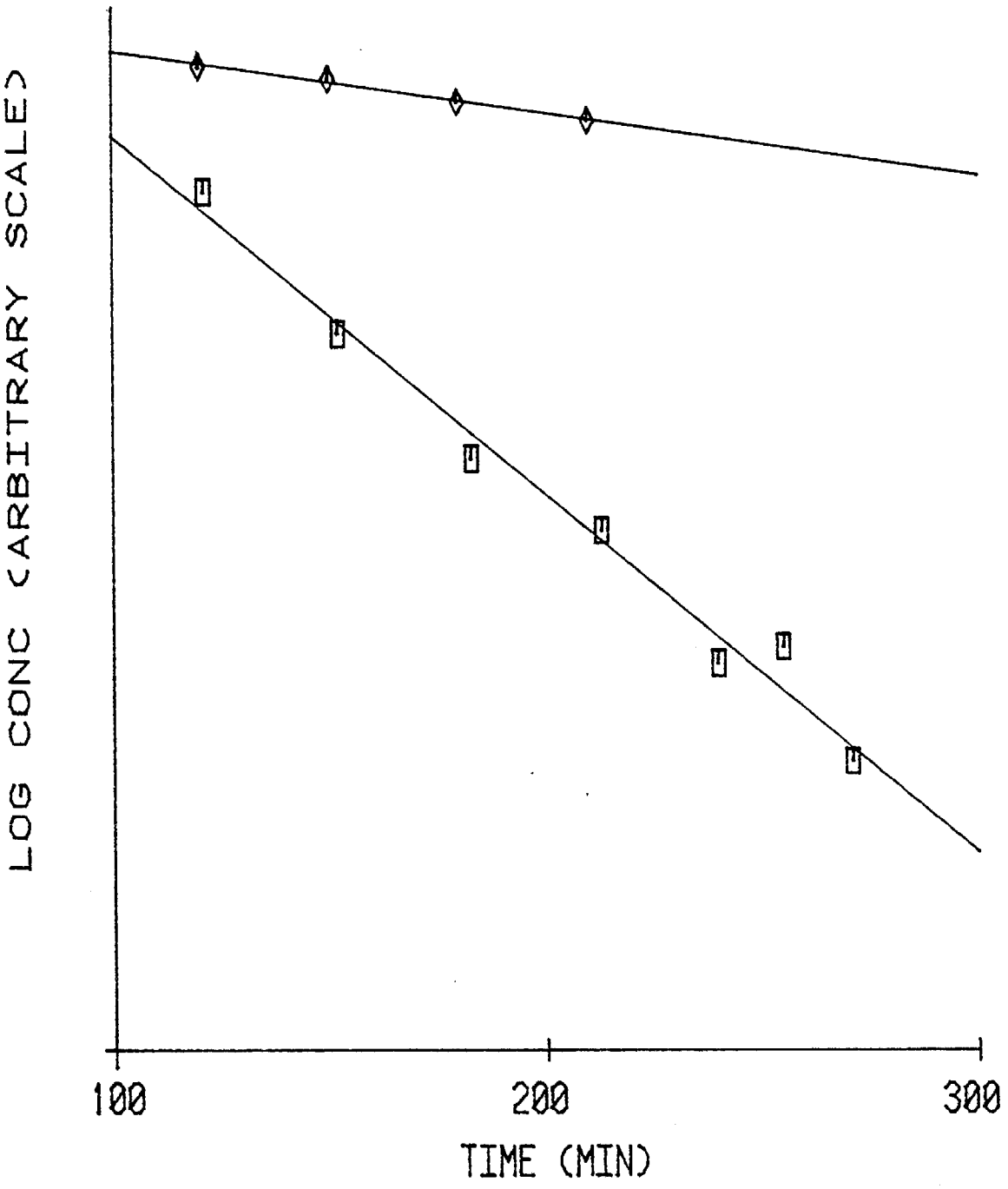

Figure 24. Plots of Logarithms of DMAE/Toluene Ratio and Toluene Concentrations vs. Time for AGC-BAG Run 3/22. ⊡ ln[DMAE/Toluene]; ◇ ln[Toluene]; —— Least Squares Lines.

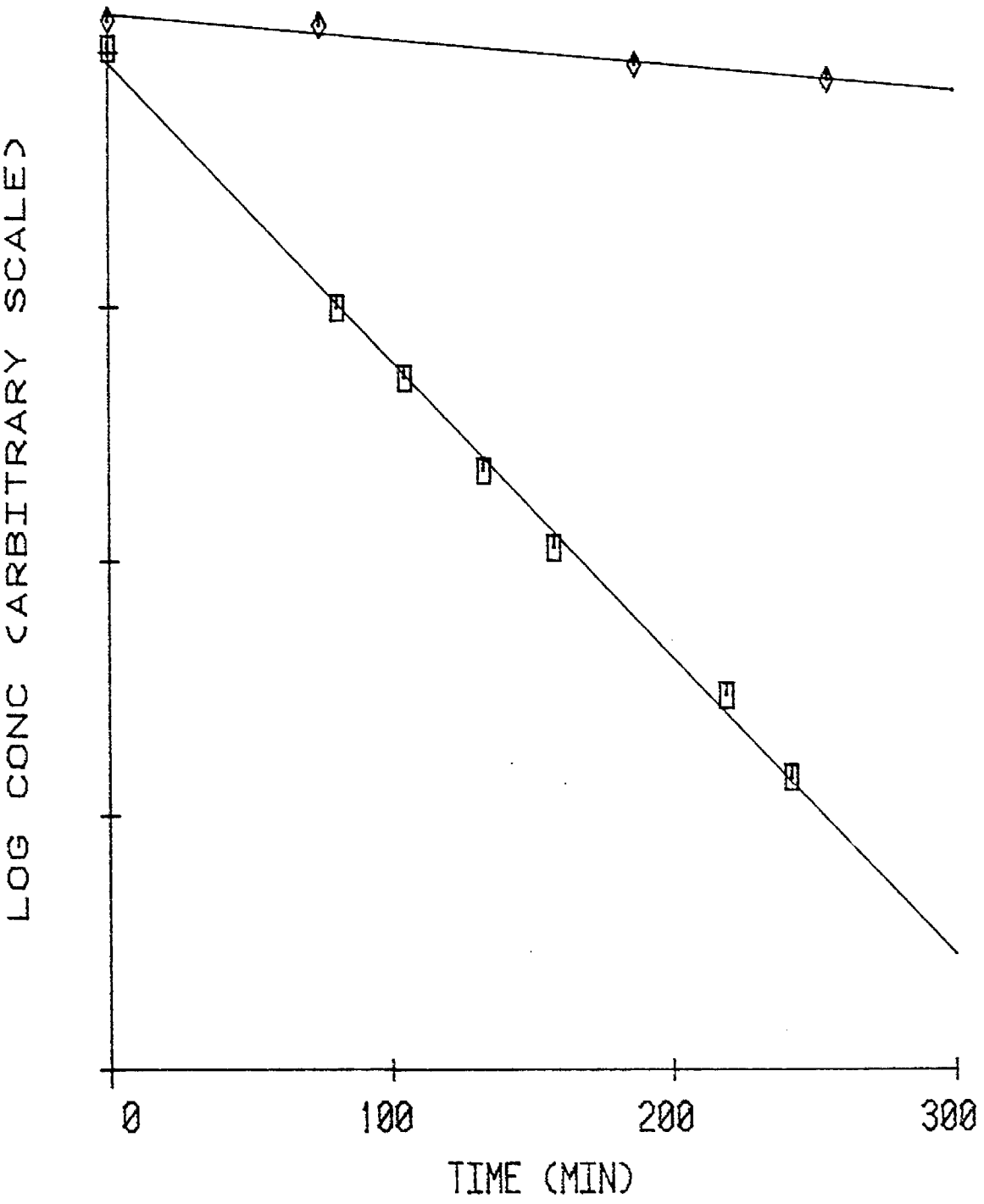

Figure 25. Plots of Logarithms of DMAE and Toluene Concentrations vs. Time for DMAE-Surrogate Hydrocarbon-NO_x Outdoor Bag Run #3. ◈ ln[Toluene]; ⧈ ln[DMAE]; —— Least Squares Lines.

F. Discussion and Conclusions

Atmospheric Lifetimes and Photooxidation Mechanisms and Products of Gas Phase DMAE and AMP. The excellent agreement we obtained between the OH + DMAE rate constant determined by the FPRF technique and that derived by its decay rates in the indoor and outdoor smog chamber irradiations indicates that the primary fate of gas phase DMAE emitted into the atmosphere must be reaction with OH. This reaction is probably also the case for AMP. Taking the average hydroxyl radical concentration to be $\cong 2 \times 10^6$ molecule cm^{-3} in urban atmospheres and the OH rate constants derived in this study, estimated lifetimes of gas phase DMAE and AMP are approximately 3 hours and 6 hours, respectively.

The most probable pathways for the atmospheric reaction of DMAE with OH are shown in Figure 26. The identification of dimethylformamide (DMF), dimethylnitramine and possibly dimethylaminoacetaldehyde by GC-MS as products of DMAE-NO_x-air photooxidation is consistent with this mechanism. Comparison of our room temperature rate constant for OH + DMAE with those for trimethylamine (Atkinson et al., 1978a) and for ethanol (Overend and Paraskevpoulos, 1978) suggests that the reaction proceeds primarily by abstraction of the hydrogen from the N-bonded carbon atoms, forming DMF, dimethylnitramine and other products, rather than abstraction from the methanolic-CH_2OH group, forming dimethylaminoacetaldehyde. Although the latter compound was detected in large yields in the initial GC-MS analysis, subsquent analysis suggests this may be an artifact (see Section II-C). However, the major product observed using GC-FID is unidentified, and the possibility of its being dimethylaminoacetaldehyde cannot be ruled out, since no authentic sample of this compound was available.

Effect of Added DMAE on O_3 Formation. Although based on its rate of reaction with OH, DMAE is a quite reactive compound, results from our chamber experiments suggest that the tendency of DMAE to form large quantities of aerosols may be a more significant factor, in terms of environmental impact, than its ozone-forming potential. In particular the replacement of large quantities of organic solvents by substantially smaller amounts of the ethanolamines should lead to lower ozone production. Also working in this direction is the lower volatility and greater "stickiness"

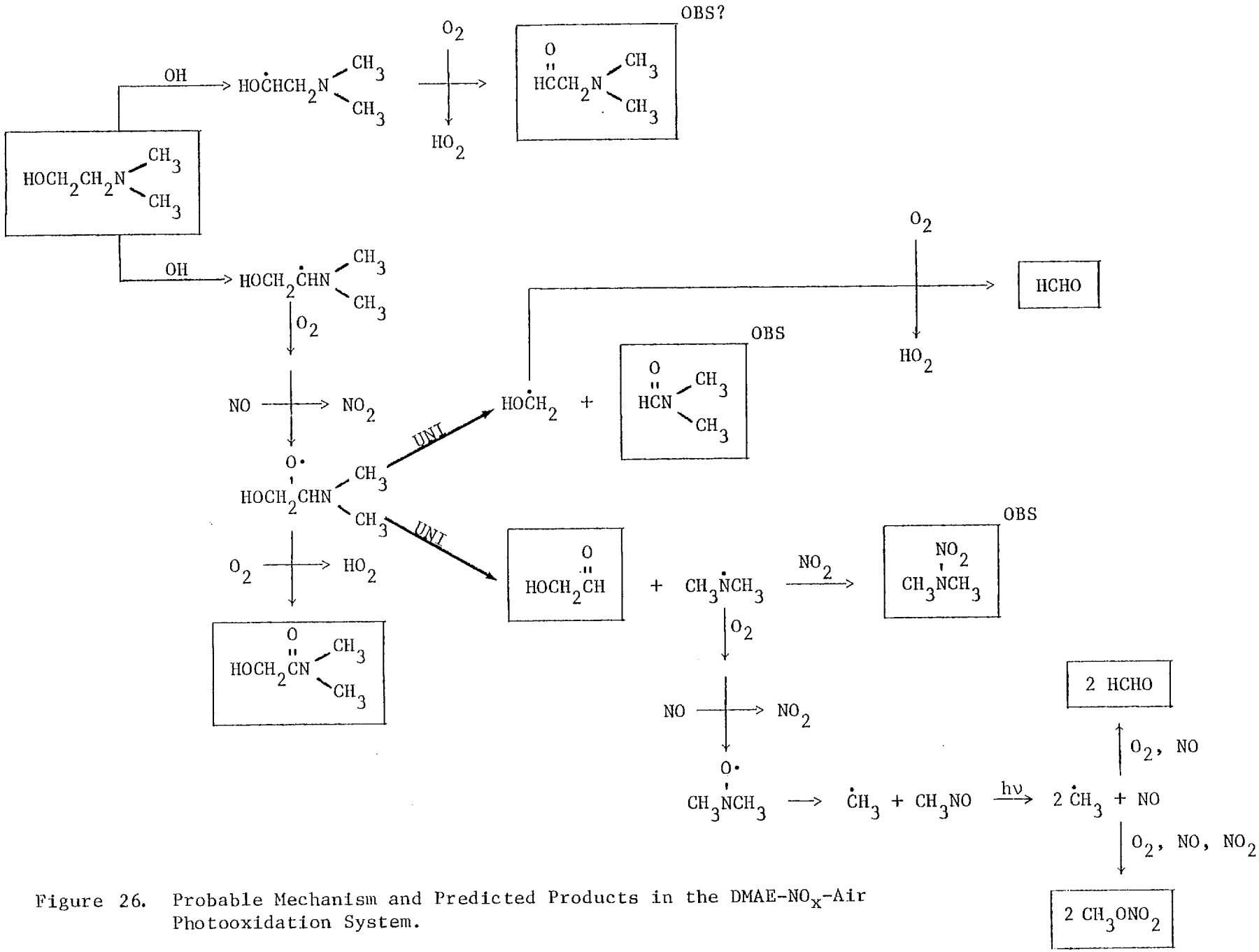

Figure 26. Probable Mechanism and Predicted Products in the DMAE-NO_x-Air Photooxidation System.

of DMAE and AMP compared with many of the organic solvents for which it is being substituted. On the other hand the propensity of DMAE and AMP to form aerosols must be considered in weighing the benefits of a water-based paint strategy since this is not a property of many of the solvents utilized in organic-based paints.

At the present time it is not possible to determine from the total amount of alcohol amines used in paint operations the actual amount which will finally react in the gas phase, but the results of our experiments lead us to believe it may be small. Chamber experiments in which special efforts are made to introduce the reactants directly into the gas phase are not suitable for such a determination. Field measurements of gas phase alcohol amine concentrations in the vicinity of their actual use in paint operations are required. Thereafter, results of smog chamber experiments can aid in assessing the practical impact of alcohol amine use on ozone formation.

Effect of DMAE on Aerosol Formation. Our studies indicate that DMAE photooxidation results in formation of large quantities of aerosol. Since aerosol formation does not occur to a measureable extent in the photooxidation of the surrogate hydrocarbon mixture in the absence of DMAE, replacing hydrocarbon solvents with DMAE may result in decreased air quality due to increased aerosol formation. How significant this effect would be is difficult to predict since it depends on the fraction of DMAE which occurs in the gas phase, and the relative importance of this amount compared to amounts of other aerosol-producing substances in the atmosphere such as other amines or SO_2.

Although the nature of the aerosol material formed in the DMAE photooxidation has not been characterized, the fact that some aerosol formation occurs in the dark in the presence of NO_x suggests the reaction of DMAE with HNO_3.

$$HOCH_2CH_2N(CH_3)(CH_3) + HNO_3 \rightarrow [\,HOCH_2CH_2\overset{+}{N}H(CH_3)(CH_3)\,]\ NO_3^-$$

HNO_3 is present in small amounts as an impurity in NO_x, and a small amount is all that is required to account for the observed formation of condensation nuclei. This reaction could also account for the buildup of

aerosol material during irradiation, since HNO_3 is a known photooxidation product of NO_x. However, the GC-MS data indicated the presence of a number of other unidentified compounds in the aerosol phase, which are undoubtedly DMAE photooxidation products. The importance of these products relative to the DMAE-HNO_3 salt in contributing to the aerosol mass is not known.

Biological Activity. Although no mutagenic activity was found from any of the samples tested, the following cautions must be emphasized. First, it was felt that the concentration of the reaction products in the gas exposure (sub-ppm) and the freeze-out samples were probably below the threshold sensitivity for the tester strains employed. Secondly, it is well documented that many nitrosamines are only detected in milligram concentrations (Ames et al., 1975, McCann et al., 1975) in the Ames test. Finally, although the Tenax cartridge method can provide adequate concentration of sample, this technique is thought to produce artifact errors during the collection and elution procedure which might change and possibly deactivate any mutagens present. Thus, failure to obtain response in the Salmonella typhimurium mutagenicity assay cannot be taken as conclusive evidence for absence of mutagenic activity of the products of the thermal or photooxidation reactions of DMAE or AMP.

III. DEVELOPMENT OF OZONE-PRECURSOR RELATIONSHIPS FOR AMBIENT AIR USING COMBINED CHAMBER DATA-MODELING TECHNIQUES

Quantitative relationships relating ambient ozone formation to the levels of its precursors, hydrocarbons and nitrogen oxides, are required if one is to predict reliably the impact of changes in emissions of these pollutants on air quality. One technique currently employed by the U. S. Environmental Protection Agency (1977, 1978) and some state and local control agencies is the "empirical kinetic modeling approach" (EKMA). This approach involves the following steps: developing a hydrocarbon-NO_x-air chemical kinetic mechanism (kinetic model) whose predictions of ozone formation can be made to be consistent with that observed in smog chamber irradiations; modifying this model by removing "chamber effects" and including appropriate diurnally-varying photolysis rate constants and realistic dilution rates and emission patterns; using the modified model to calculate isopleth plots of maximum ozone yields as a function of initial hydrocarbon and NO_x levels; and finally, using these isopleths to predict changes in ozone formation resulting from fractional changes in hydrocarbon and NO_x emissions (U. S. Environmental Protection Agency, 1977; Dimitriades, 1977).

A number of deficiencies and limitations of the EKMA technique (U. S. Environmental Protection Agency, 1977; Dimitriades, 1977; Bilger, 1978) are already well recognized by researchers and control officials. Other potentially important uncertainties of the EKMA technique which have not been adequately studied concern the validity of the chemical kinetic reaction mechanism (kinetic model) employed, and the most appropriate way to represent the nonmethane hydrocarbons in the mechanism. The kinetic model which has been used in applications of the EKMA technique is that developed for the EPA for this purpose by Dodge (1977b) (hereafter designated the EPA model), which employs the 75-step propene and n-butane mechanism developed by Durbin et al. (1975).

Studies concerning the effects of varying the mechanistic parameters or the representation of the nonmethane hydrocarbons used in the EPA model are limited. Dodge (1977a) used the EPA model to calculate the effect of varying hydrocarbon reactivity, solar energy, dilution rates, and post-9 a.m. emissions on calculated O_3 isopleths and on control

strategies derived from them. It was found that changing these parameters changed the O_3 isopleths somewhat, but that changes in the isopleths had relatively little effect on control strategies derived from them, provided the control strategies were derived in terms of relative changes in hydrocarbon or NO_x emissions. It has been inferred from this that EKMA control strategy predictions are insensitive to details of how the hydrocarbons are represented and to uncertainties in the kinetic mechanism (U. S. Environmental Protection Agency, 1977). However, we are aware of no published calculations in which different kinetic mechanisms were compared, or in which other aspects of hydrocarbon representation, such as oxygenate content, were varied. Therefore, the assumption of general insensitivity of EKMA control strategy predictions to changes in details of the kinetic mechanism or the hydrocarbon representation remains to be tested thoroughly.

In this section, we describe the results of calculations aimed at better characterizing the extent to which EKMA isopleths and control strategy predictions derived from them depend on the kinetic model and the representation of the hydrocarbon mixture. In our EKMA calculations, we used an updated independently-developed kinetic model (Carter et al., 1979) which was validated against a different smog chamber data base using different assumptions concerning chamber effects than was used in the EPA EKMA model validation. Ozone isopleths and control strategy predictions using our model are compared with those using the standard EPA EKMA model and the effect of using differing hydrocarbon compositions, particularly with and without added oxygenate, are examined. The extent to which these calculations agree or disagree gives an indication of the sensitivity of EKMA predictions to uncertainties in the kinetic mechanisms, including assumptions made in their validation, and to the representations used of reactive hydrocarbons.

Experimental.

Kinetic Mechanisms. Two different kinetic mechanisms, designated mechanisms "D" and "C," were employed in the calculations reported here. Mechanism "D" refers to the mechanism of Durbin et al. (1975) which was incorporated in the standard EPA EKMA model developed by Dodge (1977b) and which is the same as that used in the OZIPP computer programs developed for the EPA for calculating city-specific isopleth plots (Whitten and Hogo,

1978). The reactions and rate constants used in this mechanism are given elsewhere (Dodge, 1977a; Dodge, 1977b; Whitten and Hogo, 1978); photolysis rates were calculated using the absorption coefficients and quantum yields used in the OZIPP computer programs (Whitten and Hogo, 1978). Mechanism "C" is an updated and simplified version of the propene + butane-NO_x-air model of Carter et al. (1979) and the toluene-NO_x-air model of Atkinson et al. (1980) (Section IV of this Final Report). It differs from those models in the details described in the next paragraph. In addition, several calculations were done in which individual reactions or rate constants of mechanism "C" were modified to correspond to those used in the EPA mechanism.

The propene + n-butane-NO_x-air (Carter et al., 1979) and toluene-NO_x-air (Atkinson et al., 1980) mechanisms were developed to be consistent with current kinetic and mechanistic chemical data as well as with results of SAPRC evacuable smog chamber experiments (Atkinson et al., 1980; Pitts et al., 1979b; Darnall et al., 1976-78). The propene + n-butane mechanism has been updated to include recent data concerning formaldehyde photolysis (Horowitz and Calvert, 1978) and several reactions in the inorganic mechanism (Hampson and Garvin, 1978). These changes have relatively small effects on the predictions of the model, and are included in the inorganic and formaldehyde reactions listed in SAPRC's more recent toluene-NO_x-air model (Atkinson et al., 1980). In order to reduce computation time, the detailed model was simplified as follows: (1) OH radicals were assumed to react with n-butane exclusively by abstraction of a secondary hydrogen; (2) OH was assumed to react with propene only by end addition to the double bond; (3) α-hydroxy alkoxy radicals formed in the propene system were assumed to decompose much more rapidly than competing processes; and (4) secondary reactions of minor organic products formed less than 10% of the time were ignored. These simplifications affected only predictions of minor product yields, and had no significant impact on O_3 predictions.

Smog Chamber Validation. The EKMA technique requires the validation of the kinetic mechanism employed against results of smog chamber irradiations of reactant mixtures representative of those emitted into ambient air. Mechanism "D" was validated by Dodge (1977b) using irradiated auto exhaust chamber data. Mechanism "C" was validated for this study using

the extensive data base of surrogate hydrocarbon-NO_x-air irradiations in the SAPRC all glass smog chamber, details of which have been reported in previous SAPRC-ARB studies (Pitts et al., 1975; Pitts et al., 1976b). The composition of the hydrocarbon mixture in the all glass chamber irradiations was a "surrogate" for the ambient air pollutant burden in the South Coast Air Basin (Pitts et al., 1976a), and is given in Table 8 under designation "SD," for "Surrogate, Detailed". In all experiments initial NO_x consisted of approximately 10% NO_2 and 90% NO. Results of over 50 irradiations were used for validation of mechanism C. The experiments fell into four groups corresponding to initial NMHC levels of: 0.44 ± 0.09 ppmC; 0.69 ± 0.07 ppmC; 1.39 ± 0.13 ppmC; and 2.23 ± 0.16 ppmC. Initial NO_x ranged from 0.005 to 0.5 ppm.

In the calculations simulating smog chamber experiments, two representations of the surrogate hydrocarbon mixture were used. In the propene-butane-aldehyde representation of the surrogate (designated "S") all the organics in the surrogate mixture were represented by propene, n-butane and formaldehyde. The relative initial concentrations of these reactants are given in Table 8, and were chosen so that propene + n-butane in the S mixture would have the same ppmC and roughly the same OH reactivity as the "reactive" hydrocarbons in the surrogate, and so that the formaldehyde would have the same ppmC as the oxygenates in the surrogate. The "reactive" hydrocarbons in the surrogate were taken to be n-butane, 2,3-dimethylbutane and all the olefins and aromatics. Relatively unreactive methane, ethane, propane and acetylene were assumed to be inert in this model and thus were not represented in the S mixture.

In calculations using the detailed surrogate representation, SD, all reactant hydrocarbons were treated separately. Initial reactions of all organics with OH (Pitts et al., 1976b) and of the olefins with O_3 (Hampson and Garvin, 1978; Japar et al., 1974), $O(^3P)$ (Hampson and Garvin, 1978; Atkinson and Pitts, 1977; Furuyama et al., 1974), and NO_3 (Japar and Niki, 1975; Graham and Johnston, 1978) were included in the model with the appropriate rate constants. The simplification was made that products of the initial attack (by OH, O_3, etc.) were assumed to be the same for all hydrocarbons of the same class. In particular, all alkanes were assumed to give the same products as n-butane (Carter et al., 1979), all alkenes were

Table 8. Representations of the Non-Methane Organic Reactants Used in EKMA Model Calculations

Designation of Hydrocarbon Representation:	SD	S	E	E-
	Relative Concentration (ppb/ppmC NMHC)[a]			
Alkanes				
Ethane	32.6	--	--	--
Propane	5.4	--	--	--
n-Butane	79.9	172	188	188
2,3-Dimethylbutane	41.8	--	--	--
Olefins				
Ethene	17.1	--	--	--
Propene	4.8	60	83	83
Cis-2-butene	6.1	--	--	--
2-Methyl-2-butene	5.7	--	--	--
Aromatics				
Toluene	6.7	--	--	--
m-Xylene	16.5	--	--	--
Oxygenates				
Formaldehyde	22.0	26	20	--
Acetaldehyde	1.0	--	15	--
Acetone	0.8	--	--	--
Others				
Acetylene	20.6	--	--	--
CO	2800	2800	--	--
Total OH Reactivity[b] (10^3 ppm^{-1} min^{-1})	4.2	4.4	4.4	3.7
Total Oxygenate Content (ppm>C=O/ppmC NMHC)	0.024	0.026	0.035	0

[a]Does not necessarily sum up to 1000 ppbC because CO not covered in total NMHC in surrogate representations, and oxygenates not counted in EPA representations.

[b]Sum of relative concentration x OH rate constant (Atkinson et al., 1979) for each reactive organic and CO.

assumed to give the same products as propene (Carter et al., 1979), and all aromatics were assumed to give the same products as toluene (Atkinson et al., 1980). Thus the model using the SD hydrocarbon mixture does not conserve carbon and is consequently still highly approximate. The approximations are of a different nature from those in calculations using the S mixture; hence comparison of predictions using the two mixtures should be useful in assessing the effects of lumping together the initial consumption reactions of the reactive hydrocarbons.

In order to simulate the smog chamber results, the kinetic mechanism must include provisions for chamber effects. The major chamber-dependent portions of our mechanism concern: (1) the photolysis rate constants; (2) radical input from unknown chamber sources; (3) HNO_3 formation from the $N_2O_5 + H_2O$ reaction; and (4) ozone and H_2O_2 destruction on the walls.

The photolysis rate constants can be calculated using published or estimated absorption coefficients and quantum yields (Carter et al., 1979; Atkinson et al., 1980), and the measured intensities and spectral characteristics of the photolyzing radiation in the glass chamber. The rate of ozone destruction by the walls was determined by ozone dark decay experiments. The other two chamber-dependent portions of our kinetic mechanism are more uncertain, and had to be represented by adjustable parameters in our chamber simulation calculations.

The important uncertain chamber effects concern the radical input rate from unknown sources and the $N_2O_5 + H_2O$ rate constant. It is necessary to assume a significant radical input from unknown sources in order to account for radical initiation in smog chamber runs (Carter et al., 1979; Hendry et al., 1978; Bufalini et al., 1972; Wu et al., 1976; Bufalini et al., 1977). We found that the most satisfactory fits to the data are obtained by assuming an input of hydroxyl radicals at a constant rate throughout the run, where the rate was adjustable for each run (Carter et al., 1979). An hydroxyl input rate of 0.15 ppb min^{-1} is generally the minimum value required for model calculations to fit chamber experiments, while a rate of 0.4 ppb min^{-1} is more typical of experiments with the initial NO_x in the 0.2 - 0.5 ppm range. The maximum $N_2O_5 + H_2O$ rate constant appears to be ~2 x 10^{-5} ppm^{-1} min^{-1} (Morris and Niki, 1973), but significantly lower values are often required to fit NO_2 consumption

rates in some smog chamber experiments (Carter et al., 1979; Demerjian et al., 1974). The effect of varying these parameters within these ranges was tested in our chamber simulation calculations.

Ambient Air Simulations. Calculations were performed using diurnally varying photolysis rates with no provisions for chamber effects. The photolysis rates were calculated using the actinic irradiations as calculated as a function of zenith angle by Peterson (1976) using his "best estimate" surface albedos. Except for the kinetic mechanism and the hydrocarbon representation, the conditions employed in all ambient air simulations were those used in standard EPA isopleth calculations (Roth et al., 1974; Dodge, 1977b; Whitten and Hogo, 1978). In particular, full pollutant loading was assumed to occur at 7:00 a.m. local standard time, with the simulation terminating at 6:00 p.m.; a constant dilution rate of 3% hr^{-1} was used; initial NO_x was assumed to consist of 25% NO_2; and all calculations were done for a latitude of 34.1°N and a solar declination of 23.5°, which is appropriate for Los Angeles in the summer.

In addition to varying the kinetic mechanisms, calculations were done using different representations of the reactive organic mixture. These are summarized in Table 8 which gives the designation for each hydrocarbon mixture, the total OH reactivity, and the total oxygenate content of the mixtures. Mixtures SD and S represent the SAPRC "detailed surrogate" (Pitts et al., 1975; Pitts et al., 1976a; Pitts et al., 1976b) and the propene-n-butane-aldehyde surrogate (Carter et al., 1979), respectively. Mixture E consists of propene, n-butane, formaldehyde and acetaldehyde in the relative amounts used in the standard EPA EKMA model (Dodge, 1977a; Dodge, 1977b; Whitten and Hogo, 1978); this composition was derived in order to fit irradiated auto exhaust data (Dimitriades, 1970). Mixture E- is the same as the E mixture, but without the aldehydes. Calculations were done using mechanism C with all mixtures and mechanism D with mixtures E and E-. Table 9 outlines the matrix of mechanisms and hydrocarbon mixtures with corresponding model designations used in this study.

Computational Methods. The computational methods and computer programs employed in this study were the same as those described previously in our smog chamber modeling studies (Carter et al., 1979) except that for the ambient air simulations the diurnally varying photolysis rate

Table 9. Designations of Models (Kinetic Mechanism + Hydrocarbon Mixture) Used in Ambient Air Simulation Calculations

Hydrocarbon Mixture	Kinetic Mechanism	
	Carter et al. (1979) Atkinson et al. (1980) (C)	Durbin et al. (1975) Dodge (1977b) (D)
SAPRC detailed surrogate (SD)	C_{SD}	Not used
SAPRC propene-butane-aldehyde (S)	C_S	Not used
Standard EPA propene-butane-aldehydes (E)	C_E	D_E
EPA propene-butane (E-)	C_{E-}	D_{E-}

constants were updated at each time step in the integration. As before (Carter et al., 1979), the integration employed the Gear algorithm (Gear, 1971; Hindmarsh, 1972) and the quasi-steady state approximation was used for all reactive radical and atomic intermediates except HO_2. Points on the isopleth plots were derived manually from the calculated O_3 yields using a quadratic interpolation routine. Unfortunately, the OZIPP programs (Whitten and Hogo, 1978) could not be used in this study because they provided no convenient way to vary the kinetic mechanism.

Isopleth Analysis Technique. In order to test the effect of varying the kinetic mechanism or the hydrocarbon representation on predictions related to control strategies, isopleth plots were analyzed using the standard "relative" EPA EKMA isopleth analysis technique to compare their

predictions concerning one specific control strategy problem (U. S. Environmental Protection Agency, 1977; Dimitrades, 1977). The specific problem chosen here is similar to one studied by Dodge (1977a), namely, to determine the amount of NMHC control required to reduce O_3 from 0.3 ppm to the federal air quality standard of 0.12 ppm, assuming NO_x emissions remain constant. The relative EKMA isopleth analysis technique is illustrated here by means of an example. Referring to Figure 29, if we assume the NMHC/NO_x ratio is 8:1 and construct isopleths calculated using the standard EPA model (D_E), the situation of O_3 = 0.3 ppm is indicated by point a. In order to achieve a reduction of O_3 from 0.3 ppm to 0.12 ppm, the D_E isopleths indicate a reduction of NMHC is required corresponding to moving from point a to point b, which amounts to a 67% reduction in hydrocarbon emissions. Analogously, the C_E and the C_S isopleths in the same figure indicate reductions corresponding to moving from points a′ to b′ and from a" to b", respectively, amounting to required NMHC reductions of 58% and 41%. Similar analyses can be done assuming different initial NMHC/NO_x ratios and using isopleths calculated using other kinetic mechanisms and hydrocarbon representations.

Results and Discussion

Smog Chamber Validation of Mechanism C. Use of the EKMA isopleth analysis technique requires that the kinetic mechanism used be validated against results of smog chamber irradiations of a reactive mixture representing ambient air. Thus, for the purpose of validating Mechanism C, four sets of chamber simulation calculations were performed, the results of which are compared to the experimental results in Figures 27 and 28. Calculations P, P_R and P_N employed the propene-butane-aldehyde representation of the SAPRC surrogate hydrocarbon mixture and show the effect of varying the most uncertain chamber effect parameters. In order to give the best fit to the chamber data, calculations P employed a constant radical input rate of 0.4 ppb min^{-1} and assumed the $N_2O_5 + H_2O$ reaction was negligible. Calculations P_R show the effect of reducing the radical input rate to 0.2 ppm min^{-1}, and calculations P_N show the effect of using a maximum $N_2O_5 + H_2O$ rate constant of ~1.4×10^{-20} cm^3 mol^{-1} sec^{-1} (Morris and Niki, 1973). Calculations S employed the detailed representation of the surrogate hydrocarbon mixture (SD in Table 8) but used the same chamber effect

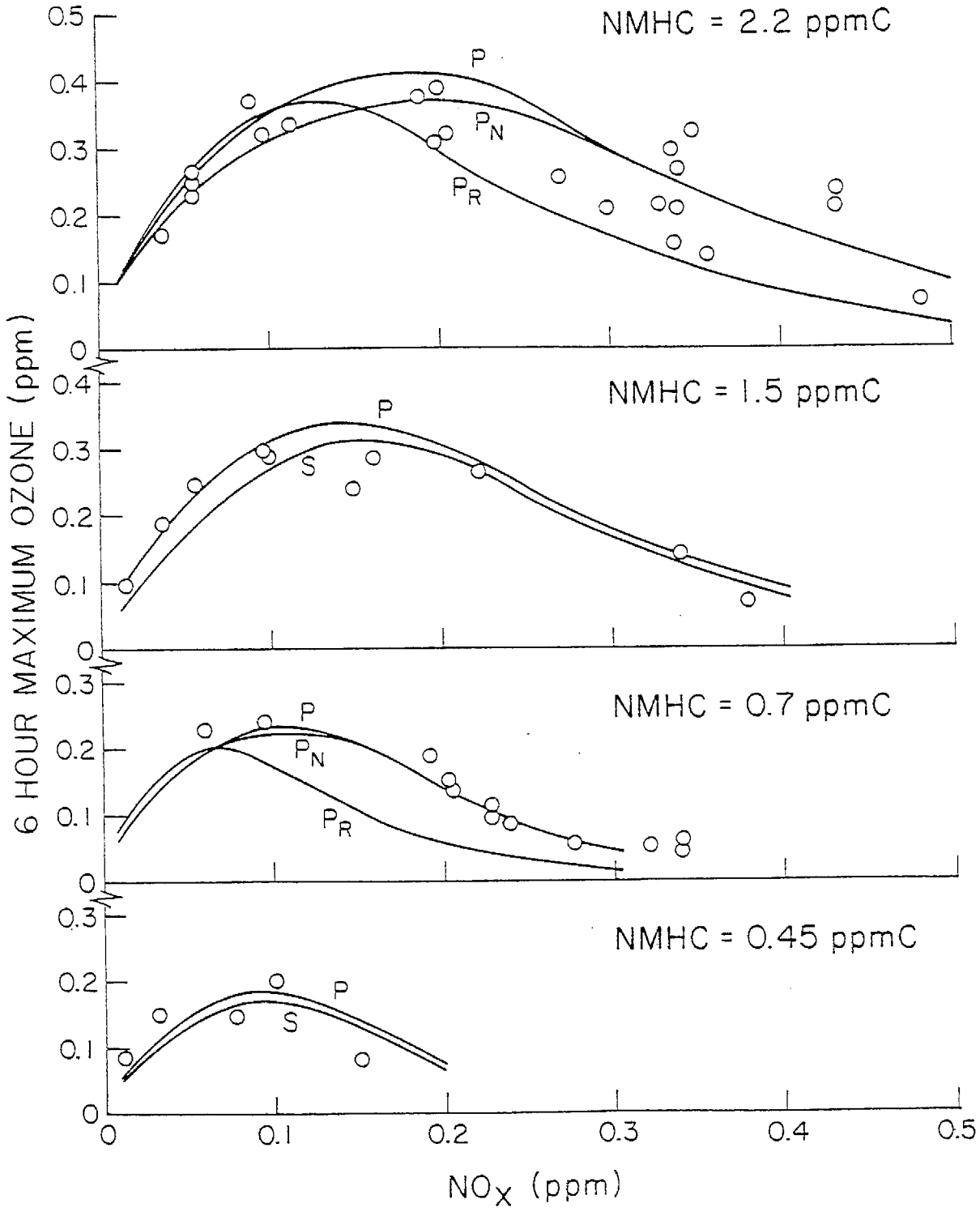

Figure 27. Experimental and Calculated Six-Hour Maximum Ozone for Various Initial Surrogate Hydrocarbon and NO_X Levels for Photolysis in the SAPRC Glass Chamber. o = experimental; —— = calculated.

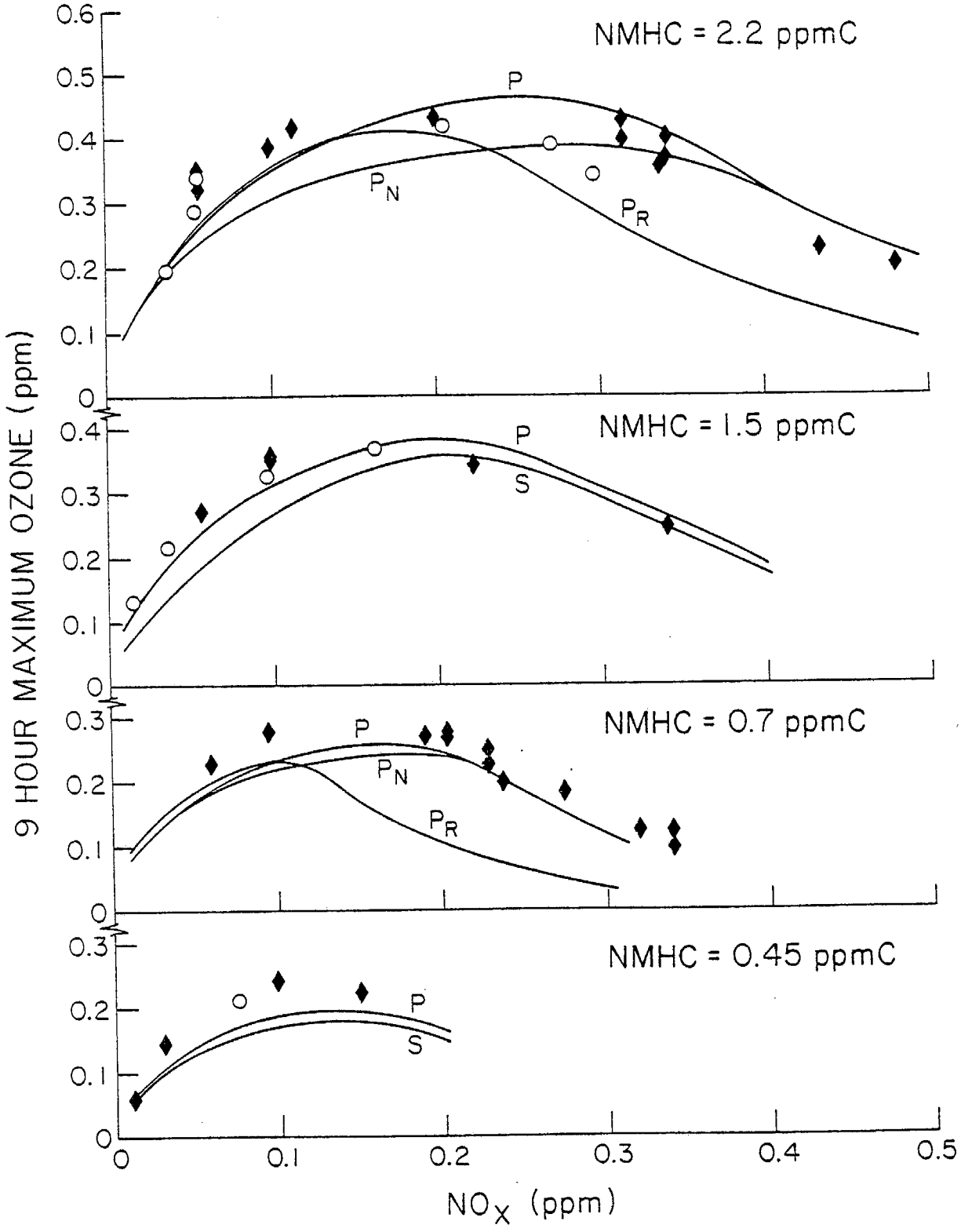

Figure 28. Experimental and Calculated Nine-Hour Maximum Ozone for Various Initial Surrogate Hydrocarbon and NO_X Levels for Photolysis in the SAPRC Glass Chamber. o = experimental; ◆ = extrapolated; —— = calculated.

parameters as calculation P. (The chamber simulation calculations P, P_R, P_N and S should not be confused with the corresponding ambient air simulation calculations C_S and C_{SD} (see below), since the latter do not include provisions for chamber effects and use different initial $[NO_2]/[NO]$ ratios than used in the chamber simulation calculations.)

Figures 27 and 28 compare six- and nine-hour maximum ozone yields observed in the surrogate hydrocarbon glass chamber experiments with those predicted by the four model calculations. Because of the limited number of nine-hour irradiations, most of the nine-hour ozone values are extrapolated from six-hour irradiations using a curve-fitting technique described elsewhere (Pitts et al., 1976b).

It can be seen from Figures 27 and 28 that the predicted O_3 maximum yields at higher NO_x levels are extremely sensitive to the chamber radical input rate used in the calculation and that good fits to the data can be attained if an input rate of 0.4 ppb min^{-1} is used. This value is consistent with the results of our modeling studies of SAPRC evacuable chamber experiments (Carter et al., 1979), where radical input rates required for calculations to fit the data range from 0.2 to 0.5 ppb min^{-1}, depending primarily on initial NO_x levels.

It can also be seen from Figures 27 and 28 that the O_3 yields at moderate NO_x levels are affected by the uncertain $N_2O_5 + H_2O$ rate constant (curves P_N), and that the magnitude of this effect increases with time and with increasing hydrocarbon level. The glass chamber data appear to be better fit if it is assumed that the $N_2O_5 + H_2O$ reaction is negligible, although in our evacuable chamber experiments the data are best fit by assuming that the reaction is not negligible (Carter et al., 1979). In general, one would expect the rate constant for this heterogeneous reaction to depend on the nature of the chamber employed.

Finally, Figures 27 and 28 show that the ozone maxima predicted using the detailed representation of the surrogate hydrocarbon mixture (S) are similar to those predicted by the corresponding propene-butane-aldehyde representation (P). In general the detailed mixture gives slightly lower O_3 predictions than calculations using the propene-n-butane-aldehyde representation, the discrepancy being largest at low NO_x and high hydrocarbon levels. This effect could be due to the slightly higher OH reac-

tivity of the propene-n-butane-aldehyde mixture (see Table 8). The fact that the discrepancy between the S and the P curves is relatively small suggests that representing complex hydrocarbon mixtures by propene + n-butane + aldehyde may be a good approximation, at least with respect to ozone formation. The small discrepancy is somewhat surprising in view of the fact that the atmospheric chemistry of aromatics (Atkinson et al., 1980; Hendry et al., 1978) is considerably different from that of alkanes and olefins (Carter et al., 1979; Hendry et al., 1978; Whitten et al., 1979; Falls and Seinfeld, 1978). Use of the simpler hydrocarbon mixture as an approximation may not yield valid results if one is representing mixtures which are higher in aromatic content than the detailed surrogate mixture used here.

The results of these calculations show that mechanism C used in calculation P can give acceptable fits to the maximum ozone yields observed in the extensive SAPRC surrogate hydrocarbon-NO_x-air smog chamber data base, provided that appropriately adjusted values of the "chamber effects" parameters are used. Given our current uncertainty of the nature and appropriate magnitudes of these parameters, this is the best that can be expected of any kinetic mechanism at the present time. Therefore, mechanism C can be considered to be "validated" for the purpose of use in EKMA calculations.

Ambient Air Simulations and EKMA Analyses. O_3 isopleth plots calculated using the two kinetic mechanisms and three different hydrocarbon representations are shown in Figures 29 through 31. The effect on the isopleths of varying both mechanism and mixture is shown in Figure 29. Isopleths using mechanism C and the standard EPA mixture (C_E) are compared with those calculated using the same mechanism and the SAPRC propane-butane-aldehyde surrogate (C_S), and those calculated using both the EPA mechanism and mixture (D_E). Figures 30 and 31 show the effects of the added aldehydes in the EPA hydrocarbon mixture on the calculated O_3 isopleths for mechanisms C and D, respectively. It can be seen from Figure 29 that although calculations using the SAPRC propene-butane-aldehyde mixture (S) give different isopleths than those using the EPA propene-butane-aldehyde mixture (E), this effect is not as great as that resulting from varying the kinetic mechanism. Mechanism C predicts that increasing NO_x

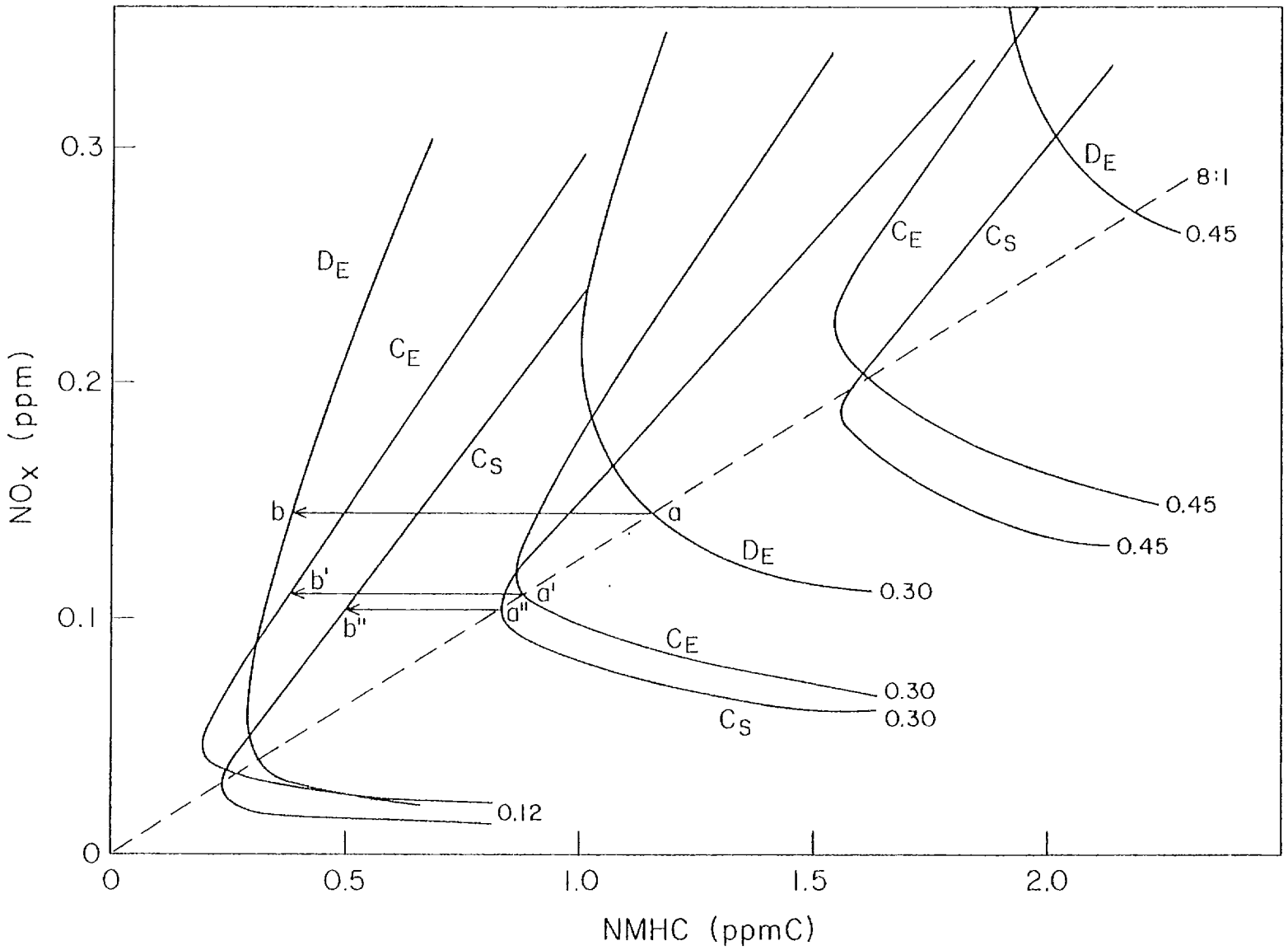

Figure 29. Isopleth Plots for O_3 = 0.12, 0.30 and 0.45 ppm Calculated for Mechanism D and the EPA Hydrocarbon Mixture (D_E); Mechanism C and the EPA Hydrocarbon Mixture (C_E); Mechanism C and the Propene-Butane-Aldehyde Representation of the SAPRC Surrogate Hydrocarbon Mixture (C_S). --- = NMHC/NO_x = 8:1.

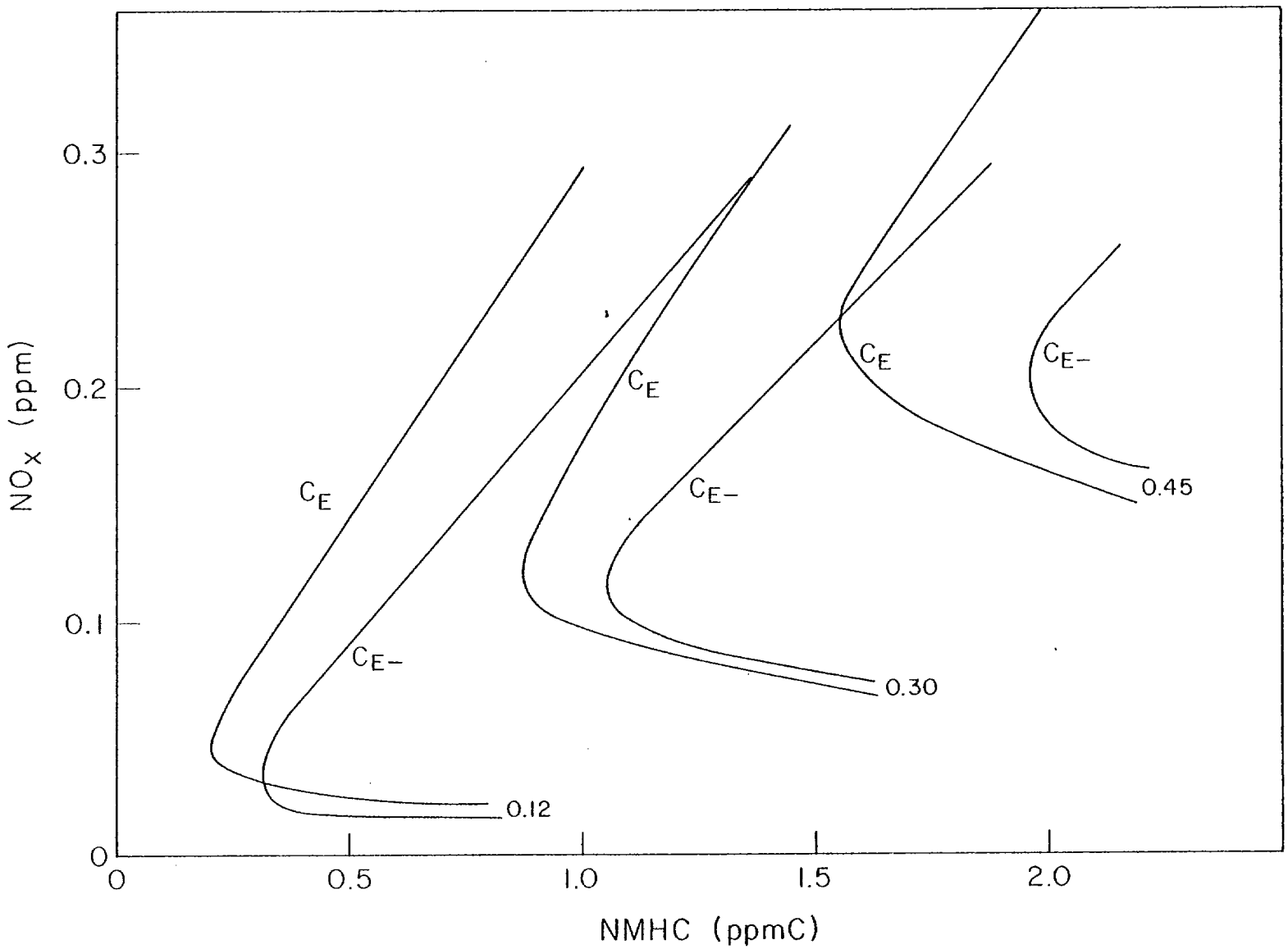

Figure 30. Isopleth Plots for O_3 = 0.12, 0.30 and 0.45 ppm Calculated for Mechanism C and the EPA Hydrocarbon Mixture With Aldehydes (C_E) and Without Aldehydes (C_{E-}).

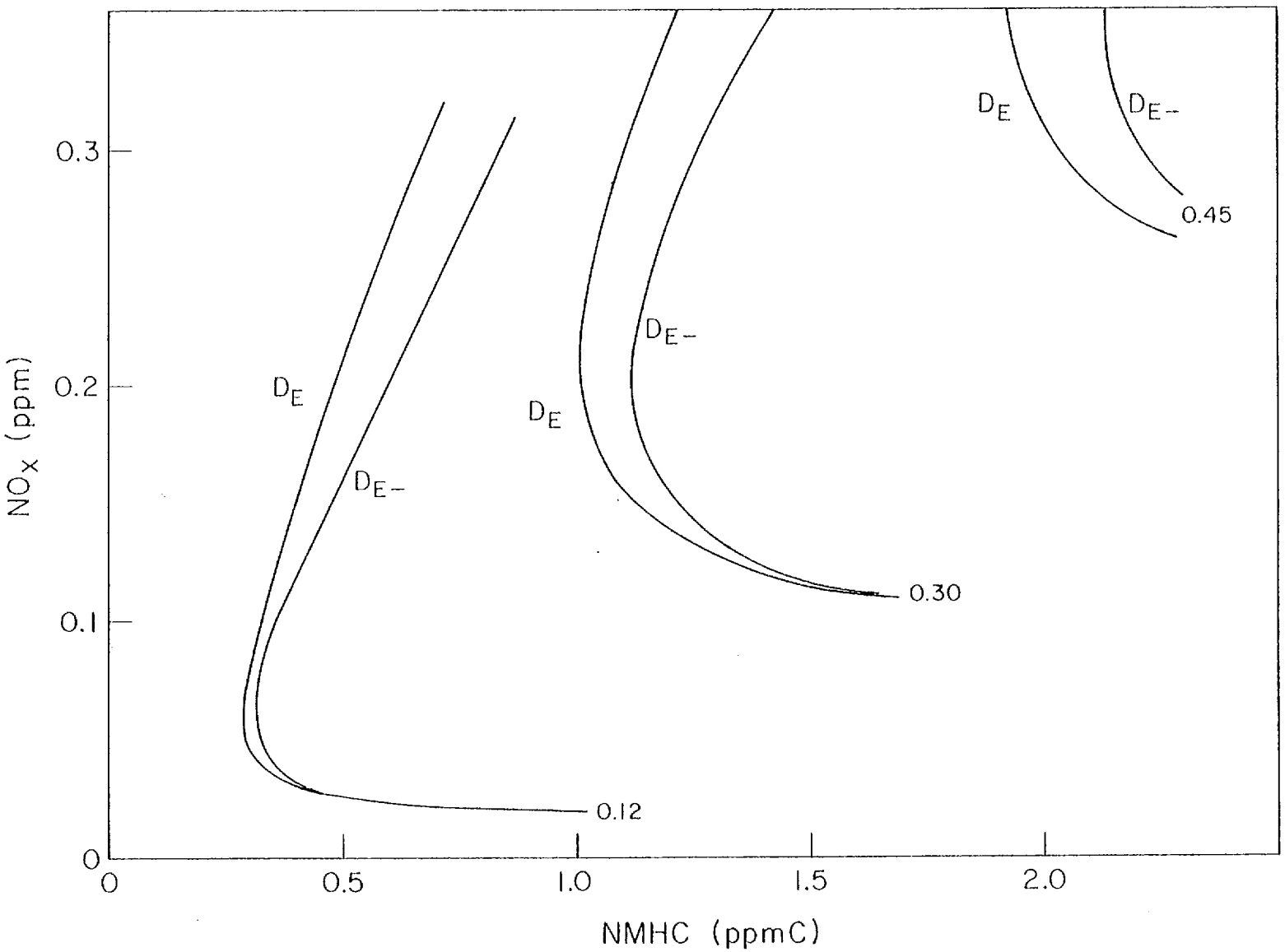

Figure 31. Isopleth Plots for O_3 = 0.12, 0.30 and 0.45 ppm Calculated for Mechanism D and the EPA Hydrocarbon Mixture With Aldehydes (D_E) and Without Aldehydes (D_{E-}).

inhibits O_3 formation more efficiently than does mechanism D. Additionally, comparison of Figures 30 and 31 shows that mechanism C predicts a larger effect of added aldehydes on the calculated O_3 isopleth than does mechanism D.

Plots are shown for the six different mechanisms and mixtures simulated in Figure 32 of the maximum O_3 concentrations which can be formed as a function of initial NMHC concentrations, and in Figure 33 of the NO_x concentrations at which these maximum O_3 concentrations are formed (hereafter referred to as "optimum NO_x"). Because of the three-dimensional nature of the isopleth plots shown in Figures 29 - 31, Figures 32 and 33 show more clearly some of the effects of using the different kinetic mechanisms or hydrocarbon representations on the model predictions. It can be seen that mechanism C predicts higher maximum O_3 values (Figure 32) and lower optimum NO_x values (Figure 33) than does mechanism D, if the same hydrocarbon mixture is used. When the same mechanism is used, mixtures with greater OH reactivity (Table 8) give higher maximum O_3 values (Figure 32), while mixtures with greater aldehyde content (Table 8) give higher optimum NO_x values (Figure 33). Otherwise, there are no obvious relationships between maximum O_3 and optimum NO_x values calculated by the various models. For example models D_E and C_E- give almost exactly the same maximum ozone values (Figure 32), yet give respectively the highest and lowest predicted optimum NO_x (Figure 33).

In order to test whether the differences in ozone isopleths calculated by the various models will affect control strategies derived from them, the isopleths in Figures 29 - 31 were analyzed to determine their predictions of hydrocarbon control required to reduce O_3 levels from 0.3 ppm to the current federal air quality standard of 0.12 ppm. The isopleth analysis technique, described above, is similar to that used by Dodge (1977a). The results of our analyses are summarized in Figure 34, in which percent hydrocarbon control predicted using the isopleths of Figures 29 - 31 are plotted against the initial NMHC/NO_x ratios used in the analyses.

Contrary to the results of Dodge's sensitivity study (1977a), Figure 34 shows that the differences in our calculated O_3 isopleths cause significant differences in predictions of hydrocarbon reduction required to meet the federal ozone standard, even when the isopleths are analyzed in

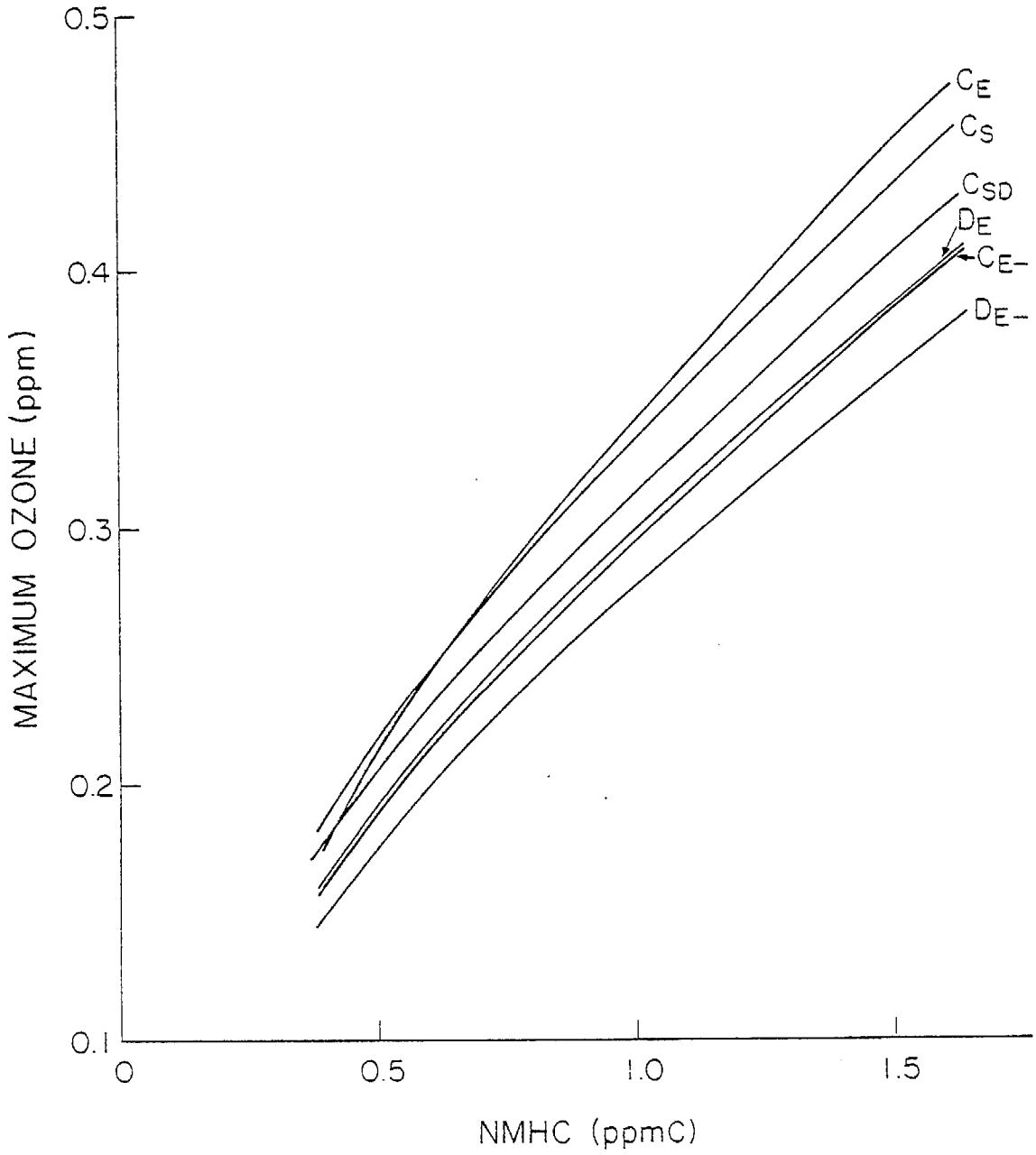

Figure 32. Calculated Maximum O_3 as a Function of Initial NMHC Levels for Mechanisms C and D and the EPA Hydrocarbon Mixture With and Without Aldehydes (C_E, C_{E-}, D_E, D_{E-}, respectively); and for Mechanism C and the Detailed and Propene-Butane-Aldehyde Representations of the SAPRC Surrogate Hydrocarbon Mixture (C_{SD} and C_S, respectively).

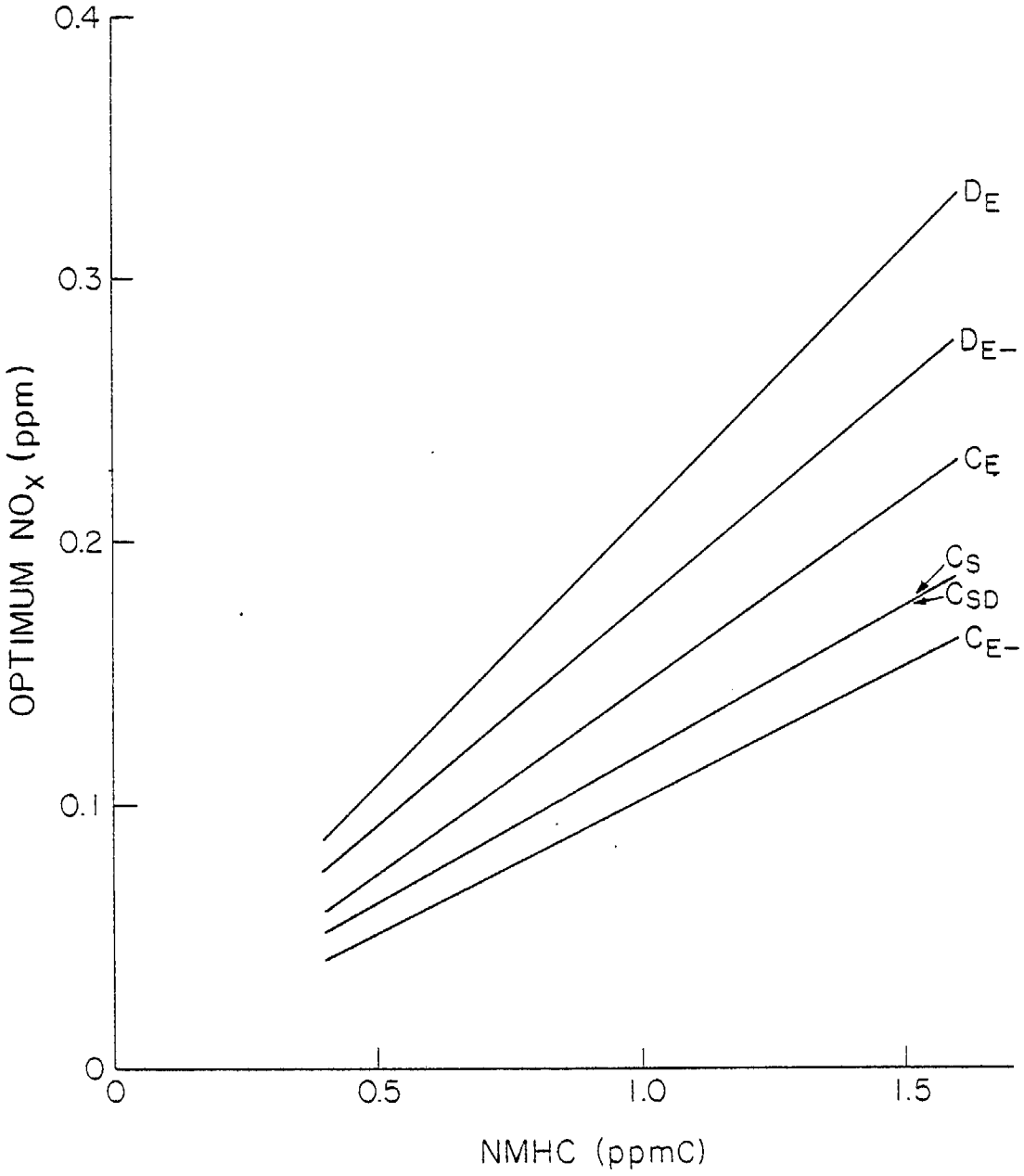

Figure 33. Calculated Initial NO_x Levels at which Maximum O_3 Formation Occurs for Mechanisms C and D and the EPA Hydrocarbon Mixture With and Without Aldehydes (C_E, C_{E-}, D_E, D_{E-}, respectively); and for Mechanism C and the Detailed and Propene-Butane-Aldehyde Representations of the SAPRC Surrogate Hydrocarbon Mixture (C_{SD} and C_S, respectively).

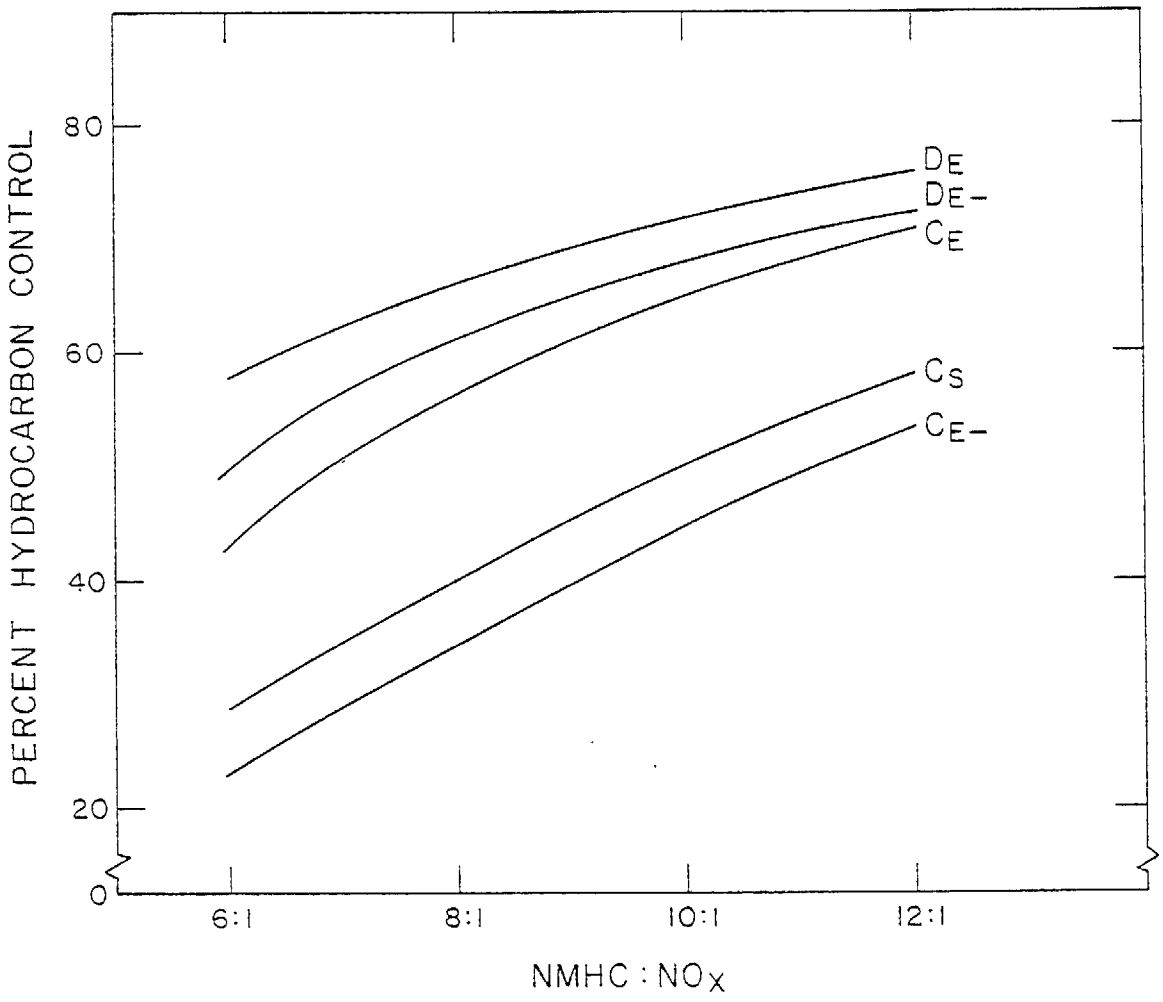

Figure 34. Percent Hydrocarbon Control Required to Reduce Ambient O_3 from 0.3 ppm to the Federal Air Quality Standard of 0.12 ppm as a Function of Initial MNHC/NO_X Ratios Derived from EKMA Isopleth Analysis. Calculations for Mechanisms C and D and the EPA Hydrocarbon Mixture With and Without Aldehydes (C_E, C_{E-}, D_E, D_{E-}, respectively) and for Mechanism C and the Propene-Butane-Aldehyde Representation of the SAPRC Surrogate Hydrocarbon Mixture (C_S).

the recommended "relative" sense (U. S. Environmental Protection Agency, 1977; Dimitriades, 1977). For example, assuming an 8:1 NMHC/NO_x ratio, and using the EPA hydrocarbon representation, mechanism D predicts a 66% NMHC reduction is required, while mechanism C predicts a 57% reduction is needed. The difference between the predictions of the kinetic mechanisms is greater if aldehydes are excluded from the hydrocarbon representation; in that case mechanism D predicts a 62% reduction is required, while mechanism C predicts only 34%. The hydrocarbon mixture is also important in affecting predictions of required hydrocarbon reductions, with mechanism C being more sensitive to the hydrocarbon representation than mechanism D (compare the difference between curves C_E and C_{E-} in Figure 34 with the difference between curves D_E and D_{E-}). The smaller sensitivity of mechanism D to hydrocarbon representation could contribute to the conclusion (Dodge, 1977a) that control strategies derived using the relative isopleth analysis technique (U. S. Environmental Protection Agency, 1977; Dimitriades, 1977) are relatively insensitive to changes in model parameters.

The percent required hydrocarbon reductions shown for the different models in Figure 34 correlate well with the predicted optimum NO_x levels (Figure 33) but correlate poorly with the predicted maximum O_3 levels (Figure 32). In terms of predicted required hydrocarbon control, the order of the models is $D_E > D_{E-} > C_E > C_S \approx C_{SD} > C_{E-}$, which is the same as the order of optimum NO_x levels for O_3 formation calculated by these models, but has no obvious relation to the $C_E > C_S > C_{SD} > D_E \approx C_{E-} > D_{E-}$ order for maximum O_3 formation. Like the calculated optimum NO_x, required hydrocarbon reduction predictions appear to be more strongly correlated with the aldehyde content in the hydrocarbon representation than with total OH reactivity (see Table 8). Thus the kinetic mechanism and the aldehyde content of the hydrocarbon mixture appear to be more important in affecting EKMA predictions of control strategies than the overall OH reactivity of the hydrocarbon mixture.

Comparison of EKMA Predictions with Ambient Air Data. In a validation study of the EKMA isopleth analysis technique, Trijonis and Hunsaker (1978) compared historical air quality trends for sites in the Los Angeles region and predictions of the EKMA isopleth method. The isopleth analyses used 1965 to 1974 air quality data for oxidant, hydrocarbon and NO_x, with the

data divided into four sets of three-year averages, 1964-1966, etc. The standard EPA isopleths (Dodge 1977b; Whitten and Hugo, 1978) were calculated using mechanism D and hydrocarbon mixture E. Trijonis and Hunsaker estimated that the 6-9 a.m. summertime ambient NMHC/NO_x ratio was ~12:1; however, a much better fit was obtained of "predicted" oxidant to the 1965-1974 historical oxidant data if an NMHC/NO_x ratio of 7:1 were used. A number of explanations for this discrepancy were offered, but the possibility of its being due to errors in the kinetic mechanism was not considered.

We examined the question of what the results of the Trijonis and Hunsaker (1978) study would have been using different kinetic mechanisms or hydrocarbon mixtures. The analysis was repeated for an example case using the same techniques and input data, but employing the isopleths calculated for this study. Oxidant trends observed in the 95th percentile of the daily maxima at Azusa were chosen as being representative. Results of predicted trends, derived using models D_E, D_{E-}, C_E, C_{E-} and C_S, and assuming the estimated initial NMHC/NO_x ratio of 12:1, are shown in Figure 35 and compared with the historic oxidant trend data (Trijonis and Hunsaker, 1978).

It can be seen that predicted oxidant trends, like the predicted hydrocarbon control requirements, are affected by the kinetic mechanism and the hydrocarbon mixture used to calculate the isopleths. Predictions of mechanisms C and D are similar if the standard EPA hydrocarbon mixture (E) is used, but are dramatically different if aldehydes are removed from the mixture (compare curves D_E with C_E and D_{E-} with C_{E-}). The predictions using mechanism C are more sensitive to the hydrocarbon mixture than mechanism D, and the aldehyde content of the mixture appears to be more important in affecting the results than total OH reactivity.

Trends calculated using mechanism C and the propene-butane-aldehyde representation of the SAPRC surrogate hydrocarbon mixture (model C_S) give the best fit to the historical oxidant data, better than the standard EPA EKMA model (D_E). The fit need not be taken as a validation of the C_S model since the large uncertainties in historical emissions and air quality data may render it coincidental. The major result of our re-examination of the Trijonis and Hunsaker analysis is the demonstration that calculated

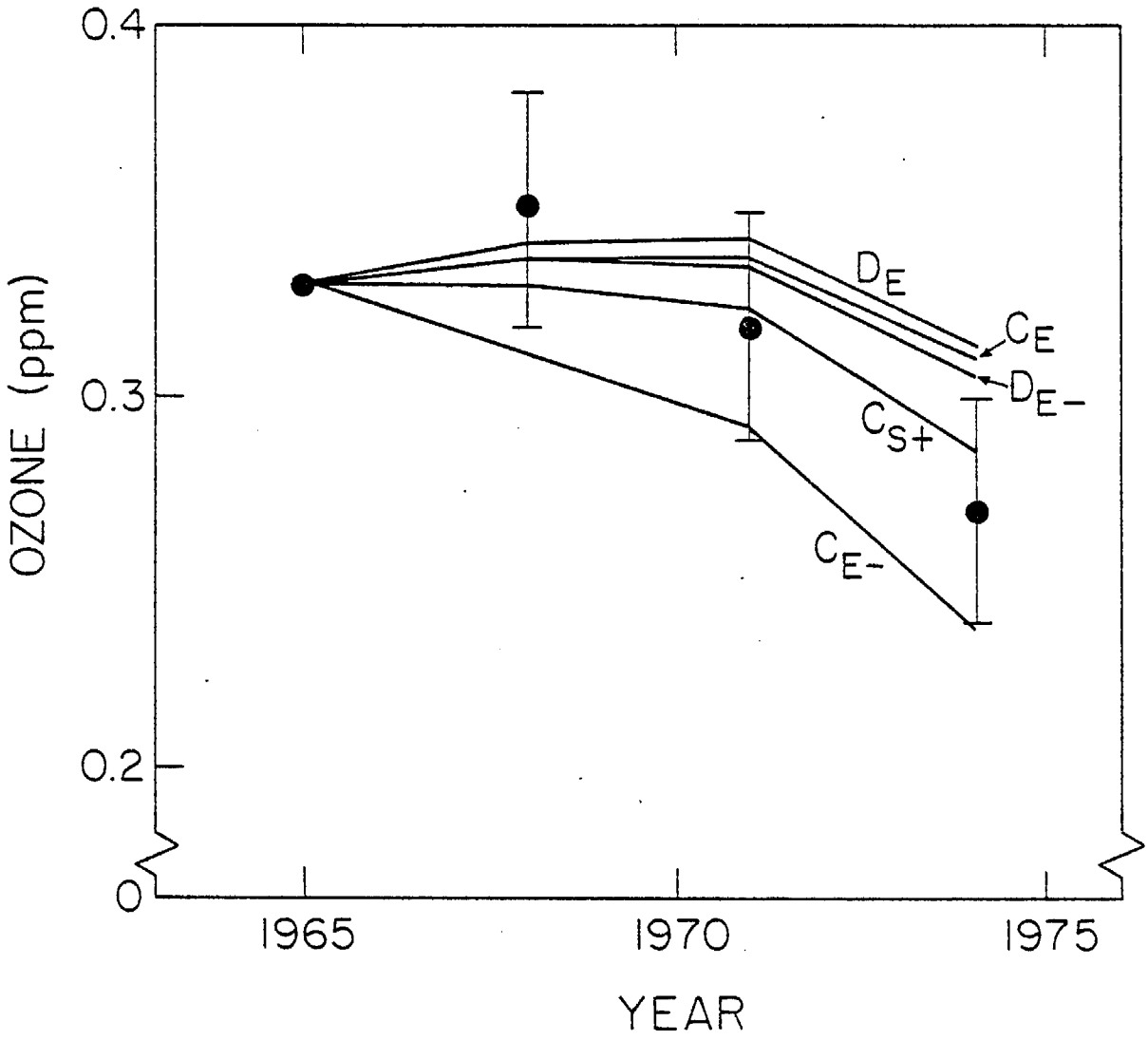

Figure 35. Oxidant Trends for the 95th Percentile of the Daily Maximum at Azusa: • = Observed, (error bars indicate measurement uncertainty); —— = Predicted from EKMA Isopleth Analysis. Calculations for Mechanisms C and D and the EPA Hydrocarbon Mixture With and Without Aldehydes (C_E, C_{E-}, D_E, D_{E-}, respectively) and for Mechanism C and the Propene-Butane-Aldehyde Representation of the SAPRC Surrogate Hydrocarbon Mixture (C_S).

trends are shown to be sensitive to both the kinetic mechanism and the hydrocarbon representation employed.

Sources of Discrepancies Between Predictions of the Kinetic Mechanisms. Since the development of mechanism D, knowledge has increased concerning rates and mechanisms of many reactions occurring in hydrocarbon-NO_x-air irradiations. This more recent information has been incorporated into mechanism C. The following differences in rate constants and mechanistic details are considered to be the most important ones between the two mechanisms.

(1) Mechanism D uses an HO_2 + NO rate constant which is a factor of ~10 lower than is currently accepted (Hampson and Garvin, 1978). This reaction is radical-propagating and indirectly causes O_3 formation by converting NO to NO_2, and it competes with the HO_2 + HO_2 reaction which is radical-terminating. The competition between these two reactions determines the minimum NO_x level at which continued O_3 formation can occur, and it has been shown that predicted O_3 maximum yields are very sensitive to this rate constant ratio (Carter et al., 1979).

(2) Mechanism D assumes maximum efficiency for radical production from the O_3 + propene reaction, while mechanism C assumes only 20% efficiency (2 radicals formed per molecule reacted, vs. 0.4). This reaction can be an important radical initiator in the system.

(3) Mechanism D, as implemented in the OZIPP programs (Whitten and Hogo, 1978), uses higher quantum yields for radical production in formaldehyde photolysis at wavelengths greater than 330 nm than those reported by Horowitz and Calvert (1978), which are used in mechanism C. Formaldehyde photolysis is an important radical initiator, and affects the model predictions by way of the aldehyde content of the hydrocarbon representation.

(4) Mechanism D uses a rate constant for the OH + NO_2 reaction which is a factor of 2 lower than currently accepted (Hampson and Garvin, 1978). This reaction is a very important radical-terminating process, and is also an important radical-terminating process, and is also an important NO_x sink.

(5) Mechanism D uses different quantum yields for $O(^1D)$ formation from O_3 photolysis; different rate constants for the reaction $O(^1D)$ + H_2O; and different rate constants for $O(^1D)$ deactivation by N_2 or O_2 than are

currently accepted (Hampson and Garvin, 1978). The combined result is that mechanism D predicts a radical input from the reaction

$$O(^1D) + H_2O \rightarrow 2\ OH$$

by a factor of ~1.25 greater than that predicted by mechanism C. This reaction is an important source of OH radicals in ambient air systems.

(6) Mechanism D used rate constants for OH reaction with propene and n-butane which are respectively 30% and 11% lower than used in mechanism C. This has the effect of making the OH reactivity of mixture E- ~60% lower for mechanism D than for mechanism C.

The effects of modifying mechanism C to resemble mechanism D in the above respects are shown in Table 10. All calculations used the E- hydrocarbon mixture, because calculations using this mixture appear to be the most sensitive to the mechanism used. It can be seen from Table 10 that using a slow HO_2 + NO rate constant or using slow OH + propene and n-butane rate constants tend to decrease both the predicted maximum O_3 and optimum NO_x while increasing radical production from the O_3 + olefin reaction or from formaldehyde or O_3 photolysis, or decreasing radical termination from the OH + NO_2 reaction all have the opposite effect. If all the modifications are made together, there is relatively little change in predicted maximum O_3, yet the predicted optimum NO_x increases significantly, and thus accounts for at least ~75% of the optimum NO_x discrepancy between the two mechanisms.

Since, as discussed previously, EKMA control strategy predictions are more closely correlated with predicted optimum NO_x than maximum O_3, the discrepancy between the mechanisms related to optimum NO_x predictions are clearly highly significant in affecting EKMA analyses. From Table 10, it can be seen that most of the discrepancy between optimum NO_x predictions of mechanism C and D can be accounted for by mechanistic differences relating to radical initiation or termination. The relationship between radical levels and predictions of NO_x dependence is due to the fact that reactions of radicals with NO_x are the major radical sinks in these hydrocarbon-NO_x-air systems. Under conditions of high NO_x which is not completely consumed during the irradiation (thus ending O_3 formation), maximum O_3 levels are determined by how rapidly O_3 is generated, which in turn is determined by

Table 10. Effect of Selected Modifications of Mechanism C on Predicted Maximum Ozone and Optimum NO_x Values Calculated for NMHC = 1.0 ppmC, and Comparison with Predictions of Mechanism D

Mechanism Used	Mechanistic Option[a]						Predicted Maximum O_3		Predicted Optimum NO_x	
	Slow HO_2+NO	O_3 + OL Maximum Radicals	$HCHO+h\nu$ Radicals	Slow $OH+NO_2$	Fast $O(^1D)+H_2O$	Slow OH+HC	(ppm)	Change[b]	(ppm)	Difference[c]
C	No	No	No	No	No	No	0.29	0	0.107	-0.069
C	YES	No	No	No	No	No	0.23	-0.06	0.095	-0.081
C	No	YES	No	No	No	No	0.32	0.03	0.132	-0.044
C	No	No	YES	No	No	No	0.32	0.03	0.138	-0.038
C	No	No	No	YES	No	No	0.37	0.08	0.137	-0.039
C	No	No	No	No	YES	No	0.30	0.01	0.116	-0.060
C	No	No	No	No	No	YES	0.27	-0.02	0.097	-0.079
C	YES	YES	YES	YES	YES	YES	0.31	0.02	0.159	-0.017
D	YES	YES	YES	YES	YES	YES	0.28	-0.01	0.176	0

[a]YES = Same as used in Mechanism D, "No" = This aspect of Mechanism C not changed.

[b]Change = Result of this calculation - result of calculation of unmodified Mechanism C.

[c]Difference = Result of this calculation - result of calculation of Mechanism D.

the radical levels which initiate the NO to NO_2 conversion processes. Predictions of NO_x dependence on O_3 formation at moderate and high NO_x levels will thus be directly affected by aspects of the kinetic mechanism concerning radical formation or destruction.

The fact that the two mechanisms can have such significant differences concerning radical initiation and termination reactions in spite of having been validated against smog chamber data may be due in part to the way chamber effects were treated during model validation. The most important chamber effect concerns radical initiation from unknown sources, for which models must include some provision in order to fit predictions to smog chamber data (Carter et al., 1979; Hendry et al., 1978; Whitten et al., 1979; Falls and Seinfeld, 1978). In the EPA model validation (Dodge, 1977b) radical initiation was accounted for by assuming nitrous acid was present in the chamber at the beginning of the irradiation. Nitrous acid is a powerful photoinitiator (Stockwell and Calvert, 1978) which could be heterogeneously formed when NO_x is injected. In the SAPRC model (Carter et al., 1979) better fits to the data were obtained by assuming, rather than initially present nitrous acid, a continuous hydroxyl radical flux from unknown sources, an assumption also used by other modelers (Hendry et al., 1978). Experiments done at SAPRC in which the possibility of introduction of HONO with the NO_x was minimized gave essentially the same results as control runs when NO_x was injected in the usual manner (Carter, 1979). Since initially present nitrous acid will be rapidly consumed by photolysis (Stockwell and Calvert, 1978), much less overall radical initiation from chamber sources was assumed in the EPA model validation compared with that used in our validation of Mechanism C. Inappropriately low radical initiation from chamber sources could be offset in the EPA model validation by use of a homogeneous mechanism assuming inappropriately high radical initiation rates or low radical termination efficiencies. We should stress that our treatment of chamber radical sources is arbitrary, and our model predictions of radical levels may be no more valid than those of the EPA model.

Conclusions. An updated propene + n-butane-NO_x-air photochemical mechanism predicts of the dependence of maximum O_3 formation on initial hydrocarbon and NO_x levels in good agreement with those observed in the

extensive set of "surrogate" hydrocarbon-NO_x-air smog chamber experiments performed at SAPRC. Validation of models using smog chamber data remains ambiguous because of the necessity to include adjustable parameters to account for significant, but poorly characterized, chamber effects. This is particularly true of aspects of the model relating to radical initiation or termination. With our present knowledge of chamber effects, the best level of validation for which one can aim is that the models not be inconsistent with the chamber data, which has been achieved for our model.

The reasonably close correspondence between results of our semi-detailed model calculations and our propene + butane calculations suggests that representing the complex surrogate hydrocarbon mixture by propene, n-butane and formaldehyde is a reasonably good approximation for examination of O_3-NMHC-NO_x relationships. Propene, n-butane and formaldehyde can be also used to represent other complex mixtures of organics, as long as the levels are chosen to correctly simulate OH reactivity and oxygenate content of the reactive compounds of the mixture.

The EKMA analyses based on isopleths calculated using our validated kinetic mechanism and hydrocarbon representation differ from analyses based on isopleths calculated using the EPA kinetic model currently used in EKMA analysis. Differences occur even though the isopleth analyses employed the "relative" technique recommended by the EPA (U. S. Environmental Protection Agency, 1977; 1978; Dimitriades, 1977), and contrast with the results of the sensitivity study by Dodge (1977a) who found that differences in calculated isopleths resulting from changing certain aspects of the input data tended to cancel out when the "relative" technique was used. Dodge also found (1977a) that the NMHC/NO_x ratios assumed in the analyses are among the most important of the input data to affect EKMA predictions. Our study confirmed that the NMHC/NO_x ratio is important; but in addition, we found that the magnitude of differences in predictions derived assuming different kinetic mechanisms or aldehyde content can approach the magnitude of the differences which occur by using the same model but changing the NMHC/NO_x by a factor of ~2. Therefore, in terms of impact on EKMA model predictions, uncertainties in the kinetic mechanism and the oxygenate content of the hydrocarbons can be of equal or perhaps even greater importance than uncertainties in the NMHC/NO_x ratio. These

facts do not appear to be generally appreciated (U. S. Environmental Protection Agency, 1977; 1978).

The major discrepancy between the predictions of the SAPRC and EPA models is in predictions of the dependence of ozone maxima on NO_x levels, due primarily to differences in the mechanisms concerning several radical initiation or termination reactions. Chamber effects are such that such reactions are precisely the aspects of the model which are most difficult to validate unambiguously using smog chamber data. Based on our previous smog chamber modeling work (Carter et al., 1979) and other chamber studies in our laboratories (Carter, 1979) we believe that the smog chamber validation of the kinetic model currently used in EKMA calculations assumes an inappropriately low radical input from chamber effects, and that that error was compensated for by other aspects of the homogeneous or chamber-independent mechanism predicting too much radical initiation, or too little radical termination. However, the method used in our models to account for chamber effects may be no less appropriate than that used in the EPA model. Until smog chamber effects are better characterized, there will remain considerable uncertainty in the kinetic models predicting radical levels, and in the corresponding EKMA analyses using isopleths based on these models.